1 cy.

COO-1195-207

SEARCH FOR THE DECAY $K_S^o \rightarrow \pi^+\pi^-\pi^o$

BY

LEWIS HAMMOND JONES, IV
B.A., Ohio Wesleyan University, 1963
M.S., University of Illinois, 1965

THESIS

Submitted in partial fulfillment of the requirements
for the degree of Doctor of Philosophy in Physics
in the Graduate College of the
University of Illinois at Urbana-Champaign, 1971

Urbana, Illinois
February, 1971

This research was supported in part by the
U.S. Atomic Energy Commission under Contract AT(11-1)-1195

DISCLAIMER

COO-1195-207

SEARCH FOR THE DECAY $K_S^o \rightarrow \pi^+\pi^-\pi^o$

BY

LEWIS HAMMOND JONES, IV
B.A., Ohio Wesleyan University, 1963
M.S., University of Illinois, 1965

THESIS

Submitted in partial fulfillment of the requirements
for the degree of Doctor of Philosophy in Physics
in the Graduate College of the
University of Illinois at Urbana-Champaign, 1971

Urbana, Illinois
February, 1971

This research was supported in part by the
U.S. Atomic Energy Commission under Contract AT(11-1)-1195

SEARCH FOR THE DECAY OF THE SHORT-LIVED NEUTRAL K MESON INTO TWO CHARGED PI MESONS AND ONE NEUTRAL PI MESON

Lewis Hammond Jones, IV, Ph.D.
Department of Physics
University of Illinois at Urbana-Champaign, 1971

A spark chamber experiment was run at Argonne National Laboratory to search for the decay $K_S^o \rightarrow \pi^+\pi^-\pi^o$. CP does not forbid this decay, but the CP conserving states are strongly suppressed by centrifugal barriers. Therefore, observation of a large amplitude for $K_S^o \rightarrow \pi^+\pi^-\pi^o$ would indicate probably CP violation in this decay mode. The method used was to measure the time distribution of $K^o \rightarrow \pi^+\pi^-\pi^o$ decays in the region from 0.5 to 6.5 K_S^o lifetimes. The K^o mesons were produced in a 3 cm. long carbon target via the reaction $\pi^- p \rightarrow K^o\Lambda$ at a beam momentum of 3 GeV/c. Identification of the Λ insured that there was no $\overline{K}^o$ contamination in the data at t = 0. The momenta of the charged decay products were measured using thin foil spark chambers placed in a 10 kG magnetic field. Photons from π^o decay were identified by observation of showers in heavy plate spark chambers. Two charged particle tracks and one photon track, consistent with $K_{\pi 3}^o$ decay, were required. The time distribution for the 99 events in the final sample was fit by the method of maximum likelihood for the complex amplitude ratio

$$x + iy = \frac{(K_S^o \rightarrow \pi^+\pi^-\pi^-)}{(K_L^o \rightarrow \pi^+\pi^-\pi^o)} .$$

The result is

$$x = -0.09 \pm 0.19, \qquad y = 0.56 \pm 0.43.$$

This result indicates a possible violation of CP in $K^0_{\pi 3}$ decays but is also consistent with CP conservation at the one-standard deviation level. The value of χ^2 for $x = y = 0$ is 6.10 for four degrees of freedom with χ^2 probability = 19.2%. A second result found in the likelihood fit is statistically preferred over the first result but is ruled out on theoretical and experimental grounds.

ACKNOWLEDGEMENTS

I wish to express sincere appreciation to my advisor, Professor James H. Smith, for his guidance and encouragement in all phases of my thesis experiment. In particular, his enthusiasm for physics has been an inspiration.

I am deeply grateful to Professor Alexander Abashian for his active and untiring participation in the experiment and the analysis and especially for his eternal optimism.

The assistance, advice, and insight of Professor Rich Orr were invaluable throughout the experiment.

I wish to thank Professor Michael J. Glaubman of Northeastern University, who flew to Argonne weekly from Boston to lend valuable assistance during the data taking.

I am very grateful to fellow graduate students Mike Graham, Paul Mantsch, and Dick Stutzke for their hard work on the experiment and for their companionship during my graduate studies.

I would also like to thank the following for their help with the experiment:

Bob Cullum and Stan Vrschaj for their clever and efficient programming.

Cloyd Smock and Leonard Seward for their competent assembly, operation, and maintenance of much of the experimental apparatus.

Jim Frank, Mick Jordan, Siegbert Raither, Sam Pederson, Pierre Sokolsky, and Steve Turk for help building and setting up the apparatus writing some of the programs.

The scanning, measuring, and bookkeeping crew including Nancy Hartog, Dan Gardner, Keith Kahl, Roberta Klos, Judy Lee, Barbara Miller, Sandy O'Meara, Jerry Pike, Terry Shephard, Estelle Thomas, Norma Vanselow, and Chin-Wen Yao, and their supervisor Patricia Martin.

Sherry Kallembach for her efficient typing of the thesis.

Dr. H. F. Haggerty and Dr. David Berley and collaborators for furnishing unpublished results.

The staff at the Argonne Z.G.S. and Applied Math Division for much valuable assistance.

The U. S. Atomic Energy Commission for financial support of the experiment.

Finally, I wish to thank my parents, family, and friends for constant encouragement throughout my graduate career.

The universe is not only queerer than we imagine, but it is queerer than we can imagine.

---J. B. S. Haldine

On ne peut pas rester toujours sur les sommets, it faut redescendre. A quoi bon, alors? Voici: le haut connaît le bas, le bas ne connaît pas le haut...
On monte, on voit. On redescend, on ne voit plus; mais on a vu. Il y a un art de se diriger dans les basses régions, par le souvenir de ce qu'on a vu lorsqu'on était plus haut. Quand on ne peut plus voir, on peut du moins encore savoir.

---René Daumal, Le Mont Analogue

Alice laughed: "There's no use trying," she said; "one can't believe in impossible things."

"I daresay you haven't had much practice," said the queen. "When I was younger, I always did it for half an hour a day. Why, sometimes I've believed in as many as six impossible things before breakfast."

---Lewis Carroll, Through the Looking Glass

TABLE OF CONTENTS

Frontispiece. Participants in the experiment, inside the instrument trailer.
Front row: C. I. Smock, R. D. Stutzke, A. Abashian.
Back row: J. H. Smith, P. M. Mantsch, M. J. Glaubman,
L. H. Jones, J. R. Orr. Not in photograph: M. F. Graham.

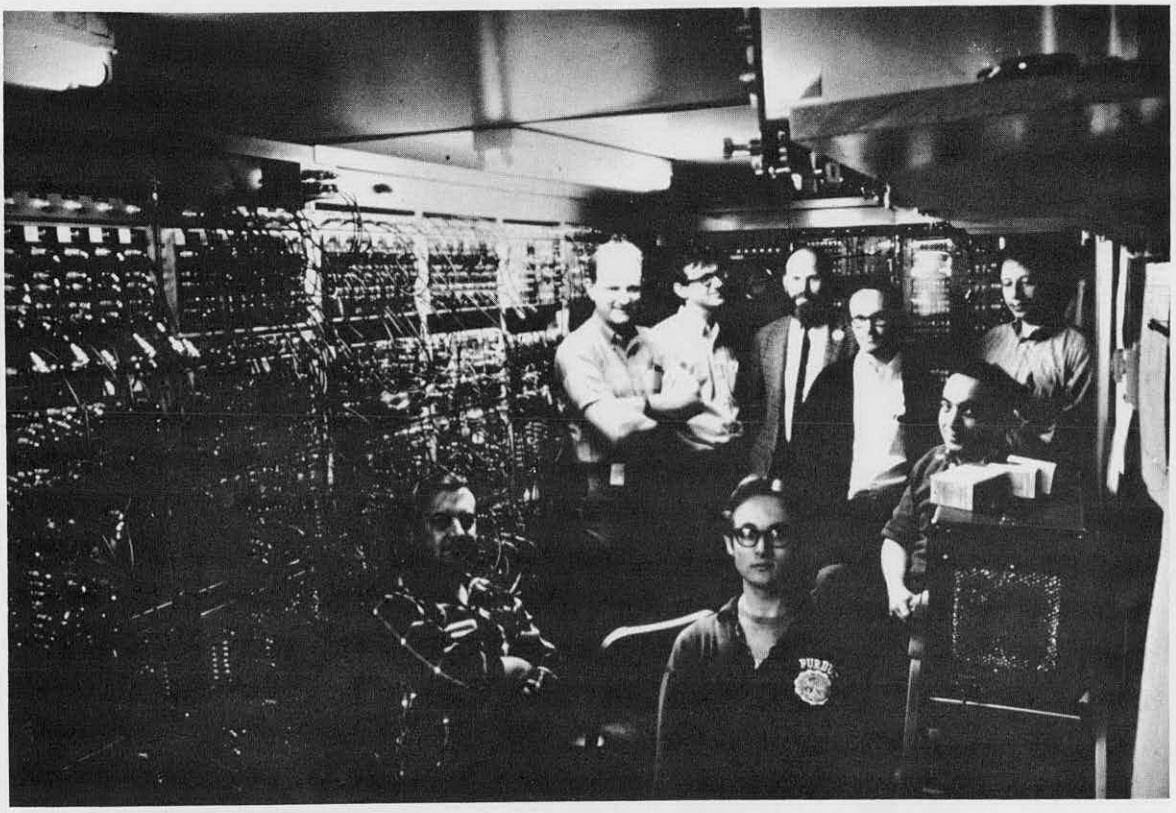

I. INTRODUCTION AND THEORY

In this experiment, a search was made for the decay $K_S^o \to \pi^+\pi^-\pi^o$. CP does not forbid this decay, but the CP conserving states are strongly suppressed by centrifugal barriers. Thus the existence of the decay $K_S^o \to \pi^+\pi^-\pi^o$ would indicate probable CP violation.

The method used was to measure the time distribution of $\pi^+\pi^-\pi^o$ decays resulting from an initial K^o state. If only $K_L^o \to \pi^+\pi^-\pi^o$ decays occur, the distribution is exponential with the K_L^o lifetime. If $K_S^o \to \pi^+\pi^-\pi^o$ decays occur as well, the two amplitudes can interfere with one another. The time distribution of $\pi^+\pi^-\pi^o$ decays would then exhibit an interference between the K_S^o and K_L^o components.

The current interest in CP experiments began in 1964 with the discovery of the CP violating decay $K_L^o \to \pi^+\pi^-$.[1,2] Since then, many experimenters have looked for other evidence for CP nonconservation. No clear evidence for CP violation outside of the neutral kaon system has been found. In the $K^o(\bar{K}^o)$ decays, it has been observed only in the existence of the decays $K_L^o \to \pi^+\pi^-$ and $K_L^o \to \pi^o\pi^o$ and in the charge asymmetry found in the leptonic decays $K_L^o \to \pi^{\pm}e^{\mp}\nu(\bar{\nu})$ and $K_L^o \to \pi^{\pm}\mu^{\mp}\nu(\bar{\nu})$. Although the CP violation in 2π decays is very small, this does not completely preclude the existence of a much larger CP violation in 3π decays. This violation would be reflected in the 2π decays through terms in the $K^o(\bar{K}^o)$ mass matrix due to 3π intermediate states.[3]

For later reference, we introduce here the following abbreviations for certain decay modes of the K^o meson:

$K_{\pi 3}^o$ for $K^o \to \pi^+\pi^-\pi^o$

K_{e3}^o for $K^o \to \pi^{\pm}e^{\mp}\nu(\bar{\nu})$

$K_{\mu 3}^o$ for $K^o \to \pi^{\pm}\mu^{\mp}\nu(\bar{\nu})$

We now state the conventions used for the $K^o(\bar{K}^o)$ system and derive the expression for the time distribution in $K^o \to \pi^+\pi^-\pi^o$ decays.

CPT is assumed to be a valid symmetry in all that follows. C is the charge conjugation operation, which transforms a particle into its anti-particle. P is the parity operation, which inverts the spatial coordinates of a particle ($\vec{r} \to -\vec{r}$). T is the time reversal operation, which inverts the time coordinate ($t \to -t$). If CPT is conserved, then CP is equivalent to T. The CP operation for the $K^o(\bar{K}^o)$ system is defined by $CP|K^o\rangle = |\bar{K}^o\rangle$.

We use the following definitions for $|K_S^o\rangle$ and $|\bar{K}^o\rangle$, the short- and long-lived components of the $K^o(\bar{K}^o)$ system:

$$|K_S^o\rangle = \frac{1}{\sqrt{2(1+|\epsilon|^2)}}\left[(1+\epsilon)|K^o\rangle + (1-\epsilon)|\bar{K}^o\rangle\right]$$

$$|K_L^o\rangle = \frac{1}{\sqrt{2(1+|\epsilon|^2)}}\left[(1+\epsilon)|K^o\rangle - (1-\epsilon)|\bar{K}^o\rangle\right]$$

Terms of the order of ϵ are negligible in this experiment and will be neglected in all subsequent discussions. Thus, for the purposes of this experiment, $|K_S^o\rangle$ and $|\bar{K}_L^o\rangle$ are taken to be equivalent to $|K_1^o\rangle$ and $|K_2^o\rangle$, the eigenstates of CP:

$$|K_S^o\rangle \approx |K_1^o\rangle = \frac{1}{\sqrt{2}}\left[|K^o\rangle + |\bar{K}^o\rangle\right]$$

$$|K_L^o\rangle \approx |K_2^o\rangle = \frac{1}{\sqrt{2}}\left[|K^o\rangle - |\bar{K}^o\rangle\right]$$

In this approximation, K_S^o is even under the operation of CP and K_L^o is odd under CP.

Define the ratio of amplitudes

$$x + iy = \frac{a(K_S^o \to \pi^+\pi^-\pi^o)}{a(K_L^o \to \pi^+\pi^-\pi^o)}$$

This ratio is the quantity measured in this experiment.

Starting from an initial state at time t = 0, $|K^o(0)\rangle = \frac{1}{2}[|K_S^o\rangle + |K_L^o\rangle]$, the amplitude for decay into $\pi^+\pi^-\pi^o$ at time t is

$$a(t) = \frac{1}{\sqrt{2}}\left[a(K_S^o \to \pi^+\pi^-\pi^o)e^{-\frac{\gamma_S t}{2} - iM_S t} + a(K_L^o \to \pi^+\pi^-\pi^o)e^{-\frac{\gamma_L t}{2} - iM_L t}\right]$$

where γ_S, γ_L = widths of K_S^o, K_L^o

M_S, M_L = masses of K_S^o, K_L^o.

Squaring a(t) and using the definition for x + iy gives the rate of $\pi^+\pi^-\pi^o$ decays, $\Gamma(t;x,y)$

$$\Gamma(t;x,y) = \frac{1}{2}\left|a(K_L^o \to \pi^+\pi^-\pi^o)\right|^2\left\{(x^2+y^2)e^{-\gamma_S t} + e^{-\gamma_L t} + 2[x\cos\delta t - y\sin\delta t]e^{-\frac{(\gamma_S+\gamma_L)}{2}t}\right\}.$$

where $\delta = M_L - M_S$.

Figures 1 and 2 show plots of this expression for several values of the magnitude and phase of x + iy.

All states of $K_S^o \to \pi^+\pi^-\pi^o$ except the CP violating I = 1 state are expected to be suppressed by angular momentum barriers or the $\Delta I = 1/2$ rule.[4/]

Figure 1. Theoretical time distribution curves with $|x + iy| = 0.2$.

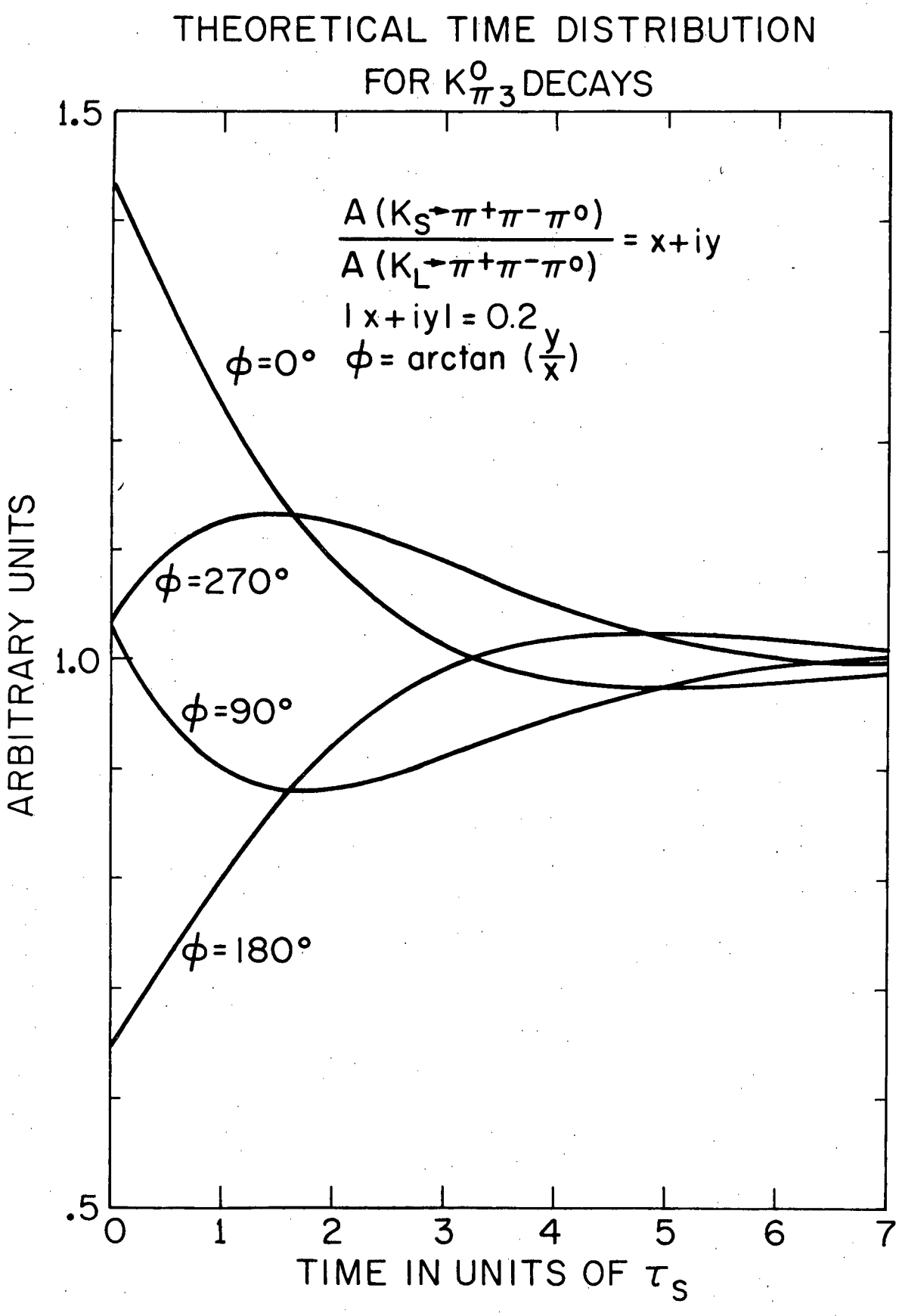
THEORETICAL TIME DISTRIBUTION
FOR $K^0_{\pi 3}$ DECAYS
$\frac{A(K_S \to \pi^+\pi^-\pi^0)}{A(K_L \to \pi^+\pi^-\pi^0)} = x+iy$
$|x+iy| = 0.2$
$\phi = \arctan(\frac{y}{x})$
ϕ=0°
ϕ=270°
ϕ=90°
ϕ=180°
ARBITRARY UNITS
1.5
1.0
.5
0
1
2
3
4
5
6
7
TIME IN UNITS OF τ_S

Figure 2. Theoretical time distribution curves with $|x + iy| = 1.0$.

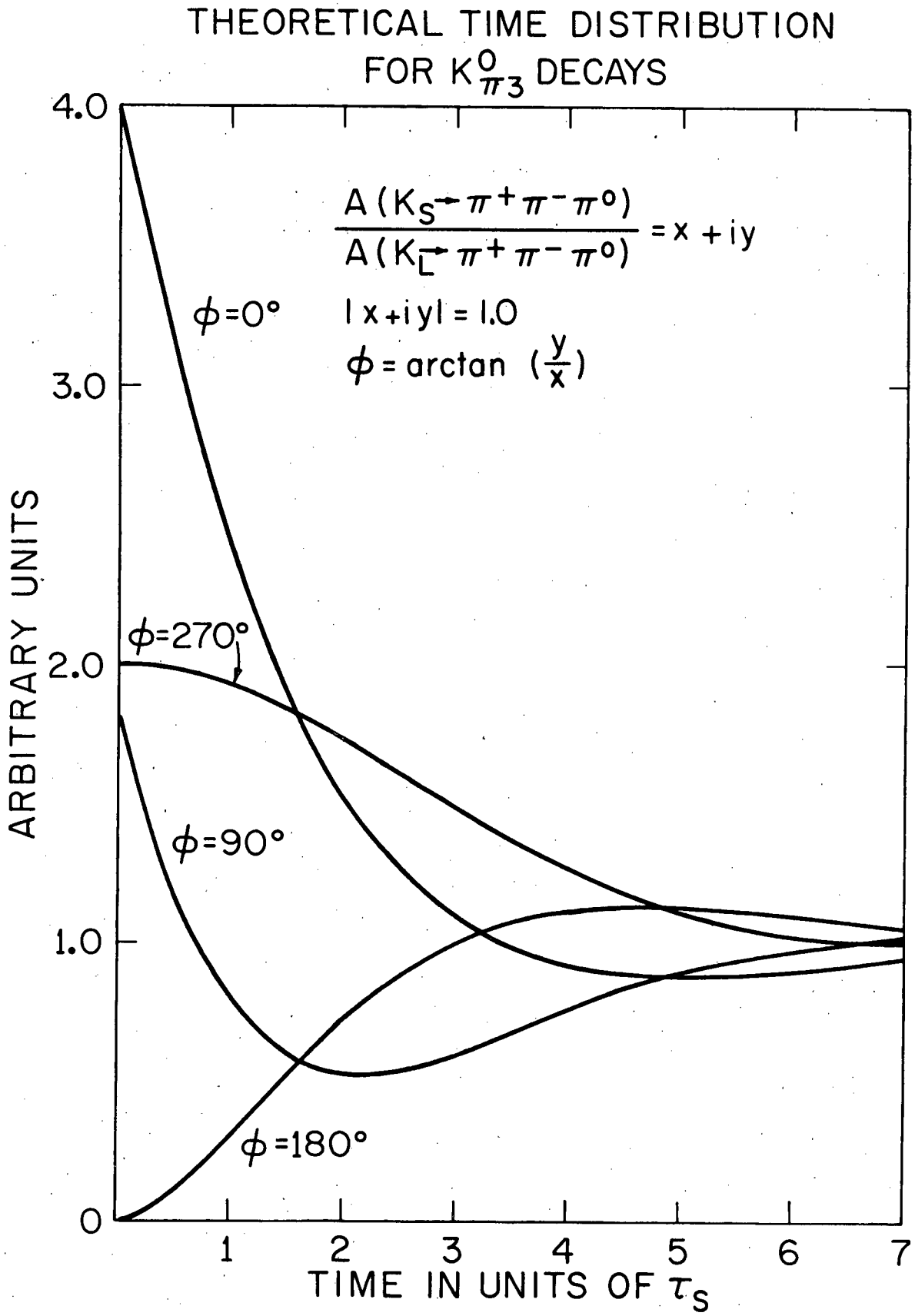
THEORETICAL TIME DISTRIBUTION
FOR $K^0_{\pi 3}$ DECAYS
$\frac{A(K_S \to \pi^+\pi^-\pi^0)}{A(K_L \to \pi^+\pi^-\pi^0)} = x + iy$
$\phi = 0°$
$|x+iy| = 1.0$
$\phi = \arctan(\frac{y}{x})$
$\phi = 270°$
$\phi = 90°$
$\phi = 180°$
ARBITRARY UNITS
4.0
3.0
2.0
1.0
0
1
2
3
4
5
6
7
TIME IN UNITS OF τ_S

Therefore a nonzero value for x + iy suggests that CP is violated in this mode.

The following discussion considers briefly the allowed states of the $\pi^+\pi^-\pi^o$ system. A more detailed discussion is found in reference 5.

Bose statistics requires that the isospin state be multiplied by the appropriate space state to give total symmetry of the wave function.

There are seven isospin states for the neutral 3π system:[6] one I = 0 state ($\Delta I = 1/2$), three I = 1 states ($\Delta I = 1/2, 3/2$), two I = 2 states ($\Delta I = 3/2, 5/2$), and one I = 3 state ($\Delta I = 5/2, 7/2$). One of the I = 1 states and one of the I = 3 states are symmetric. The other states either are antisymmetric or have mixed symmetry. $J^{PG} = 0^{--}$ for all three-pi states. $CP = (-1)^I GP = (-1)^I$. Thus, for $K_S^o \to \pi^+\pi^-\pi^o$ decays, the even isospin states, with I = 0,2, are allowed by CP and the odd ones, with I = 1,3, are forbidden. Table 1 summarizes the $K_{\pi 3}^o$ isospin states.

Table 1.

$K_{\pi 3}^o$ Isospin States

Isospin	Number of States	Symmetry	CP
I = 0	1	Antisymmetric	+1
I = 1	3	Symmetric, Mixed	-1
I = 2	2	Mixed	+1
I = 3	1	Symmetric	-1

Now consider the space states.[4] Let the angular momentum of the π^+ and the π^- in their rest frame be ℓ and the angular momentum of the π^o with respect to the center of mass frame of the π^+ and π^- be L. This is indicated schematically in the diagram below.

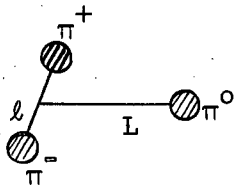

Since the spin of the K^o is zero, the total angular momentum of the three-pion system must be zero. Therefore, $\ell = L = 0,1,2,\ldots$ All states except the dipion s-state with $\ell = L = 0$ have centrifugal barriers and hence are strongly suppressed. Therefore, the three-pion decay rate is dominated by the s-state. Since the spatial wave function for the s-state is symmetric, the corresponding isospin state must also be symmetric. Thus the symmetric $I = 1,3$ states, which violate CP in K_S^o decays, are favored over the $I = 0,2$ states, which conserve CP in K_S^o decays.

Another reason for suppression of certain isospin states is the $\Delta I = 1/2$ rule, which is thought to hold to a few percent. The $\Delta I = 1/2$ rule allows $I = 0,1$ but forbids $I = 2,3$. Thus the suppression due to centrifugal barriers and to the $\Delta I = 1/2$ rule indicates that the $I = 1$ symmetric s-state is preferred, except for the effect of CP.

Interference between K_S^o and K_L^o occurs in the total rate only if both K_S^o and K_L^o both decay to the same final state, since states with different values of I,ℓ are orthogonal. A nonzero value of $x + iy$ should be attributed

primarily to interference in the dominant I = 1 symmetric s-state, which is CP violating for K_S^o and CP conserving for K_L^o. Thus $x + iy \neq 0$ would imply CP violation. Interference in the I = 0,2 states, which are CP conserving for K_S^o and CP violating for K_L^o, is also possible, but would be too small to observe in this experiment.

Several theoretical estimates have been made of the amount of $K_S^o \to 3\pi$ which might be expected. Lee and Wu [7] suggest that the ratio of amplitudes of CP violating $K_S^o \to 3\pi$ to CP conserving $K_L^o \to 3\pi$ should be of order of magnitude η where $\eta \approx \frac{\alpha}{\pi} \approx \eta_{+-} = \frac{a(K_L^o \to \pi^+\pi^-)}{a(K_S^o \to \pi^+\pi^-)} = 1.96 \times 10^{-3}$ where α is the fine structure constant. They estimate the strength of the $\Delta I = 3/2, 5/2$ amplitudes, $\xi_{3/2}$, $\xi_{5/2}$, to be $\sim \pi\alpha$ of the $\Delta I = 1/2$ amplitude. The centrifugal barrier effects should go as $(kR)^{2\ell}$ where k is the average pion momentum, R is the effective interaction radius, and ℓ is the dipion angular momentum. One factor $(kR)^{\ell}$ is due to the centrifugal barrier of π^+ with respect to π^-, and the other factor $(kR)^{\ell}$ is due to the centrifugal barrier of π^o with respect to the $\pi^+\pi^-$ system. $(kR) \sim 1/3$ if R $\sim$ the pion Compton wavelength. $\ell = 3$ for I = 0 and $\ell = 1$ for I = 2. Using these approximations for the effects of the suppression due to $\Delta I = 1/2$ and centrifugal barriers, Lee and Wu estimate the ratios of the amplitudes for the different isospin states to be:

$$a[K_S^o \to (3\pi)_{I=0}] : a[K_S^o \to (3\pi)_{I=1}] : a[K_S^o \to (3\pi)_{I=2}] :$$
$$a[K_S^o \to (3\pi)_{I=3}] : a[K_L^o \to (3\pi)_{I=1}]$$

$$\approx (kR)^6 : \eta : (kR)^2 \xi_{3/2} : \eta\, \xi_{5/2} : 1$$

$$\approx 10^{-3} : 2 \times 10^{-3} : 2.5 \times 10^{-3} : 5 \times 10^{-5} : 1$$

For the total branching ratio, Lee and Wu estimate

$$\frac{\Gamma(K_S^o \to 3\pi)}{\Gamma(K_L^o \to 3\pi)} \approx |\eta|^2 + |(kR)^2 \xi_{3/2}|^2 \approx 10^{-5}$$

The notation (3π) in these expressions includes $\pi^o\pi^o\pi^o$ as well as $\pi^+\pi^-\pi^o$. Lee and Wu state that their estimated values could conceivably be wrong by several orders of magnitude due to the limited understanding of CP symmetry.

Eliezer and Singer[8] have also estimated the strength of the CP conserving (CPC) $\Delta I = 1/2$ partial rate for $K_S^o \to 3\pi$ using a Hamiltonian constructed phenomenologically from three meson field products. The obtain the ratio

$$\frac{\Gamma[K_S^o \to (3\pi)_{I=0}]_{CPC}}{\Gamma[K_L^o \to (3\pi)]_{CPC}} \approx 10^{-7} - 10^{-6}$$

Glashow has proposed a Hamiltonian model of weak interactions which allows for a large CP violating $K_S^o \to 3\pi$ rate.[9] In this model a modification of the usual current-current weak interaction is employed in which vector and axial-vector currents transform differently under SU(3), yet each transforms like a member of a unitary octet. Glashow's model predicts that $\Gamma(K_S^o \to 3\pi)$ and $\Gamma(K_L^o \to 3\pi)$ may be comparable in magnitude.

Glashow and Weinberg[10] have pointed out that if the magnitude of $(x + iy)$ is near unity, then CPT invariance and $\Delta I \leq 3/2$ require the phase of $(x + iy)$ to be approximately $\pm 90^o$.

This experiment is not sensitive enough to detect the very small amplitudes predicted by Lee and Wu or by Eliezer and Singer. The experiment could expect to observe only a large CP violating $K_S^o \rightarrow \pi^+\pi^-\pi^o$ amplitude in the $I = 1$, $\ell = 0$ state. That is, a K_S^o amplitude an order of magnitude smaller than the K_L^o amplitude could not be resolved due to the limited statistical accuracy of the experiment.

A large value for the $K_S^o \rightarrow \pi^+\pi^-\pi^o$ amplitude can be related to ϵ, the CP violation parameter in the definitions of K_S^o, K_L^o given above. Given a coherent mixture of K^o and $\overline{K}^o$ at time t

$$\Psi(t) = a(t)|K^o\rangle + b(t)|\overline{K}^o\rangle \quad ,$$

the evolution of the system is given by the equation [3]

$$-\frac{d\Psi(t)}{dt} = (\Gamma + iM)\Psi(t)$$

where Γ and M are (2 x 2) Hermiteam matrices, generally termed the decay matrix and the mass matrix. [3] ϵ may be written in terms of elements of Γ and M as follows, neglecting terms of order ϵ^2: [3]

$$\epsilon = \frac{\Gamma_{12} - \Gamma^*_{12} + i(M_{12} - M^*_{12})}{(\gamma_S - \gamma_L) + 2i(M_S - M_L)}$$

Under the assumption of a large, direct, CP-violating amplitude for $K_S^o \rightarrow \pi^+\pi^-\pi^o$, occurring primarily in the state with $I = 1$, $\ell = 0$, Haggerty has shown [5] that the contribution of decays to ϵ is

$$\epsilon_{3\pi} \approx 2y\ (1-i)(10^{-4}) \ .$$

When the data of this experiment are fit by the method of maximum likelihood, as discussed later, two maxima are found with the following values of x, y:

$$x = -0.09 \pm 0.19, \quad y = +0.56 \pm 0.43$$

$$x = -2.94 \pm 0.36, \quad y = -0.10 \pm 0.55$$

The second result is statistically preferred by two standard deviations over the first. However, such a large magnitude for x is not only theoretically very unlikely because it would imply a large violation of the $\Delta I = 1/2$ rule or CPT, but this particular value is also ruled out by other experiments using $\overline{K}^0$ initial states. Therefore, we place more credence upon the first result.

II. EXPERIMENTAL DETAILS

The experiment was performed in the 17° beam line at the Argonne National Laboratory Zero Gradient Synchrotron using optical spark chambers and scintillation counters. The apparatus was designed to be sensitive to the following sequence of reactions.

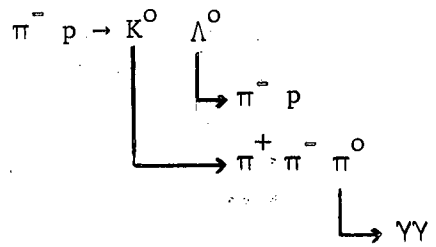

Detection of two charged particles from K^o decay and one from Λ^o decay were required. The π^+ and π^- from the K^o decay were momentum analyzed in a 10 kG magnetic field in order to reconstruct the decay. During scanning, one gamma ray from the π^o decay was required to shower in heavy plate spark chambers downstream of the magnet.

A. The Beam

A schematic drawing of the 17° beam line is shown in Figure 3 . Circulating protons in the Z.G.S. struck an internal beryllium target. A secondary beam of 3 GeV/c negative particles was directed down the 17° line and focused onto our target by a system of two bending magnets, three quadrupole doublets, and a collimating slit. A detailed description of the beam optics is given elsewhere.[11] Included in the beam line were two CO_2 threshold Čerenkov counters, which are discussed in the next section. The beam intensity was regulated by adjusting the width of the collimating slit

BEAM TRANSPORT SYSTEM
ARGONNE ZGS EXPERIMENT E-155

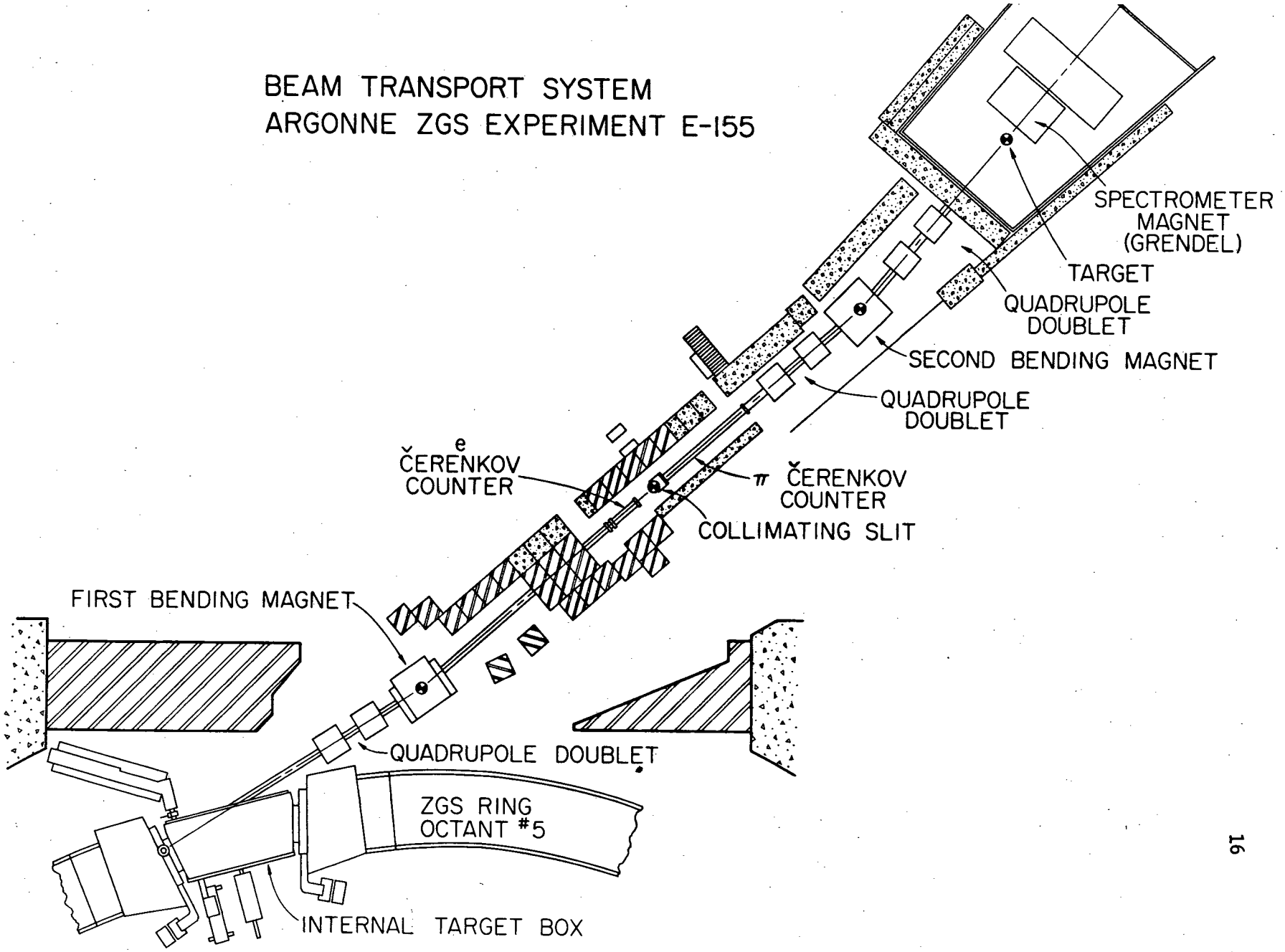

to allow approximately 200,000 negative pions per accelerator pulse to reach the apparatus. The beam spill was spread over a 450 msec. flattop. The period between the start of successive beam pulses was about 2.5 seconds. At the final focus of the 17° line the beam particles struck a cylindrical target, 3 cm. long and .875 inch in diameter, made of dense carbon (2.2 gm/cc).

B. Experimental Arrangement

The arrangement of the spark chambers and scintillation counters is shown in Figure 4 . There were six sets of spark chambers designated π chamber, Λ chamber, K chamber, K' chamber, magnet chambers, and shower chambers. There were two Čerenkov counters, $\check{C}_{\pi}$ and $\check{C}_{e}$; four beam defining counters, π_1, π_2, π_3, and A; and three counter hodoscopes, $\lambda dE/dx$, ϕ, and ρ.

The incident beam particle was identified as a π^- by signals from the CO_2 threshold Čerenkov counters, $\check{C}_{\pi}$ and $\check{C}_{e}$. The upstream counter, $\check{C}_{e}$, was set to veto beam electrons. The downstream counter, $\check{C}_{\pi}$, was set to accept pions but reject heavier particles. The beam pion was required to give a pulse in π_1, π_2, and π_3 before entering the carbon target. The anticoincidence counter A, located immediately downstream of the target, ensured that only neutral particles emerged from the target.

Decay of the Λ was signaled by a pulse from one of the $\lambda dE/dx$ hodoscope counters. This hodoscope was a circular array of eight triangular counters centered on the beam line. The diameter of the array was 19.75 inches and the thickness of the counters 1/8 inch. A 3/4 inch hole in the center of the array allowed beam particles to pass through without hitting the counters. The $\lambda dE/dx$ hodoscope was designed to be triggered by the slow proton (or pion) from Λ decay but not by the more energetic charged particles

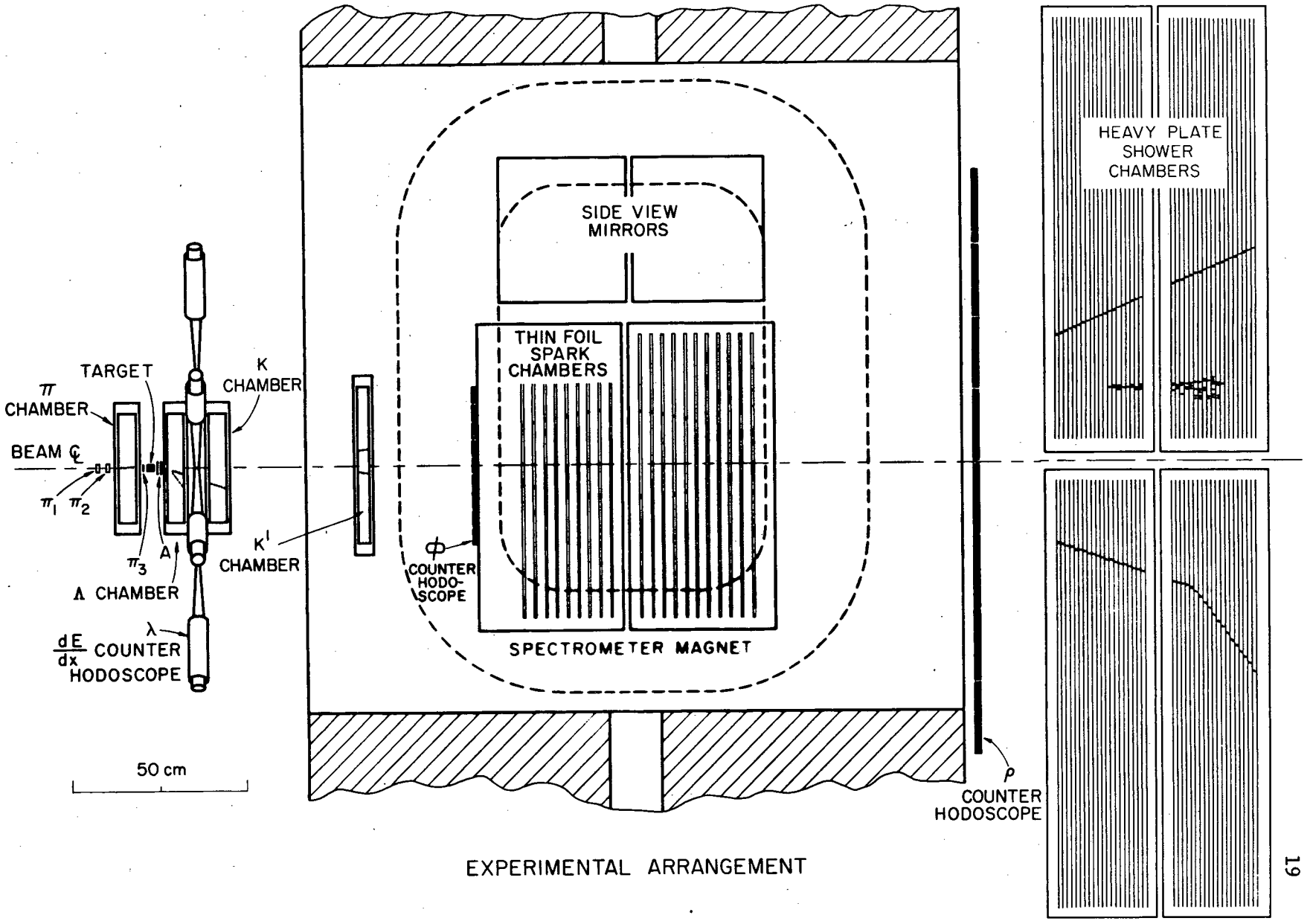

EXPERIMENTAL ARRANGEMENT

produced in K^O decay. To achieve this, the discriminator levels for the hodoscope counters were set to trigger on 550 MeV/c protons hitting the counters straight on. Particles producing a smaller pulse than a 550 MeV/c proton would not trigger the array.

The rationale behind the $\lambda dE/dx$ hodoscope is further explained as follows. The lambda from associated production is peaked backward in the production rest frame. In the laboratory frame it is typically emitted with an angle of about 40^O and a kinetic energy of a few hundred MeV. Due to its low energy and short lifetime, the lambda generally decays in the region before the hodoscope (2/3 of the time to the charged mode $\pi^- p$). The proton and/or pion from lambda decay is generally about twice minimum ionizing and can trigger the hodoscope by dE/dx. The K^O, on the other hand, is strongly peaked forward in both the production rest frame and the laboratory frame and is emitted with a lab kinetic energy of about 2.2 GeV. If it decays upstream of the hodoscope, its decay products are usually too energetic to cause a large enough pulse in the $\lambda dE/dx$ counters to trigger the hodoscope. In some events, the K^O decay products both pass through the same $\lambda dE/dx$ counter and thus deposit enough energy to trigger the counter. Events of this type were eliminated during scanning. The Monte Carlo calculations, described later, show that lower energy K^O's and $\overline{K}^O$'s from the three-body production processes $\pi^- p \rightarrow K^O \Lambda \pi^O$ and $\pi^- p \rightarrow K^O \overline{K}^O n$ do not trigger the hodoscope.

The decay volume for the K^O was the region between the anticounter A and the ϕ hodoscope. K^O decays were signaled by pulses from the ϕ and ρ hodoscopes, which were two vertical arrays of counters located before and after the 10 kG magnetic field region. Two signals in coincidence from each of these hodoscopes were required in order to ensure two charged particles

entering and two leaving the magnet. The ϕ hodoscope consisted of nine scintillators, each 12 inches high by 2 inches wide by 1/8 inch thick. The ρ hodoscope contained eight scintillators, each with dimensions 24 inches high by 8 inches wide by 1/8 inch thick.

All counters were fabricated from Pilot B scintillator.* RCA 8575 photomultiplier tubes with bialkali photocathodes were used for the $\lambda dE/dx$ counters. RCA 7746 and RCA 6810 photomultiplier tubes were employed for the other counters. As protection from the fringing field of the magnet, all tubes were surrounded by cylindrical magnetic shields composed of Netic, Co-netic,** and soft iron. This precaution was taken to minimize any dependence of pulse height on the magnetic field. With no shielding, the pulse heights from photomultiplier tubes in the fringing field showed pronounced dependence on the magnetic field strength. For a given counter, differences of as much as 40% were observed between pulse height with field on and pulse height with field off. With the shielding in place, the greatest difference observed was about 5% for the ϕ and ρ counters. The $\lambda dE/dx$ counter pulse heights showed negligible change between field-on and field-off runs with shields in place.

C. Triggering

Pulses from the scintillation counters were fed into Illinois and EG&G logic modules. A schematic diagram of the triggering logic is shown in

---

*Pilot B is a trade name for plastic scintillation material manufactured by Pilot Chemicals Inc.

**Netic and Co-netic are trade names for magnetic shielding materials manufactured by Magnetic Shields Division, Perfection Mica Co.

Figure 5 . A desirable event was one in which one charged pion entered the target, no charged particles emerged from the target, one heavily ionizing particle passed through a $\lambda dE/dx$ counter, and two charged particles traversed the magnetic field region. The final coincidence which signaled this type of event was:

$$\check{C}_{\pi}\check{C}_{e}\pi_1\pi_2\pi_3\bar{A}\ (\lambda dE/dx)(2\phi)(2\rho)$$

When this coincidence occurred, high voltage pulses were applied to fire the spark chambers and the event was recorded on film.

D. Spark Chambers

The trajectories of the charged particles for each event were recorded using optical spark chambers. In the drawing of the apparatus, Figure 4 , the spark chambers are shown with typical tracks sketched.

Four small thin foil chambers located upstream of the magnetic field region recorded the early stages of each event. Figures 6 and 7 show the upstream spark chambers and counters. The incoming beam track was seen in the π chamber. Eigher one or two tracks from the lambda decay were seen in the Λ and K chambers. The start of the two charged tracks from K^{o} decay was recorded in the Λ, K, and K' chambers. The π, Λ, and K chambers were identical six-gap chambers. The foils in these three chambers were 1 mil aluminum, 12.75 by 12.75 inches. The distance between the centers of adjacent gaps was 5/16 inch. The K' chamber had four gaps with 3/8 inch spacing between the centers of adjacent gaps. The K' foils were also 1 mil aluminum.

Figure 5. Triggering logic.

TRIGGERING LOGIC

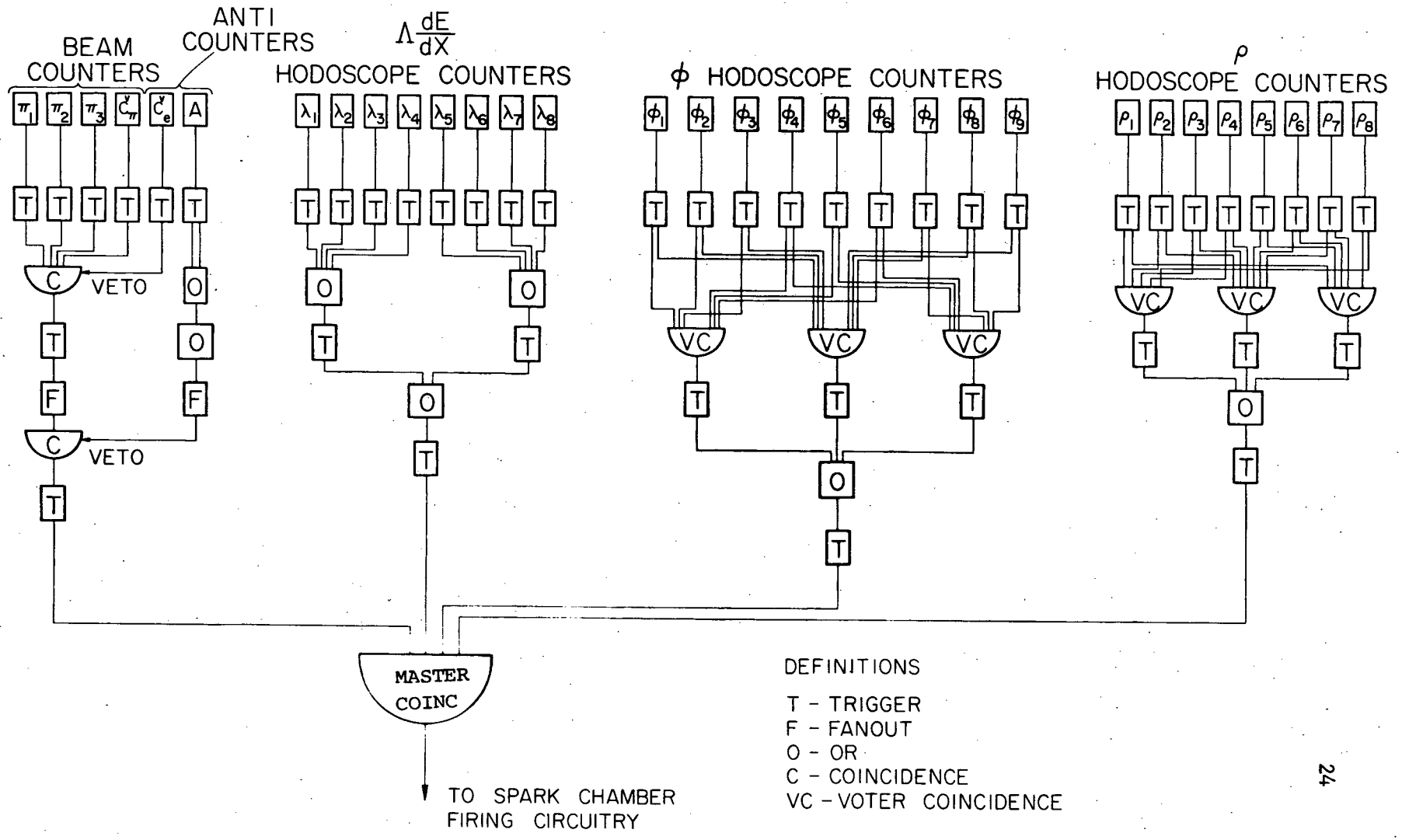

Figure 6. Upstream spark chambers and counters seen from above. Shown in the photograph are the beam defining counters, anticoincidence counter, π chamber, Λ chamber, $\lambda dE/dx$ hodoscope. "Grendel" is the spectrometer magnet.

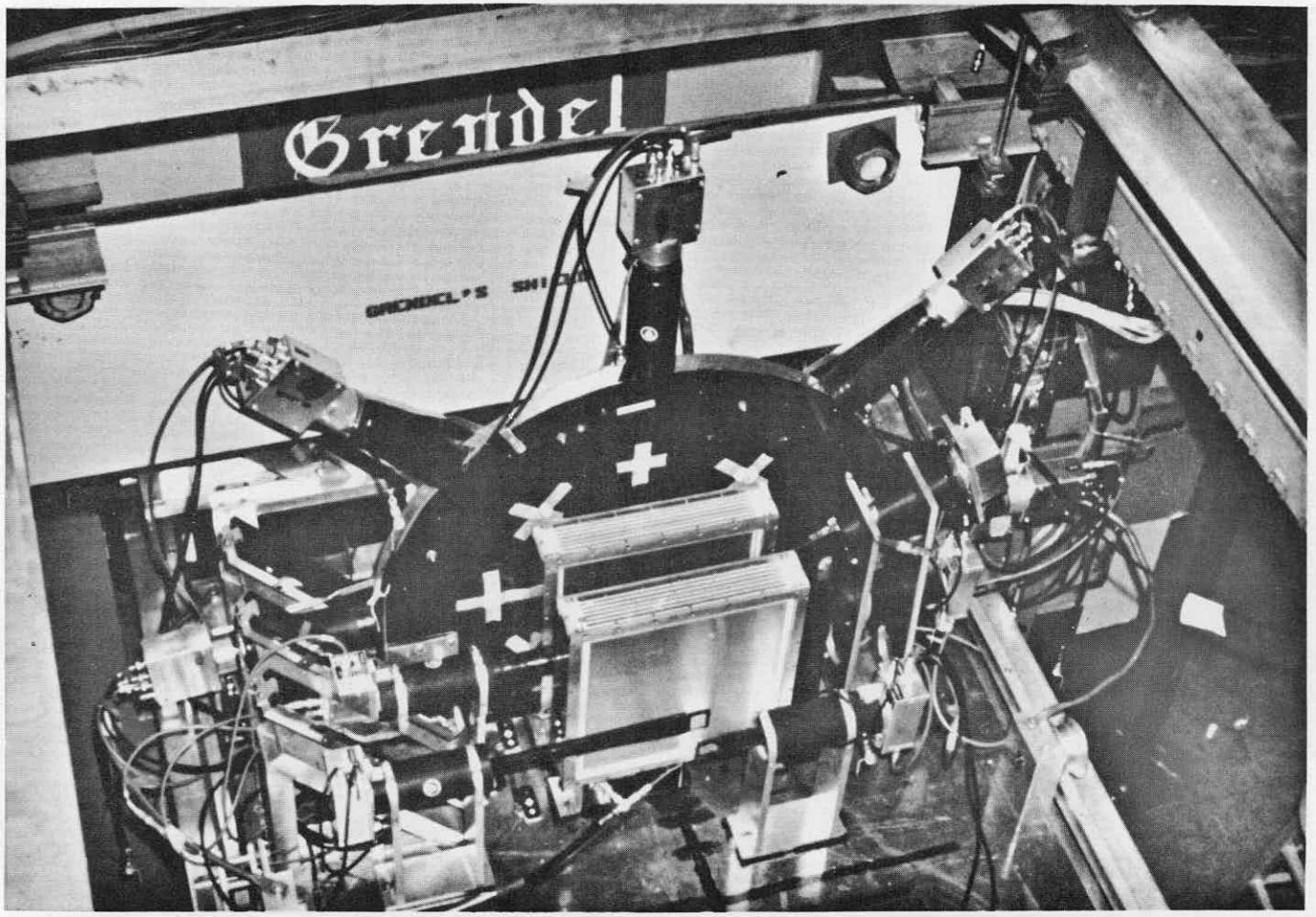
Grendel

Figure 7. Upstream spark chambers and counters seen from the side.

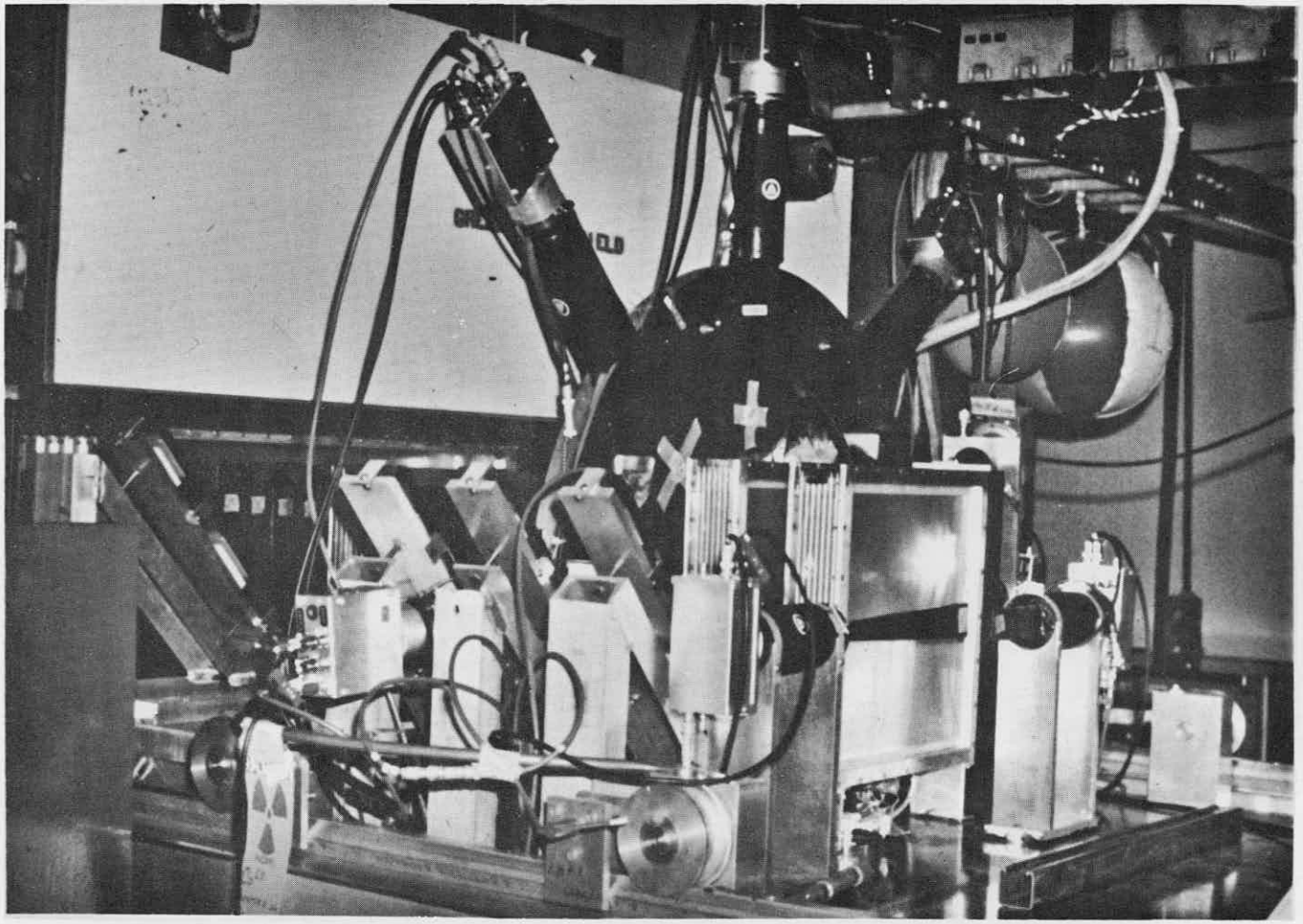

The magnet chambers, shown in Figures 8 and 9 , were thin foil chambers located within the 18 inch high gap of the magnet and viewed through slots in the upper pole piece. These chambers were used to measure the curvature of the track in the 10 kG magnetic field in order to determine the momenta of the charged particles. The chambers contained 20 visible gaps, each 1/4 inch wide, with a distance of 25.4 inches between the centers of the first and last gaps. The foils were 1 mil aluminum with dimensions 14.5 by 31.2 inches.

The π, Λ, K, K', and magnet chambers were mounted on wheeled transport plates which could be rolled upstream on hexagonal transport rails for servicing. During the data taking, both transport plates were securely clamped in place.

Downstream of the magnet were four heavy plate shower chambers, shown in Figure 10. These were used to identify and differentiate between pion, electron, and photon tracks by observation of their interactions and showering in the plates. Each shower chamber contained twenty-one plates, with dimensions 3 feet by 4 feet by 1/8 inch. The plates were alternately aluminum and stainless steel. Every third plate in a given chamber, starting with the second plate, was stainless steel. Lead, 3/16 inch thick, was placed between the upstream and downstream chambers to enhance the showering of electrons and photons. The chambers contained a total of 4.4 radiation lengths of material.

E. Photography

All spark chambers were viewed in 90° stereo using a system of mirrors. Two cameras recorded the spark chamber tracks for each trigger.

Figure 8. The magnet chambers.

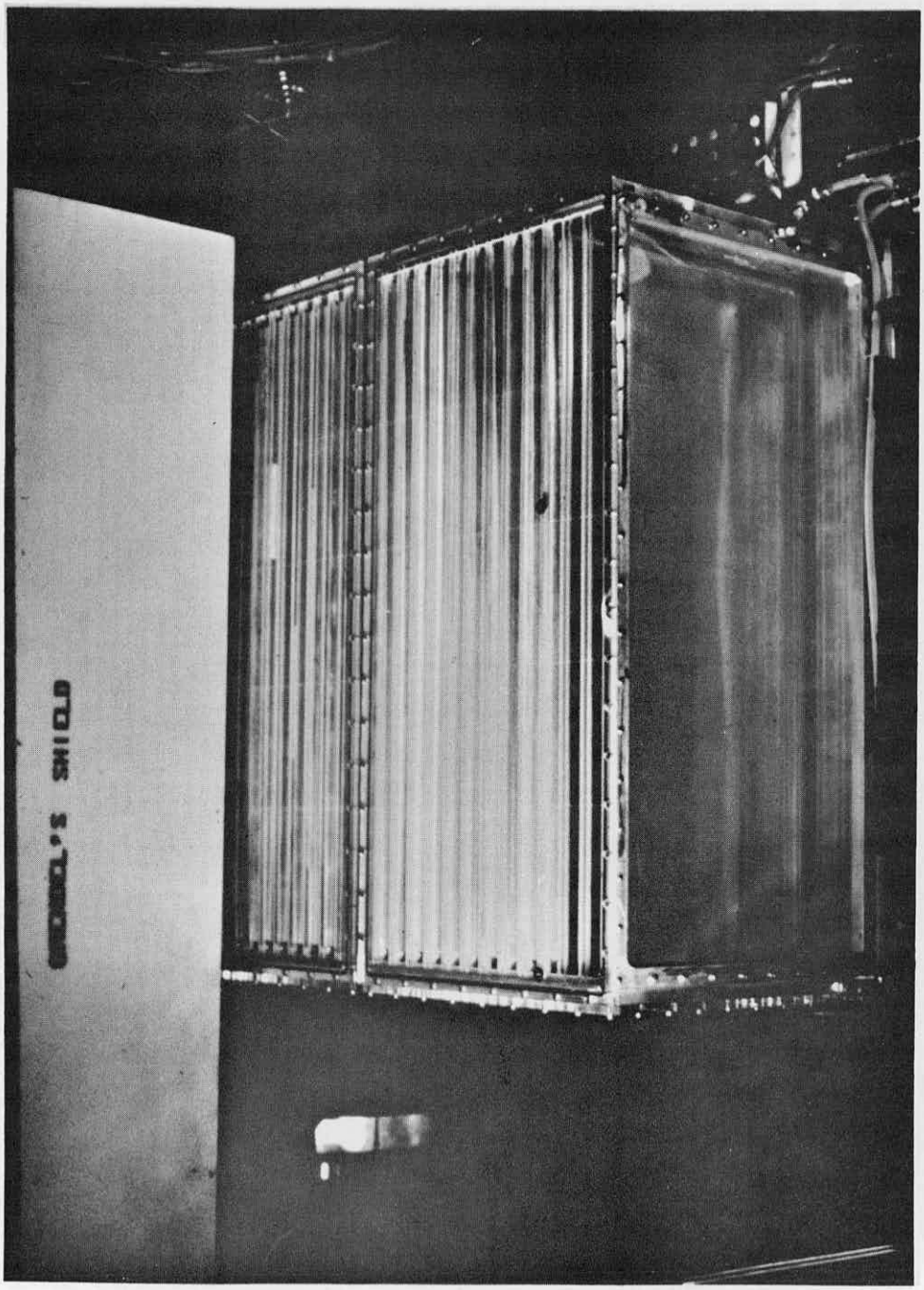
GOMEL'S SHIELD

Figure 9. The magnet chambers seen from the side, partially rolled out of the magnet. At left are the π and Λ chambers.

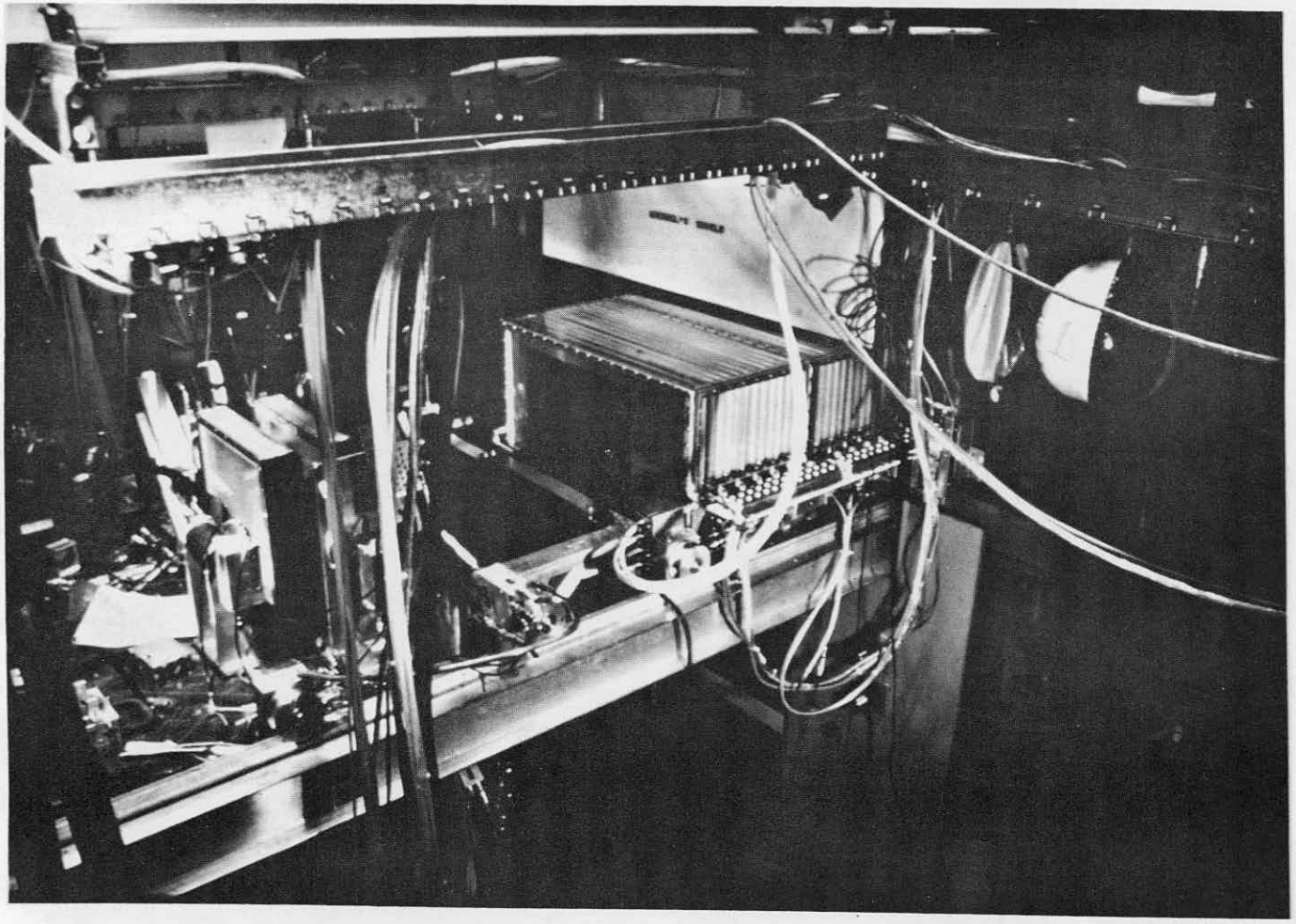

Figure 10. The four heavy plate shower chambers and some of the associated mirrors.

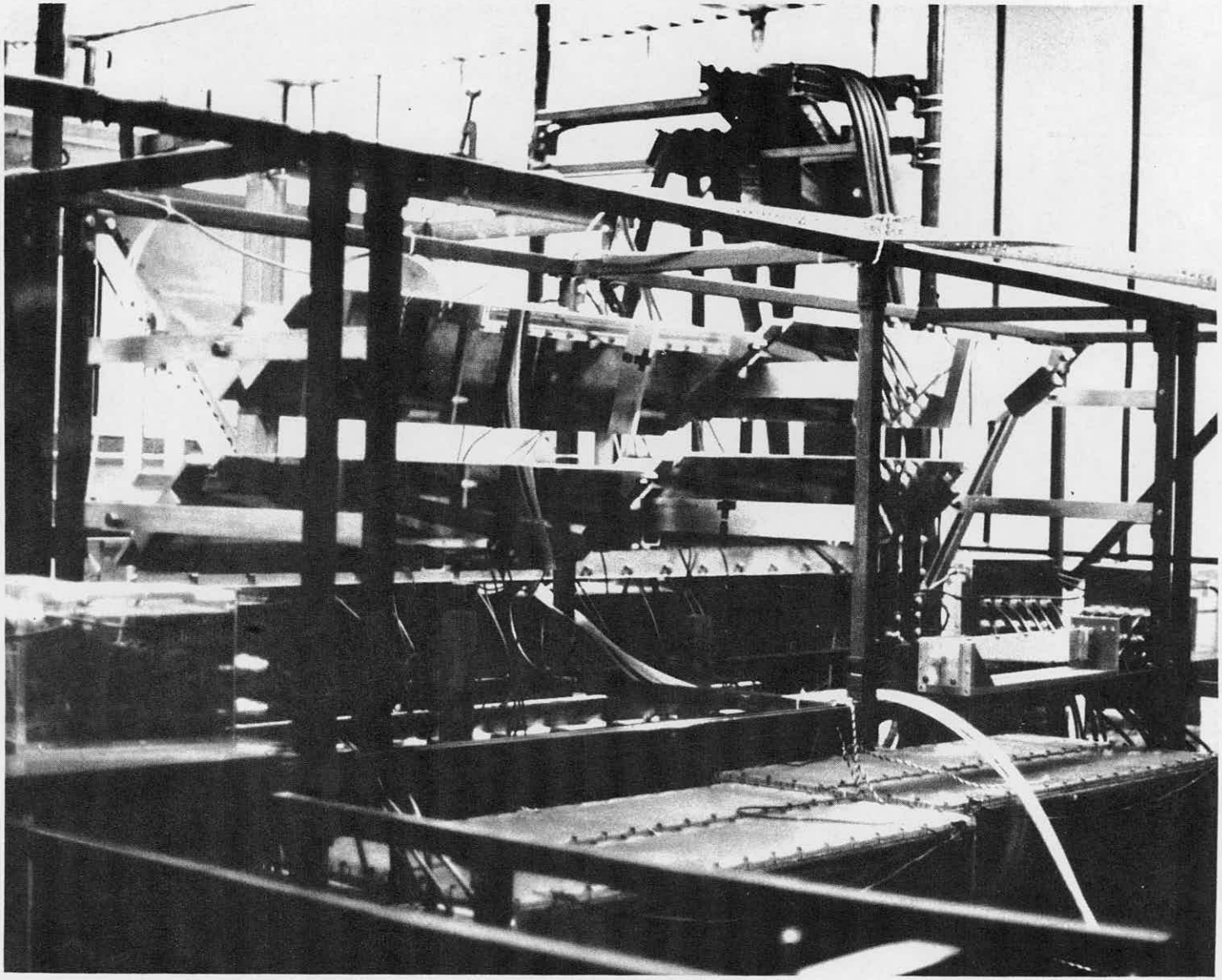

One camera photographed the π, Λ, K, K', and magnet chambers, and the other photographed the shower chambers. In addition to the spark chamber tracks, the cameras photographed arrays of neon lights which were flashed with each trigger to indicate the frame and roll numbers as well as which counters fired.

Figure 11 shows the two frames from a $K^{o}_{\pi 3}$ event. In the lower frame, which shows the upstream chambers, the top views are on the right and the side views on the left. In the π chamber, one incoming beam track is seen. The Λ chamber shows the two tracks from Λ decay, one of which continues into the K chamber. The vertex for the K^{o} decay is seen in the K chamber. The two π tracks from K^{o} decay continue through the K' chamber and the magnetic chambers, where their curvature due to the magnetic field can be seen. Between the π and Λ chambers are the binary frame and roll number lights and the counter lights. The paired circle and cross which appear in various positions on the frame are fiducials. These fiducials were electroluminescent panels which were mounted on each spark chamber and flashed each time the spark chambers fired.

The upper frame shows the shower chamber tracks. The top views appear in the upper half of the frame, and the side views in the lower right and left. Right and left in the picture correspond to beam right and beam left respectively. One of the π tracks passes through the shower chambers undeflected, while the other indicates a scatter between the front and rear chambers. The photon shower, which originates in the lead plates between front and rear chambers, appears between the two π tracks in the top view and on the right in the side view. Lighter marks parallel to the π tracks are reflections. These sometimes appear in the shower chamber pictures but

Figure 11. A $K^{o}_{\pi 3}$ event.

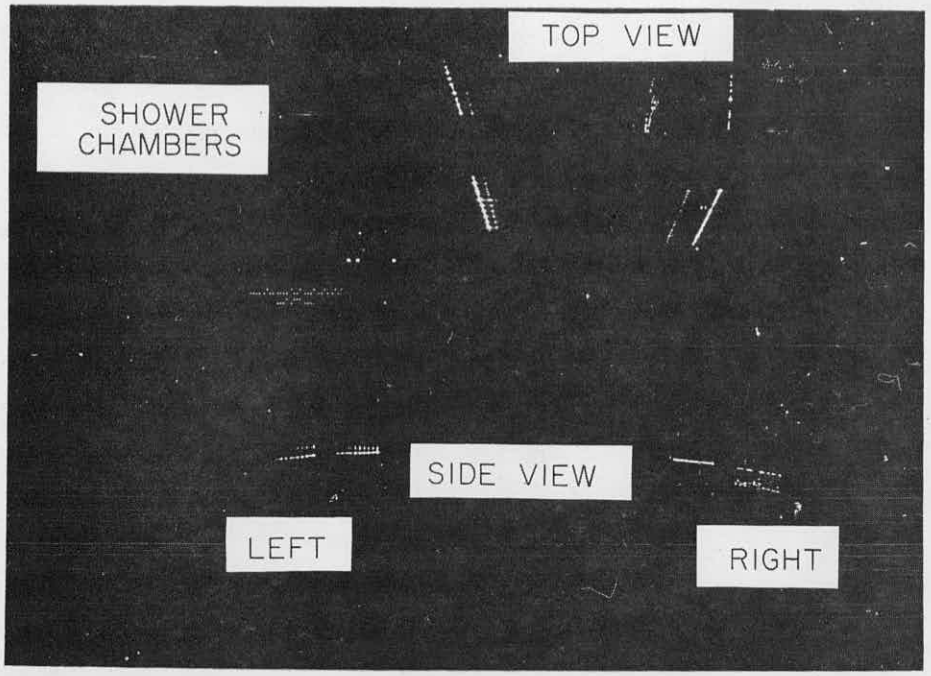

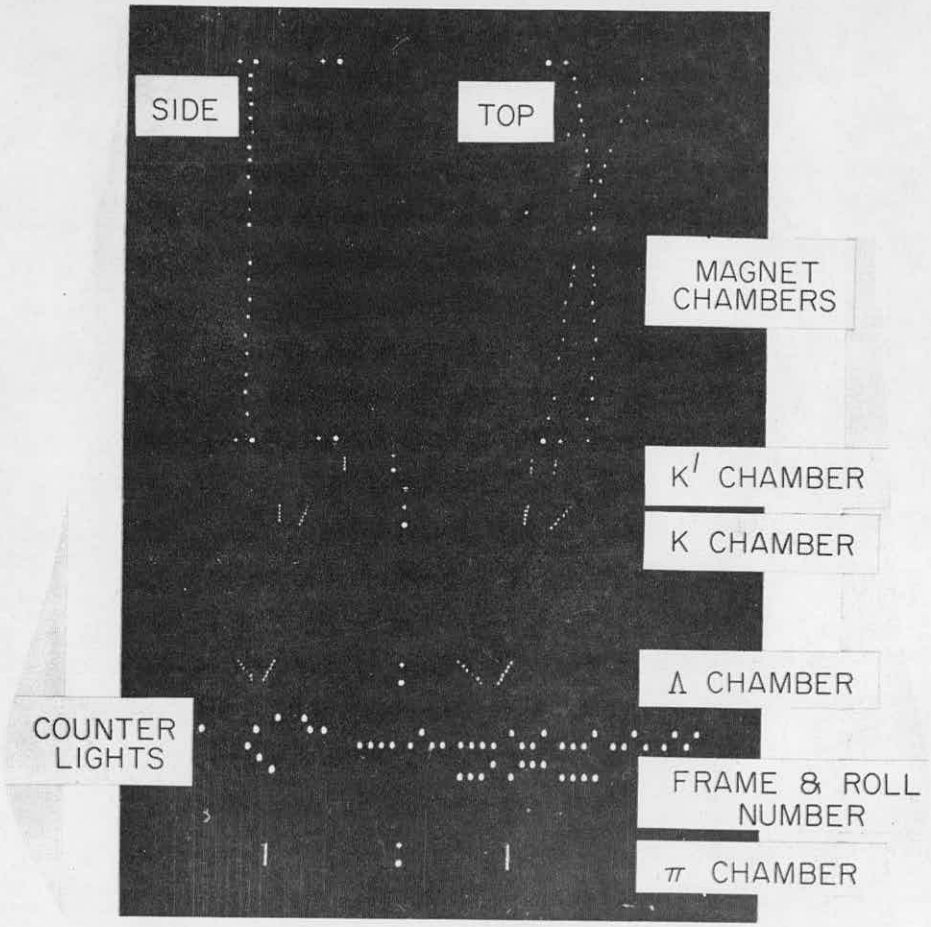

TYPICAL EVENT
$K^{o} \rightarrow \pi^{+} \pi^{-} \pi^{o}$

are easy to recognize and therefore cause little difficulty. The binary lights and ρ counter lights appear in the center left portion of the frame.

159 retroreflective fiducial crosses were permanently mounted on the lower magnet polepiece and on the right wall of the magnet yoke. When the transport plates were rolled forward, these fiducials could be viewed through the magnet chamber optics. Calibration photographs of these fiducial crosses were made periodically to ensure that the magnet chamber optics remained stationary. The crosses were illuminated by flashing an annular flash lamp which was mounted surrounding the upstream camera lens. This same set of fiducials allowed optical corrections to be made for distortions in the mirrors.

The cameras were fast cycling Flight Research cameras. 35 mm. Kodak 2479 RAR film was used throughout most of the experiment.

F. Experimental Procedure

To avoid any bias associated with the magnetic field direction, the polarity of the spectrometer magnet was reversed periodically. The current in the magnet coils was monitored continuously to prevent variation of the field strength by more than a few hundredths of a per cent.

Rates of all counters and of various coincidence circuits were checked frequently in order to detect and correct for any anomalies. Tube voltages and discriminator settings were adjusted and logic circuits replaced as needed to ensure reproducible performance. Particular attention was paid to the λdE/dx counters. A 0.1 microcurie Co^{60} source was permanently mounted on each of these counters so that frequent calibrations could be conveniently carried out.

Numerous experimental settings were checked hourly and adjusted when necessary, for example spark gap high voltages, spark chamber clearing fields, Čerenkov counter pressures.

At the end of each roll of film a test strip was developed and examined in order to note and correct for any changes in spark chamber or camera performance.

III. EVENT SELECTION

Figure 12 shows a flow diagram of the stages in the selection of $K^o_{\pi 3}$ events. Table 2 lists the rejection criteria which were applied to the data, as described in the following sections.

A. Photon Scan

A total of 467,900 pairs of spark chamber photographs were taken during the experiment.

The first step in the selection of $K^o_{\pi 3}$ candidates was the scanning of the shower chamber film for photon showers. In this scan any track starting farther downstream than the fifth gap of the shower chambers and having at least five sparks was called a photon. The scanners were instructed to be very liberal in their selection of possible photon tracks. Any frame with the slightest possibility of having a photon track was to be considered a $K^o_{\pi 3}$ candidate at this stage of the analysis.

A total of 32,000 frames were selected in the photon scan.

B. Chloe Measurement

For all events selected in the photon scan, the magnet film (which included the π, Λ, K, K', and magnet chambers) was digitized on the CHLOE flying spot digitizer at Argonne.[12] This machine, controlled by an ASI 210 computer, measured the locations of all marks of sufficient brightness within specified regions on the film. CHLOE measured the spark chamber tracks as well as the binary coded frame numbers, counter lights and fiducials. In addition to the location of the centroid of each mark, CHLOE measured the area of the mark and the number of scan lines it included. This information was recorded on magnetic tapes.

Figure 12. Event selection flow diagram.

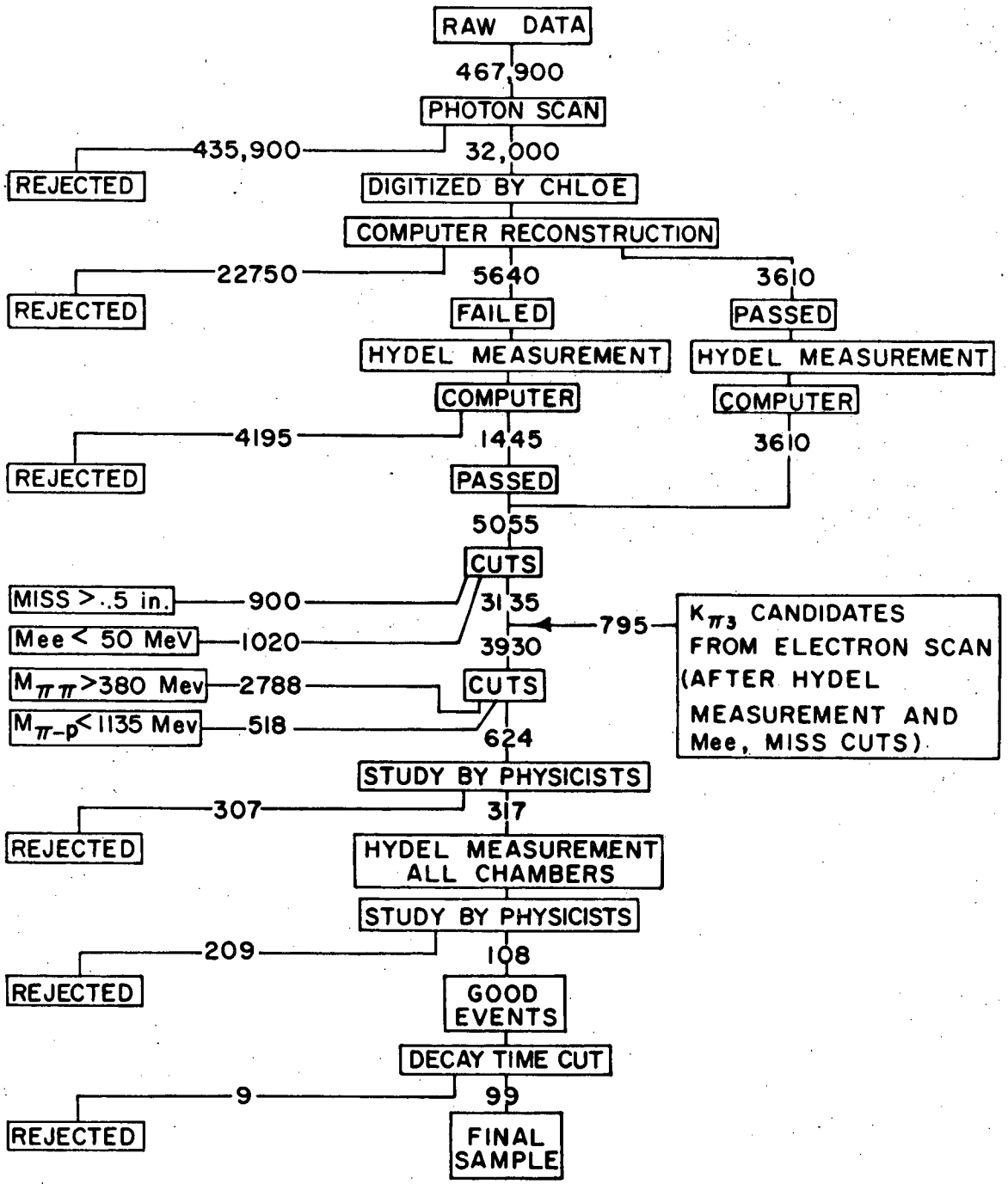
RAW DATA
467,900
PHOTON SCAN
435,900
REJECTED
32,000
DIGITIZED BY CHLOE
COMPUTER RECONSTRUCTION
22750
REJECTED
5640
FAILED
3610
PASSED
HYDEL MEASUREMENT
COMPUTER
HYDEL MEASUREMENT
COMPUTER
4195
REJECTED
1445
PASSED
3610
5055
CUTS
MISS >.5 in.
900
Mee < 50 MeV
1020
3135
795
$K_{\pi 3}$ CANDIDATES FROM ELECTRON SCAN (AFTER HYDEL MEASUREMENT AND Mee, MISS CUTS)
3930
$M_{\pi\pi}$ >380 Mev
2788
$M_{\pi-p}$ <1135 Mev
518
CUTS
624
STUDY BY PHYSICISTS
307
REJECTED
317
HYDEL MEASUREMENT ALL CHAMBERS
STUDY BY PHYSICISTS
209
REJECTED
108
GOOD EVENTS
DECAY TIME CUT
9
REJECTED
99
FINAL SAMPLE

Table 2

Summary of Rejection Criteria

1) Less than two good magnet tracks with opposite curvature

2) Hits

3) No intersection within fiducial volume

4) Momentum > 2500 MeV/c for either track

5) Miss > .500 inch

6) $M_{ee} < 50$ MeV

7) $M_{\pi\pi\pi} > 362.78$ MeV

8) $M_{\pi^- p} < 1135$ MeV

9) No photon

10) Shower chamber tracks not correlated with magnet chamber tracks or not pion tracks

11) Fakes

12) Incorrect counter lights

13) No lambda

14) Scatter before end of magnet chambers

15) Energy cuts: $\gamma_k < 3.000$ or $\gamma_k > 6.100$

16) Decay vertex before Λ chamber

17) Outside Dalitz plot

18) $t_K > 6.5$

C. Computer Reconstruction of Event

Information from the CHLOE tapes was analyzed using programs written for the IBM 360 50/75 computer. First the spark and fiducial locations were transformed to real space coordinates. A pattern recognition program attempted to organize the sparks into tracks. Only the tracks in the π and magnet chambers were used at this stage of the analysis. The momenta of all tracks passing through the field region were calculated by a least squares method with the aid of a table of measured magnetic field values. For each pair of magnet tracks having opposite curvature, the point of closest approach was calculated. This point was taken as the decay vertex for the two charged particles associated with the tracks. The production point for the decaying particle was taken to be the intersection of one of the π chamber tracks with the midplane of the target. Using the calculated momenta, decay point, and production point for each pair of magnet tracks, the complete kinematics of the event was calculated assuming several hypotheses for the decay.

D. Physicist Scan of Computer Output

The output of the CHLOE programs was scanned rapidly by physicists to eliminate obviously bad events and to determine which frames should be remeasured. Frames were rejected for any of the following reasons:

1) There were not two magnet tracks with opposite curvature.
2) Hits. Events were rejected if either magnet track hit any part of the magnet chambers or the magnet itself. To determine which tracks hit obstacles, a computer program stepped the tracks downstream through the field and checked for hits.
3) The computer programs could not find an intersection point for the two tracks within the fiducial volume.

4) The calculated momentum of either track was greater than 2500 MeV/c. This condition eliminated beam tracks, which sometimes appeared in the pictures. Such tracks entered the apparatus after the trigger but before the spark chambers fired.

A total of 22,750 events were summarily rejected as a result of these conditions.

E. HYDEL Measurement

5640 events which failed the pattern recognition program or which appeared to need a better measurement were remeasured on a manually operated HYDEL object plane digitizer at the University of Illinois. The HYDEL is a slower but more accurate measuring device than CHLOE. To save measuring time, only the π and magnet chambers were measured at this stage. The remeasured events were then reprocessed on the computer and examined by physicists in the manner just described. 1445 of these events survived.

In addition, 3610 events which had passed the CHLOE measurement and computer reconstruction were remeasured on the HYDEL. This was done to ensure greater consistency of measurement for all events.

5055 events were found to be acceptable at this point.

F. Kinematical Cuts

Two kinematical cuts were now applied to the data. Events were rejected for the following reasons:

5) Miss > .500 inch, where the miss is the distance of closest approach of the two magnet tracks when they are extrapolated upstream of the field region.

6) $M_{ee} < 50$ MeV, where M_{ee} is the invariant mass of the two charged particles assuming they are an electron-positron pair. This cut eliminated most of the triggers due to photon conversions upstream of the magnet chambers.

After these cuts the sample contained 3135 events.

G. Addition of Events from Electron Scan

At this point another class of $K^o_{\pi 3}$ candidates was added to the sample. In a companion experiment to test the validity of the $\Delta S = \Delta Q$ selection rule in K^o_{e3} decays[13], the same shower chamber film had been scanned for electron showers. Physicists analyzing the electron frames for K^o_{e3} candidates noted that in some cases the scanners had mistaken photon showers for electron showers. In addition, the electron scan showed that a substantial number of photon showers had not been selected in the photon scan due to the requirement that photon showers originate later than gap five of the shower chambers. Many of these had been called electrons during the electron scan. It was decided to study all events having photons which materialized later than gap one of the shower chambers. All such events not found during the photon scan but later identified by physicists studying the electron scan were now considered as possible $K^o_{\pi 3}$ candidates. These events had been measured in the same manner as the events from the photon scan and processed with the same computer programs. They were subjected to the same six rejection criteria already described. There were 795 events in this category. After these had been added, the total number of events remaining in the sample was 3930.

H. $M_{\pi\pi}$ and M_{π^-p} Cuts

Two additional kinematical cuts were now applied to the sample:

7) $M_{\pi\pi} > 380$ MeV, where $M_{\pi\pi}$ is the invariant mass of the two charged particles assuming both are pions. (The kinematic limit for $K_{\pi 3}$ is M = 362.78 MeV.)

8) $M_{\pi^-p} < 1135$, where M_{π^-p} is the invariant mass assuming the positive particle is a proton and the negative particle a pion. This cut was made to rid the sample of triggers due to $\Lambda \rightarrow \pi^- p$.

I. Physicist Study of Spark Chamber Photographs

Physicists now made a careful study of the spark chamber photographs for the 624 events which remained in the $K^o_{\pi 3}$ sample. Events were rejected for any of the following reasons:

9) No good photon track. The photon had to materialize later than gap one of the shower chambers, show evidence of showering, and have a direction consistent with the calculated decay point of the K^o.

10) Lack of correlation between "pion" tracks in the shower chambers and the tracks in the magnet chambers. The computer programs predicted where the extrapolated magnet chamber tracks should appear in the shower chambers. We required pion-like tracks to appear near these locations. To aid in distinguishing pions from electrons in the shower chambers, a series of calibration photographs of pion and electron tracks of various momenta had been taken during a special run. With the aid of these calibration photos, all tracks which showed evidence of showering

were carefully examined to determine whether they might be electrons rather than pions. Typically, electrons could be clearly identified by their showering in the shower chambers. Pions would generally do one of the following things: pass through the shower chambers undeflected, pass through with a single scatter, interact in the plates producing several new tracks at large angles to the original track, come to rest in the plates. For low momentum tracks (<500 MeV/c) electron showers were occasionally not well developed, and careful examination was necessary to distinguish them from pions. In addition, pions would occasionally charge exchange by $\pi^- p \rightarrow \pi^o n$ or $\pi^+ n \rightarrow \pi^o p$ followed by $\pi^o \rightarrow \gamma\gamma$. The photons from the π^o decay would then convert in the plates and shower. Study of the calibration pictures was very useful in distinguishing such pion charge exchange tracks from electron or photon showers. In a few frames, one pion passed through the gap between the left and right shower chambers and was not observed in the chambers. Such events were accepted if the computer programs indicated that the corresponding magnet track should extrapolate into the gap.

11) Fake events. Fakes were events in which the two magnet tracks could not have come from the same point. Fake events were detected by careful examination of the spark chamber photographs and the computer output. They would usually have large misses. Often their calculated decay point locations would

differ from the "vertex" locations seen in the upstream spark chambers. A particularly prevalent type of fake event was the following. Two vees were seen in the upstream spark chambers. One track from each vee passed through the magnet chambers, and the other two tracks left the fiducial region upstream of the magnet.

12) Incorrect counter lights. The counter lights were examined to ascertain whether the counters involved in the trigger were the ones struck by the particles. A computer program extrapolated the magnet tracks to determine which ϕ and ρ counters the particles should have passed through.

13) No evidence for a lambda. A $\Lambda \rightarrow \pi^- p$ decay appeared as either a single track or a vee in the Λ and/or K chambers. The single-track lambdas occurred when the angle between the two lambda decay particles was very small or when the second decay particle was emitted backwards in the laboratory. The lambda counter lights were examined to be sure that one of the tracks considered to be from lambda decay hit the λdE/dx counter involved in the trigger.

14) Scatter before end of magnet chambers. For a small number of events, one of the tracks made a small angle scatter. Since this could cause error in the determination of the momentum and of the decay point location, these events were discarded.

Only clearly bad events were rejected at this stage of the analysis. All questionable events were retained for remeasurement and further study. 317 events remained in the sample.

J. Complete HYDEL Measurement

Thus far, to save measuring time, only the tracks in the π and magnet chambers had been measured. All candidates remaining in the sample were now remeasured on the HYDEL. This time the Λ, K, and K' tracks were measured as well as the π and magnet tracks. An extended version of the analysis programs incorporating the front chamber tracks was used. This enabled more accurate calculation of the decay point locations for early decays.

The spark chamber photographs and new computer output were re-examined by physicists. In addition to the rejection criteria already described, events were now discarded for any of the following reasons:

15) $\gamma_K < 3.000$ or $\gamma_K > 6.100$ where γ_K is the calculated laboratory energy of the K^o in units of the K^o mass.

16) Intersection point before first foil of Λ chamber. Events having decay points before the Λ chamber were very difficult to interpret. For example, if both the K^o and the lambda decayed before the Λ chamber, there could be four Λ chamber tracks, any two of which could continue on through the magnet. It was sometimes impossible to distinguish fake events of this type since all four tracks would appear to originate at roughly the same location prior to the Λ chamber. To avoid fakes of this sort, no decays before the lambda chamber were accepted.

17) Outside Dalitz plot. All events were required to be either within the Dalitz plot boundary or not further outside than 15 MeV.

Condition 7) was now made more restrictive:

7) $M_{\pi\pi\pi} > 362.78$ MeV. This cut had earlier been 380 MeV to ensure that good events were not discarded due to small measuring errors.

After these cuts, 108 events remained as $K^o_{\pi 3}$ candidates. All of these events had been measured at least twice on the HYDEL. A few were measured a third time to be certain that no good events were eliminated because of measuring errors.

Table 3 summarizes the numbers of events rejected and the reasons for rejection during the studies by physicists described in this section and the last section.

K. Cut on Decay Time

Before the final likelihood fit, a cut on proper decay time of the K^o was made. 9 events were discarded, for which

18) $t_K > 6.5$, where t_K is the proper decay time of the K^o in units of the K^o_S lifetime.

The reason for this cut was that the geometrical detection efficiency for $t_K > 6.5$ was very low. The efficiency is discussed in a later section.

After all the rejection criteria had been applied to the data, 99 events remained in the final sample.

Table 3

Reasons for Rejection of Events during Simultaneous Examination of Photographs and Computer Output by Physicists

Reason for Rejection	First Physicist Study	Second Physicist Study	Both Physicist Studies
Hit	39	41	80
Either momentum > 2500 MeV/c	8	0	8
$M_{\pi\pi\pi} > 362.78$ MeV	0	3	3
$M_{\pi^- p} < 1135$ MeV	0	2	2
No photon	49	10	59
Tracks shower or do not appear in shower chambers	17	14	31
Fake event	152	81	233
Wrong counter lights	0	22	22
No lambda	26	4	30
Scatter before end of magnet chambers	0	3	3
K^o energy too high or low	0	6	6
Decay before Λ chamber	16	16	32
Outside Dalitz plot	0	7	7
	307	209	516

IV. MONTE CARLO PROGRAM

A Monte Carlo computer program was written for the following purposes:

1) To calculate the geometrical $K^o_{\pi 3}$ detection efficiency of the apparatus as a function of the K^o proper time.

2) To calculate theoretical distributions of kinematical quantities for comparison with the data.

3) To study the effect of various backgrounds.

The Monte Carlo program generates simulated $K^o_{\pi 3}$ events and asks whether they would trigger the apparatus. The values of all required kinematical quantities are chosen by random number techniques.

The K^o's and Λ's which trigger the apparatus are assumed to come from a mixture of the following production modes:

$$\pi^- p \rightarrow K^o \Lambda$$

$$\pi^- p \rightarrow K^o \Sigma^o \quad (\Sigma^o \rightarrow \Lambda \gamma)$$

$$\pi^- p \rightarrow K^{o*}(890)\, \Lambda \quad (K^{o*}(890) \rightarrow K^o \pi^o)$$

There is also provision for generating other production and decay processes in order to study backgrounds.

No experimental error is included in the calculations.

A longer discussion of the Monte Carlo program is presented in Appendix A.

V. CALIBRATION ROLL

To obtain estimates of the main types of events which triggered the spark chambers, a typical roll of film was examined without respect to the content of the shower chambers. The magnet film for this roll was scanned to reject frames which did not have two good tracks of opposite curvature. The 1851 remaining frames were measured on the HYDEL, processed on the computer, and studied by physicists. Based on this study, Table 4 presents estimates of the major categories of events which were seen on the spark chamber film.[13]

In addition to providing background estimates, this typical roll provided an unbiased sample of $K_S^o \rightarrow \pi^+\pi^-$ events, which were used for calibration of the K^o energy spectrum, as described in a later section.

Table 4

Estimates of Types of Events which Triggered the Apparatus

Unmeasurable events (> 4 tracks and spurious triggers)	48.4%
Fake events, events with tracks that hit the sides of the chambers or magnet	38.14%
$K^o_S \rightarrow \pi^+\pi^-$	10.0%
$\Lambda^o \rightarrow \pi^- p$	2.0%
$\gamma \rightarrow e^+e^-$	1.2%
$K^o \rightarrow \pi^{\pm} e^{\mp} \nu(\bar{\nu})$	.1%
$K^o \rightarrow \pi^{\pm} \mu^{\mp} \nu(\bar{\nu})$	.1%
$K^o \rightarrow \pi^+\pi^-\pi^o$	.06%*

* Due to the requirement that one photon be observed in the shower chambers, only about one third of the $K^o_{\pi 3}$ events which triggered the counters remained in the final sample.

VI. BACKGROUNDS

This section discusses the most significant backgrounds encountered in the experiment. The number of possible background events remaining in the final $K^o_{\pi 3}$ sample was estimated to be so small that no background corrections were made for the final fit.

A. $K^o_S \rightarrow \pi^+\pi^-$

This process, although frequently observed in the spark chamber photographs, caused no confusion with $K^o_{\pi 3}$ decays. The $\pi\pi$ invariant mass for $K^o_S \rightarrow \pi^+\pi^-$ is $M_{\pi\pi} = 497.76$, the mass of the K^o, whereas $K^o_{\pi 3}$ events must have $M_{\pi\pi} < 362.78$. Thus our $M_{\pi\pi}$ cut completely eliminated $K^o_S \rightarrow \pi^+\pi^-$ events from the sample.

B. $\Lambda \rightarrow \pi^- p$

Examination of the $M_{\pi^- p}$ invariant masses in the raw data showed a large peak in the region of the lambda mass. This effect is evident in Figure 13 , which is a histogram of $M_{\pi^- p}$ for all events which satisfied the following requirements: a photon candidate in the shower chambers, two good tracks of opposite curvature in the magnet chambers, $M_{ee} > 50$ MeV, Miss < .500 inch.

In order to rid the sample of lambdas, events having $M_{\pi^- p} < 1135$ were rejected. Monte Carlo calculations show that 3.3% of the $K_{\pi 3}$ events are lost by making this cut. Figure 14 shows a histogram of the events in the final sample. There is no evidence for peaking at low $M_{\pi^- p}$. For comparison, the Monte Carlo predicted curve, normalized to the same number of events, is superimposed on the histogram.

Figure 13. $\pi^- p$ invariant mass distribution before $M_{\pi^- p}$ cut.

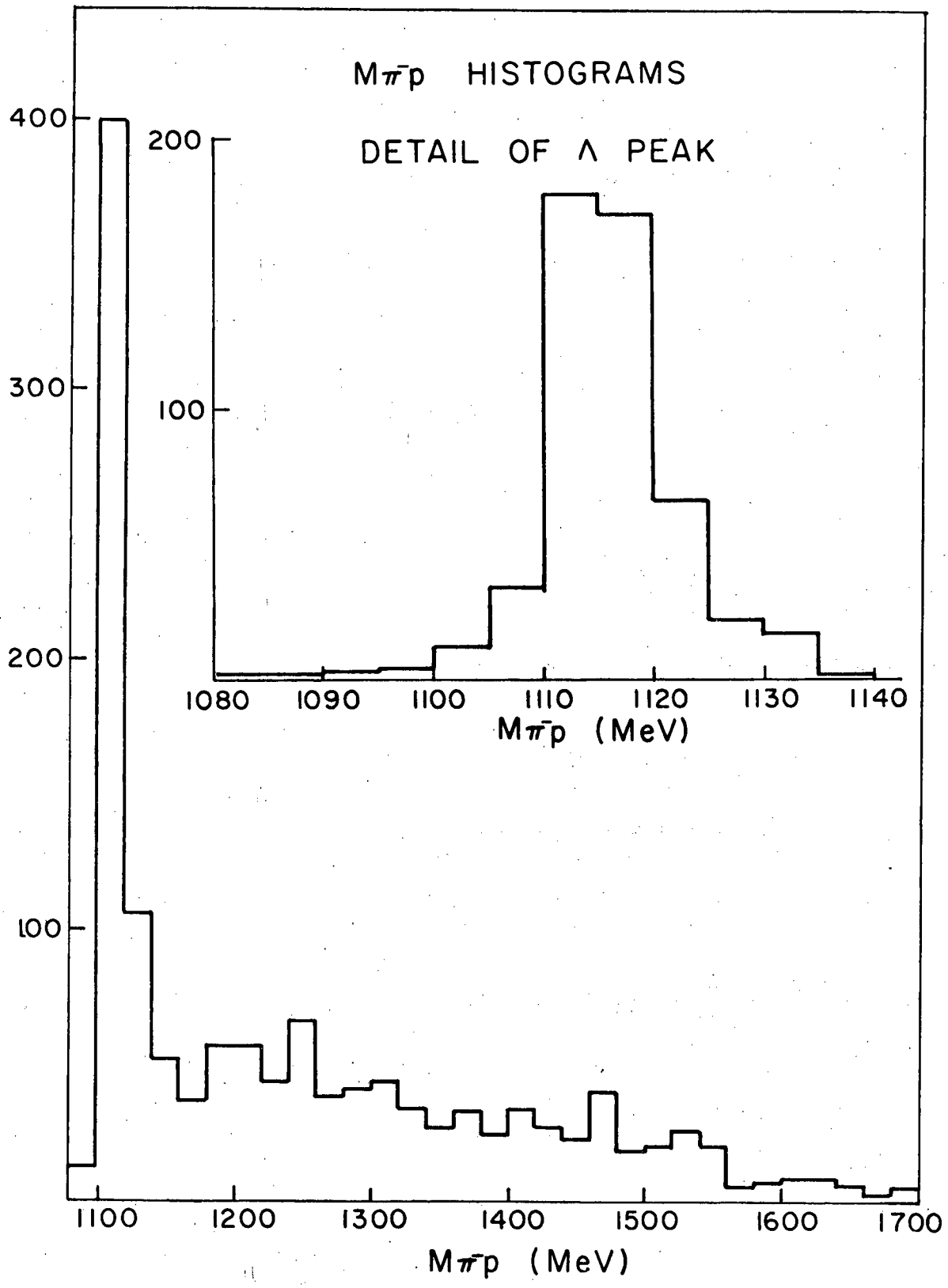
Mπ⁻p HISTOGRAMS
DETAIL OF Λ PEAK
400
300
200
100
200
100
1080
1090
1100
1110
1120
1130
1140
Mπ⁻p (MeV)
1100
1200
1300
1400
1500
1600
1700
Mπ⁻p (MeV)

Figure 14. $\pi^- p$ invariant mass distribution for final sample. Smooth curve is Monte Carlo prediction.

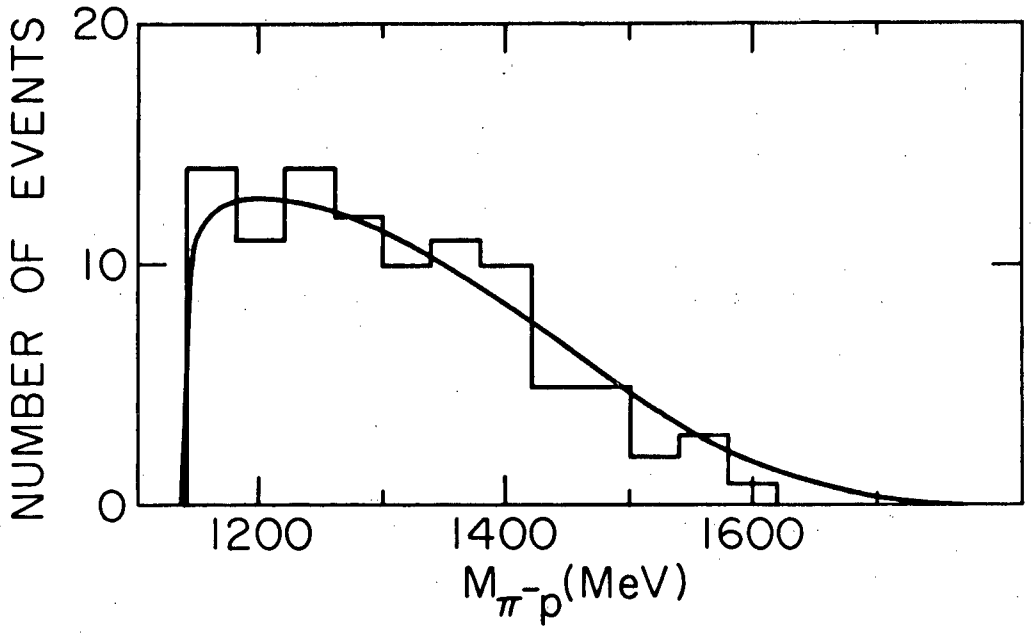
NUMBER OF EVENTS
20
10
0
1200
1400
1600
M_{π^-p}(MeV)

C. Leptonic Decays of K^o

In two companion experiments[13,14], the same spark chamber film was analyzed for K^o_{e3} and $K^o_{\mu 3}$ decays as well as for $K^o_{\pi 3}$ decays. The apparatus had been designed to be sensitive to all three decay modes. Monte Carlo calculations showed that comparable numbers of events should be expected from each process.

There were several methods for distinguishing $K^o_{\pi 3}$ decays from leptonic decays. A photon in the shower chambers was required for $K^o_{\pi 3}$ candidates, whereas leptonic decays would generally not have a photon in the shower chambers. For K^o's produced via $\pi^- p \rightarrow \Lambda K^o$, the leptonic events would not have a photon. Photons could arise from $K^o\Sigma^o$ production followed by $\Sigma^o \rightarrow \Lambda\gamma$ or from $K^o\Lambda\pi^o$ production followed by $\pi^o \rightarrow \gamma\gamma$. Monte Carlo calculations showed that only about two percent of the leptonic events should have photons appearing in the shower chambers.

For most K^o_{e3} events, the electron could be identified by its showering in the shower chambers. The calibration pictures discussed earlier were carefully studied to aid physicists in distinguishing electrons from pions. For 6 of the events in the final $K^o_{\pi 3}$ sample, one of the charged particles observed in the magnet chambers passed through the gap between the right and left shower chambers. Thus we could not determine from observing the shower chambers whether the particle might be an electron. However, each of these events gave a better kinematical fit to $K^o_{\pi 3}$ than to K^o_{e3}. Monte Carlo estimates show that about 0.4% of the K^o_{e3} events which triggered the apparatus should have had an electron in the shower gap plus a photon in the shower

chambers. Based on the number of K^o_{e3} events observed in the companion experiment, we estimate that 2 K^o_{e3} events of this type might have been mistaken for $K^o_{\pi 3}$ events before kinematical calculations were made.

The kinematics calculations performed for each event tested whether it was consistent with a $K^o_{\mu 3}$ or K^o_{e3} hypothesis in addition to the $K^o_{\pi 3}$ hypothesis. Generally the fit was considerably better for one K^o decay mode than for others. One reason is that the $K^o_{\pi 3}$ decay has a lower energy release than the leptonic decays. (Q = 83.63 for $K^o_{\pi 3}$, Q = 252.52 for $K^o_{\mu 3}$, Q = 357.67 for K^o_{e3}, where Q is the kinetic energy available in the K^o rest frame.) The leptonic events tended to have higher transverse momenta than allowed for $K^o_{\pi 3}$, and hence the reconstruction of these events under a $K^o_{\pi 3}$ hypothesis either failed entirely or gave unphysical results a large fraction of the time.

A kinematic calculation described elsewhere[15] in the literature was very useful in distinguishing $K^o_{\pi 3}$ events from leptonic events. This calculation exploits the low Q value in $K^o_{\pi 3}$ decays. For each event, the quantity Popsquare was calculated where

$$\text{Popsquare} = \frac{(M_K^2 - M_{\pi^o}^2 - M_{\pi\pi}^2)^2 - 4M_{\pi^o}^2 M_{\pi\pi}^2 - 4M_K^2 P_T^2}{4(P_T^2 + M_{\pi\pi}^2)}$$

M_K = mass of K^o

$M_{\pi\pi}$ = invariant $\pi^+\pi^-$ mass

M_{π^o} = mass of π^o

P_T = total transverse momentum of the two charged particles with respect to the K^o direction

In physical terms, Popsquare is the square of the momentum of the kaon in the reference frame in which the total longitudinal momentum of the two charged particles is zero. For a true $K^o_{\pi 3}$ event, Popsquare must be positive, although measuring uncertainties give the Popsquare distribution a small negative tail. For K^o_{e3} and $K^o_{\mu 3}$ events, the Popsquare distribution is predominantly negative, peaking around -20,000 MeV^2 with only a small positive tail. Figure 15 shows the Popsquare distributions for this experiment as well as for the K^o_{e3} and $K^o_{\mu 3}$ companion experiments. Superimposed on each experimental histogram is the expected Monte Carlo distribution. Measuring errors and experimental resolution were not included in the Monte Carlo calculations. The Popsquare histograms for the three K^o decay modes are plotted on the same scale, one above another, so that one can easily compare the overlap regions. No cut on Popsquare was actually made in any of the three experiments. For the $K^o_{\pi 3}$ final sample, all events have Popsquare greater than -5000 MeV^2/c. Based on the experimental histograms, 8% of the K^o_{e3} events and 24% of the $K^o_{\mu 3}$ events which triggered the apparatus had Popsquare greater than -5000 MeV^2. We estimated above that 2 K^o_{e3} events might have been mistaken for $K^o_{\pi 3}$ events before the kinematical calculations. Applying the Popsquare test as well, we estimate that no K^o_{e3} events remain in the final $K^o_{\pi 3}$ sample.

To aid in distinguishing muons from pions, a steel absorber with thickness 405 gm/cm^2 was placed downstream of the shower chambers. Beyond the steel was a hodoscope of counters with height 36 inches and total width 108 inches. Because of their low interaction probability, muons with total lab energy greater than 875 MeV were expected to traverse the steel and trigger the hodoscope. "Mu lights" were flashed and recorded on the shower chamber film

Figure 15. Popsquare distributions for $K^o_{\mu 3}$, K^o_{e3}, and $K^o_{\pi 3}$ experiments. Smooth curves are Monte Carlo predictions.

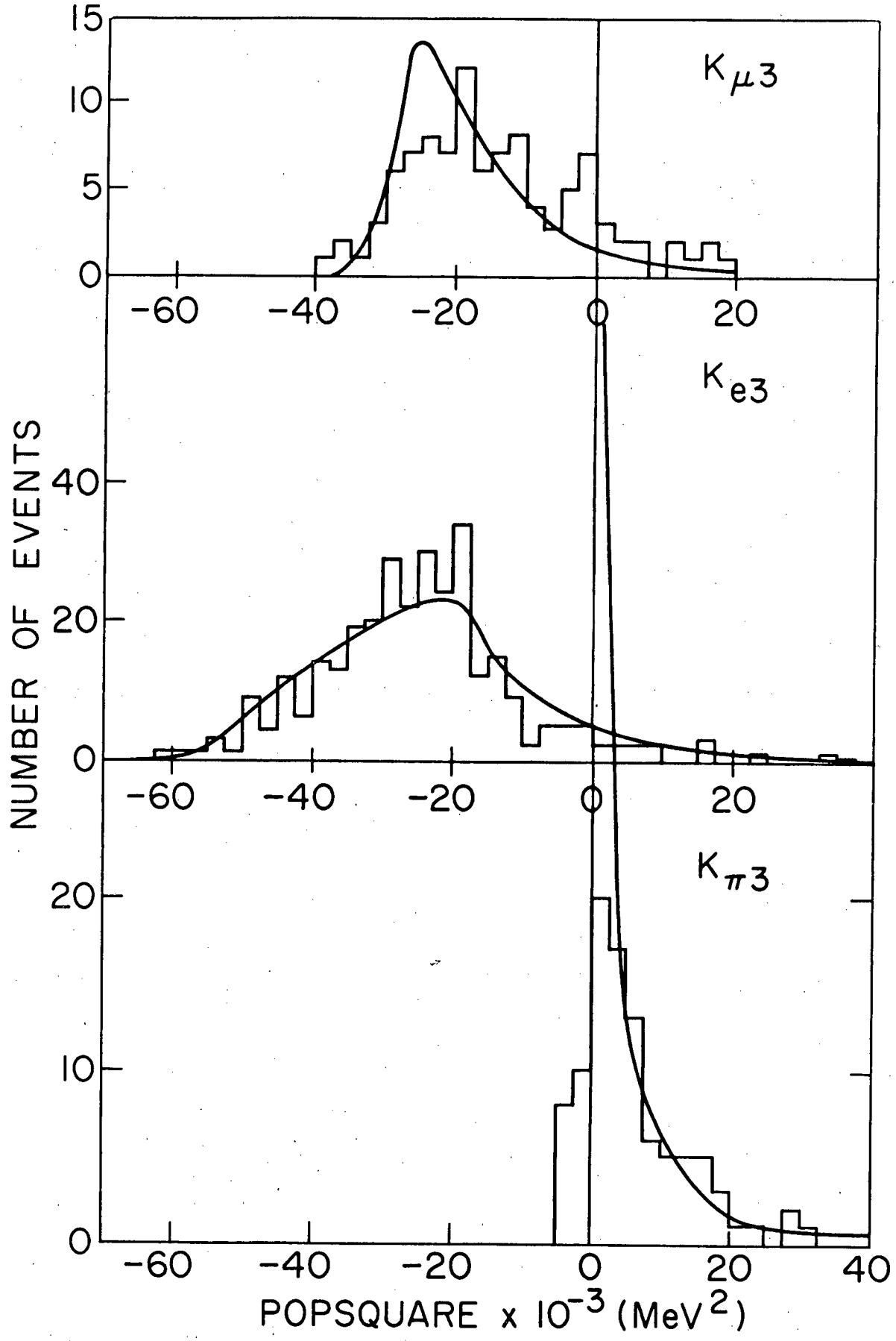
15
10
5
0
$K_{\mu 3}$
-60
-40
-20
0
20
K_{e3}
40
20
0
NUMBER OF EVENTS
-60
-40
-20
0
20
$K_{\pi 3}$
20
10
0
-60
-40
-20
0
20
40
POPSQUARE x 10^{-3} (MeV^2)

to indicate when these hodoscope counters fired. Monte Carlo studies indicated that 69% of the $K_{\mu 3}$ events which triggered the spark chamber firing logic should also trigger this muon hodoscope. Valid $K^o_{\pi 3}$ events could trigger the muon hodoscope provided one of the charged pions decayed in flight to a muon, and that muon had sufficient energy to penetrate the steel absorber. On the basis of Monte Carlo calculations we expect about 4 events of this type. In the final sample there are 3 events with mu counter lights. All of these have a better kinematic fit to the $K^o_{\pi 3}$ hypothesis than to the $K^o_{\mu 3}$ hypothesis. No events were discarded on the basis of the mu lights. 31% of the $K^o_{\mu 3}$ events would not be expected to trigger the mu counters and thus would have more chance of being confused with $K^o_{\pi 3}$ events. But only 2% of these should have a photon in the shower chambers. Based on the number of $K^o_{\mu 3}$ events observed in the companion experiment, we estimate that less than 2 $K^o_{\mu 3}$ events which did not trigger the mu counters should have had a photon in the shower chambers. From the Popsquare test described above, only 24% of these events should have a Popsquare value in the $K^o_{\pi 3}$ range ($\gtrsim$-5000 MeV^2). Thus we estimate that less than 1 $K^o_{\mu 3}$ event might remain in the $K^o_{\pi 3}$ final sample.

D. $K^o_S \to \pi^+\pi^-\gamma$

This process is assumed to occur only through inner bremsstralung and not through the direct process. The relevant Feynman graphs are [16]

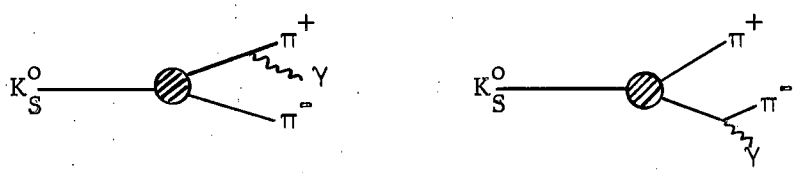

The theoretical center-of-mass photon spectrum (Figure 16) is given by [16,17,18]

$$\frac{d\Gamma(K_S \to \pi^+\pi^-\gamma)}{dk} = \frac{\alpha}{\pi}\Gamma(K_S \to \pi^+\pi^-)\frac{\beta}{\beta_o}\left(\frac{1+\beta^2}{\beta}\ln\frac{1+\beta}{1-\beta}\right)\frac{1}{k}\left(1 - \frac{2k}{m_K}\right)$$

where k is the photon momentum in the K_S^o rest frame

β is the pion velocity in units of c in the dipion rest frame

β_o is the value of β when k = 0.

For $K_{\pi 3}^o$ decay, the $\pi\pi\pi$ invariant mass is restricted to the region $M_{\pi\pi\pi} < 363$ MeV. Figure 17 shows a histogram of $M_{\pi\pi\pi}$ for the final sample and the predicted Monte Carlo distribution. Making this the restriction $M_{\pi\pi\pi} < 363$ MeV for $K_S^o \to \pi^+\pi^-\gamma$ is equivalent to the condition k > 135 MeV/c. The integral of the above expression for k > 50 MeV/c has been performed elsewhere.[16] From this integration, Webber obtains the branching ratio

$$\Gamma(K_S^o \to \pi^+\pi^-\gamma;\ k > 50\ \text{MeV/c}) = (2.56 \times 10^{-3})\Gamma(K_S^o \to \pi^+\pi^-)$$

We have performed numerical integrations from the graph in Figure to ascertain that only 2.69% of the $K_S^o \to \pi^+\pi^-\gamma$ decays with k>50 MeV/c also have k>135 MeV/c and hence could simulate $K_{\pi 3}^o$ decays. Approximately 10% of the triggers in the experiment (~46,700) were due to $K_S^o \to \pi^+\pi^-$. Thus $(46{,}700)(2.56 \times 10^{-3})(.0269) \approx 3$ triggers should have been due to $K_S^o \to \pi^+\pi^-\gamma$. Considering the photon detection efficiency of 55% (discussed later) and the fact that all photons would not reach the shower chambers, less than 1 $K_S^o \to \pi^+\pi^-\gamma$ event might have been mistaken for a $K_{\pi 3}^o$.

Figure 16. Theoretical center-of-mass photon spectrum for $K_S^o \rightarrow \pi^+\pi^-\gamma$.

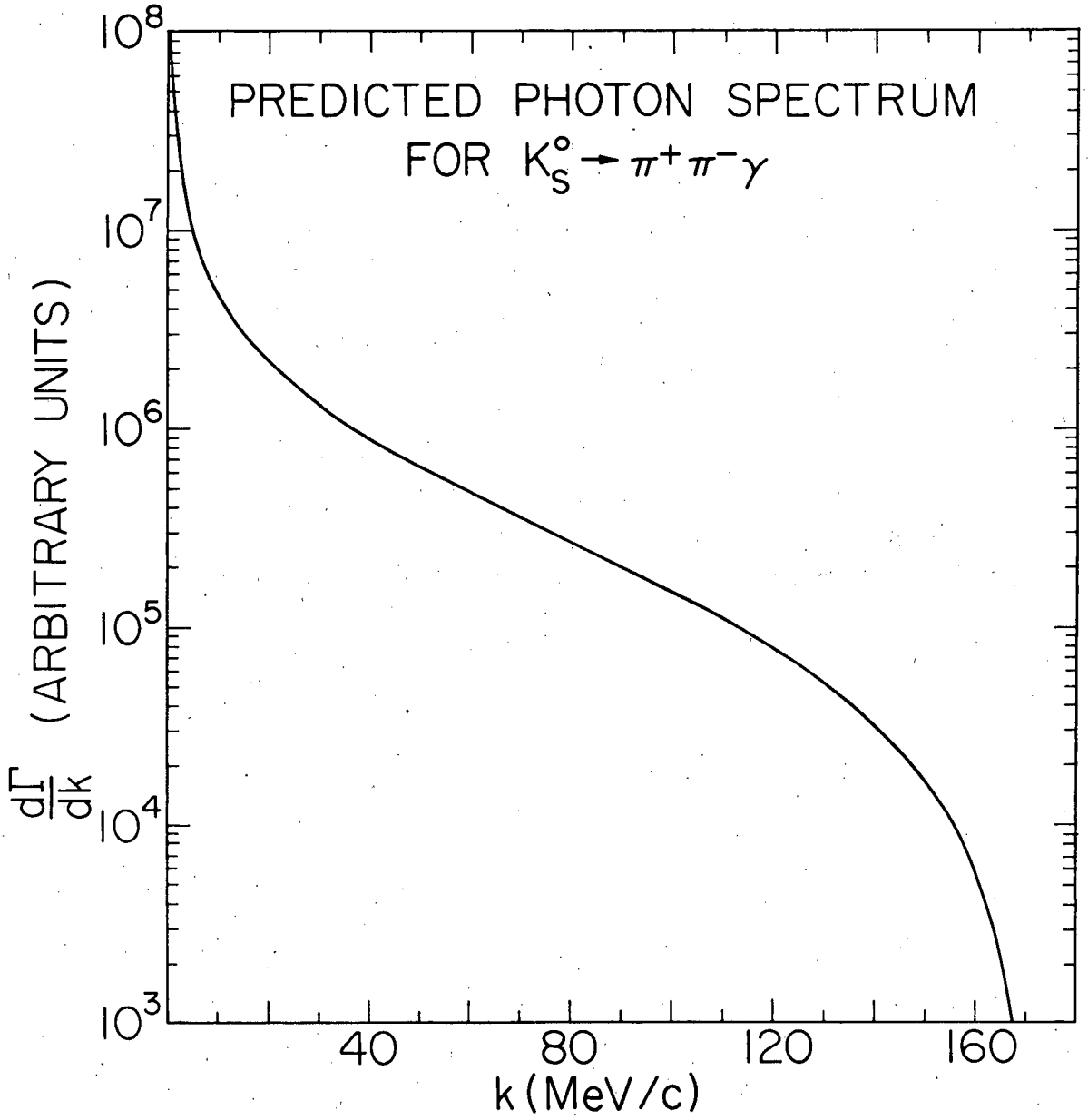
PREDICTED PHOTON SPECTRUM
FOR $K_S^\circ \rightarrow \pi^+\pi^-\gamma$
$\frac{d\Gamma}{dk}$ (ARBITRARY UNITS)
10^8
10^7
10^6
10^5
10^4
10^3
40
80
120
160
k (MeV/c)

Figure 17. $\pi^+\pi^-$ invariant mass distribution for final sample. Smooth curve is Monte Carlo prediction.

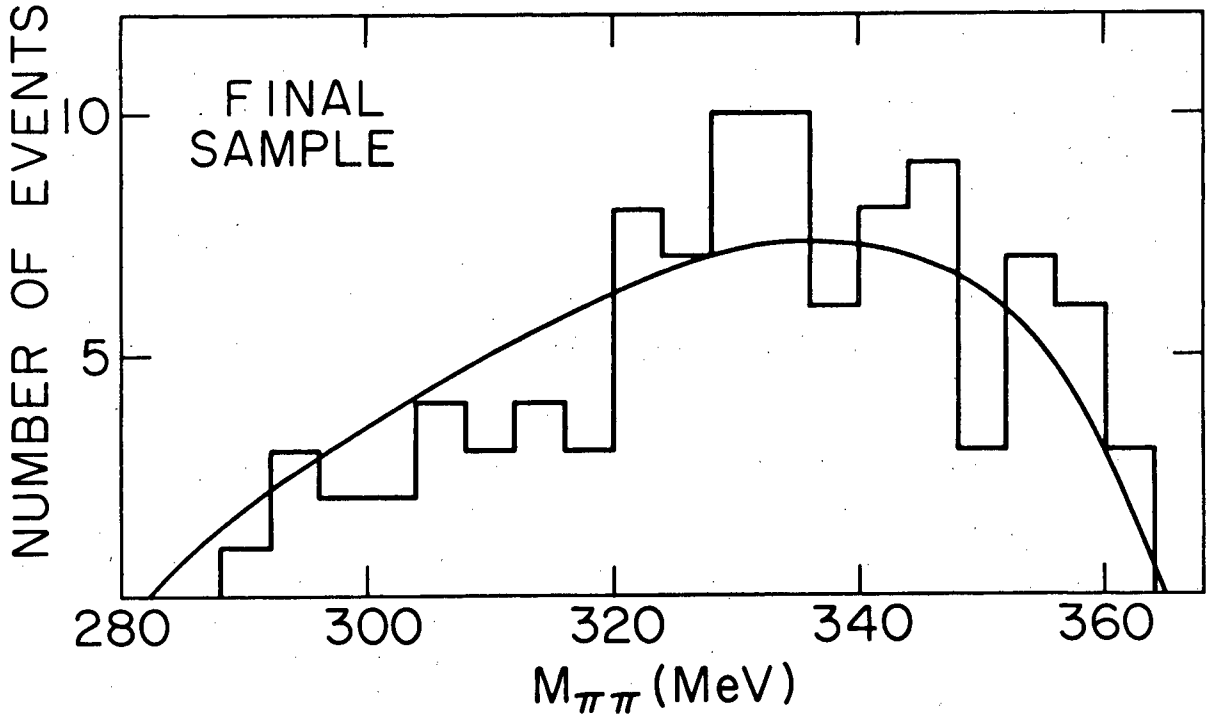
NUMBER OF EVENTS
10
5
FINAL
SAMPLE
280
300
320
340
360
$M_{\pi\pi}$ (MeV)

E. Photon conversions ($\gamma \rightarrow e^+e^-$)

Electron-positron pairs from photon conversions upstream of the magnet were responsible for approximately 1.2% of all triggers. The photons came primarily from the 2γ decay of π^o mesons which were produced through $K_s^o \rightarrow \pi^o\pi^o$, pion charge exchange, or three body production reactions.

This background was easily eliminated due to the small invariant mass of pairs and their characteristic appearance in the spark chambers.

Since the pair is produced with approximately zero opening angle, the two tracks appear together in the upstream spark chambers. In the magnet chambers, the two tracks curve apart in the top view but remain colinear in the side view. In the shower chambers both tracks shower. This topology facilitated identification of pair conversion events by examination of the spark chamber film.

The invariant mass cut $M_{ee} < 50$ MeV was applied to the data in order to virtually eliminate all pair conversions from the sample. Examination of the spark chamber photographs for events with the above topology provided an additional check that no such events remained. The Monte Carlo program indicated that 2.1% of the $K_{\pi 3}^o$ events were discarded as a result of this cut. Figure 18 shows a histogram of M_{ee} for all events in the final sample. Superimposed on the histogram is the Monte Carlo predicted curve normalized to the same number of events. There is no evidence of peaking at low values of M_{ee}, and the data agree well with the Monte Carlo prediction. We estimate that no photon conversion events remain in the final sample.

Figure 18. e^+e^- invariant mass distribution for final sample. Smooth curve is Monte Carlo prediction.

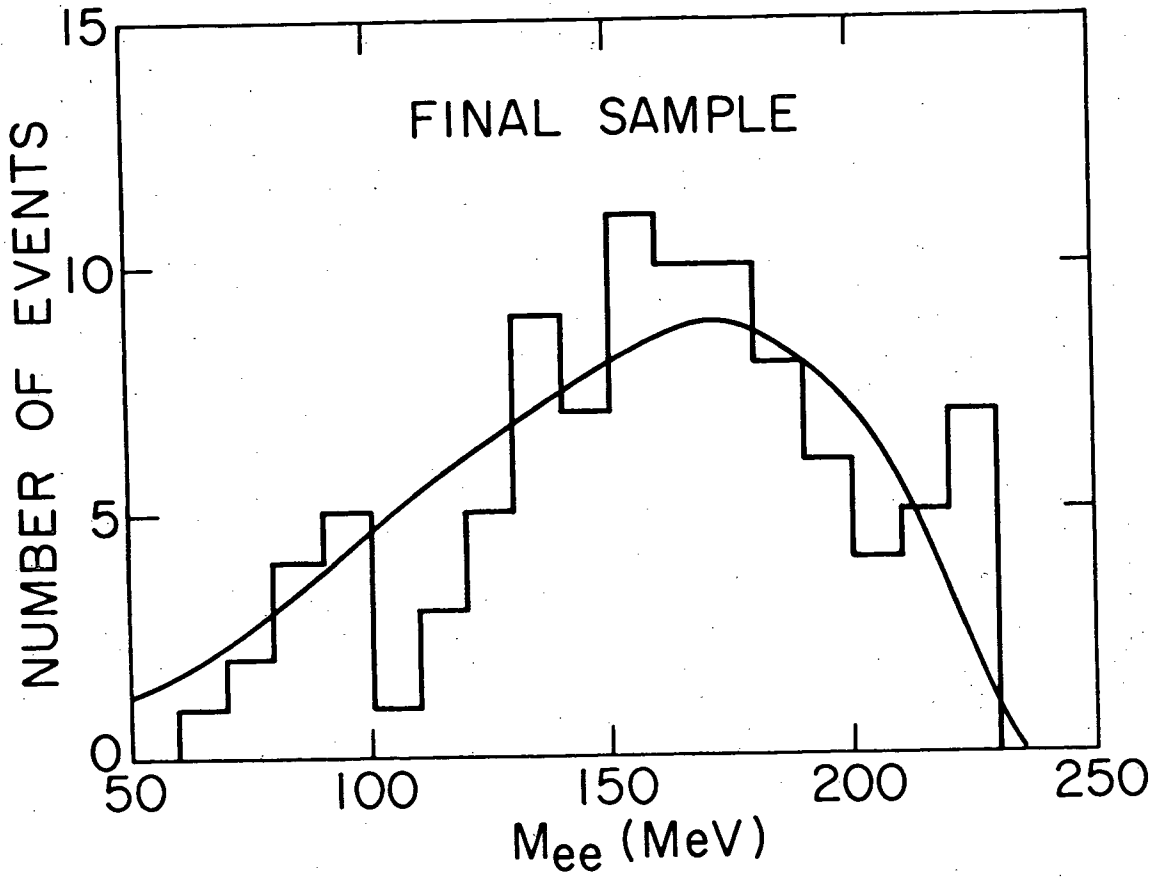
FINAL SAMPLE
NUMBER OF EVENTS
15
10
5
0
50
100
150
200
250
Mee (MeV)

F. Dalitz pairs ($\pi^o \to \gamma e^+ e^-$)

Approximately 1% of π^o decays proceed via the Dalitz mode $\pi^o \to e^+ e^- \gamma$. [18] The Dalitz pairs from this decay may have observable opening angles and sizeable invariant masses. Study of experimental invariant mass distribution for Dalitz pairs [19,20] indicates that 95% have $M_{ee} < 50$ MeV and hence are eliminated by our M_{ee} cut.

To be mistaken for $K^o_{\pi 3}$ events, the remaining Dalitz pairs would have to satisfy $K^o_{\pi 3}$ kinematics as well as not producing showers in the shower chambers. All events in the final sample having $M_{ee} < 135$ MeV were re-examined to determine whether the shower chamber tracks showed any evidence of showering. No such events were found. We estimate that no Dalitz pair events should remain in the final sample.

G. $K^o \bar{K}^o n$

This process could cause a bias in the time distribution if undetected, since it would result in a small initial $\bar{K}^o$ component. However, the Monte Carlo calculations indicate that the number of events of this type that would trigger the apparatus is negligible. For this process to be detected, one kaon would have to trigger the ϕ and ρ hodoscopes and the other kaon, decaying in the $\pi^+ \pi^-$ mode, would have to trigger the $\lambda dE/dx$ hodoscope. The Monte Carlo results indicate that even if the $\bar{K}^o$ decay products have enough energy to pass through the magnet and trigger the ϕ and ρ hodoscopes, the K^o decay products tend to be too energetic to trigger the $\lambda dE/dx$ hodoscope. Furthermore, because of its large energy and short lifetime, the K^o will often decay upstream of the anticoincidence counter and thus anti out. We estimate that no events from $K^o \bar{K}^o n$ production remain in the final sample.

VII. DISCUSSION OF PHOTONS

The requirement that one of the photons from π^o decay be seen in the shower chambers was an important check that the events were really $K^o_{\pi 3}$ events. This section describes some studies of the photons for events in the final sample and indicates the existence of some biases in the identification of photons. Whereas these biases limit the number of $K^o_{\pi 3}$ events in the final sample, they have little effect on the time distribution.

Figure 19 shows a histogram of the starting gap for the photon showers in the shower chambers. The vertical marks along the abscissa indicate the position of the heavy plates in these chambers. The designations "S" and "Pb" with arrows indicate the locations of the stainless steel plates and the lead sheets. The plates not marked by arrows were aluminum. The histogram clearly indicates that showers are most likely to begin in the gaps immediately following the stainless steel plates or the lead sheets, as anticipated. One expects the distribution of photon conversions as a function of distance z to be exponential, decreasing as $e^{-\lambda z}$. Thus the histogram suggests that our photon detection efficiency is low for the first five gaps of the shower chambers compared with the later gaps, as would be expected. A calculation based on the histogram indicates that the photon detection efficiency for these early gaps is about 35% relative to the later gaps. This low efficiency is due to the manner in which events in the early gaps were obtained, which has been described in the section on selection of events.

The detection efficiency for photons converting later than gap 5 is estimated to be 70%. The overall photon detection efficiency is

Figure 19. Starting gap for photon showers. Numbers along abscissa are gap numbers for front and rear shower chambers. "S" and "Pb" indicate locations of stainless steel plates and lead. The other plates are aluminum.

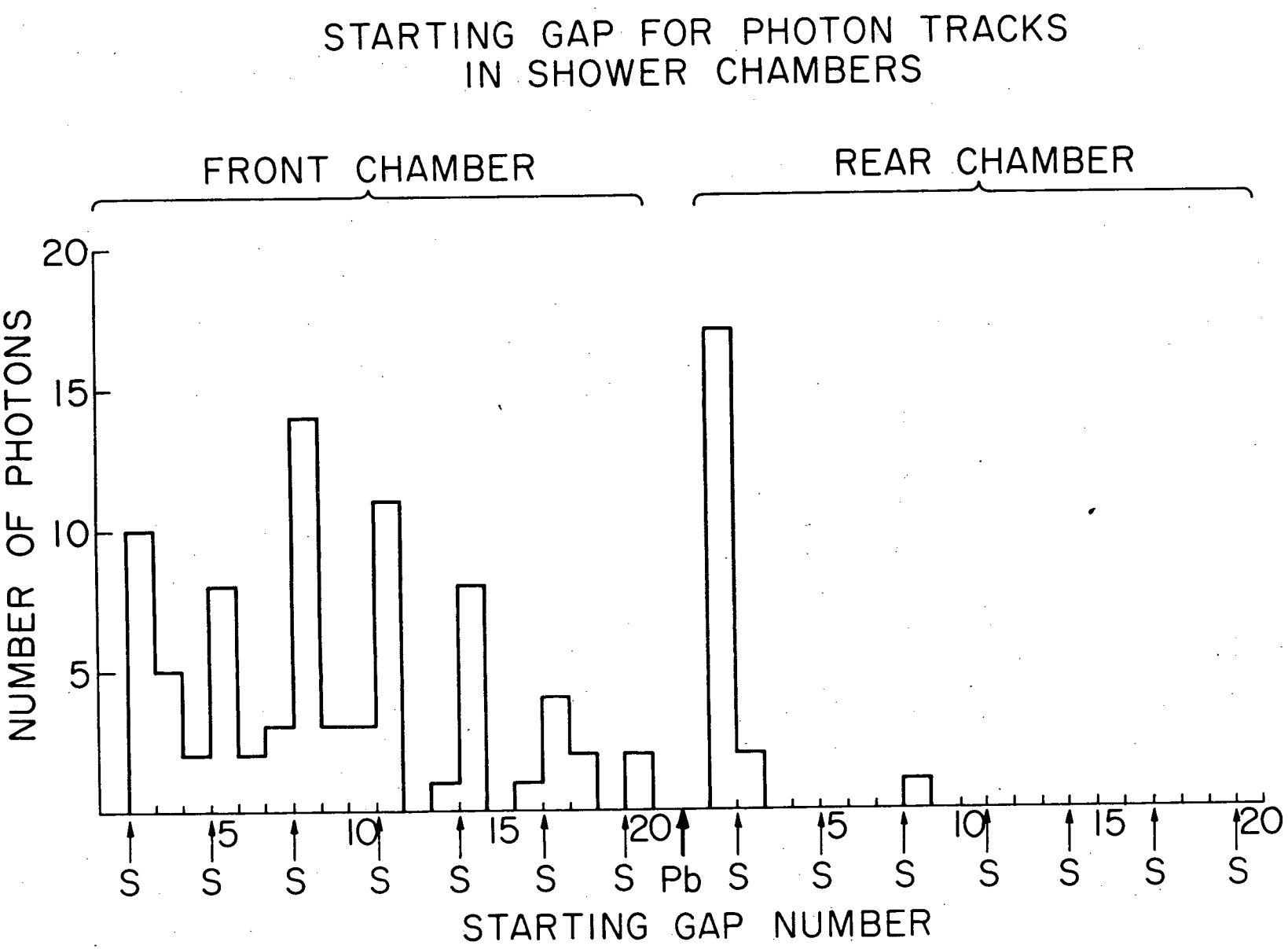
STARTING GAP FOR PHOTON TRACKS
IN SHOWER CHAMBERS
FRONT CHAMBER
REAR CHAMBER
NUMBER OF PHOTONS
20
15
10
5
S
Pb
STARTING GAP NUMBER

estimated to be 55%. These estimates were computed from the relative numbers of photons found by different scanners examining the same shower chamber film.

Figure 20 shows histograms of the laboratory energy and angle θ_{π^o} of the π^o, computed with the kinematical data from the two visible charged particles. θ_{π^o} is the angle between the π^o direction and the beam centerline. The Monte-Carlo predicted curves, normalized to the number of events in the final sample, are superimposed on these histograms. These plots indicate a bias against low energy, wide angle π^o's. This effect is presumably a result of the low photon detection efficiency.

The energies and directions of both photons from π^o decay can be calculated provided the following quantities are known:

1) π^o energy
2) π^o direction
3) Location of decay vertex
4) Shower origin for observed photon

The first three quantities were known from the K^o reconstruction and kinematics calculations. Rough measurements were made of the photon shower origins in the shower chambers. Since the shower chambers were intended for visual identification only, the optical constants needed for accurate measurements were not well known. The measurements were made from a Recordak film viewer, based on the known locations of six fiducial marks. A rough parallax correction was then applied. It is estimated that a few of these measurements could be incorrect by as much as 2-3 inches.

Figure 20. Distributions of calculated laboratory energy and polar angle of π^0 for events in the final sample. Smooth curves are Monte Carlo predictions.

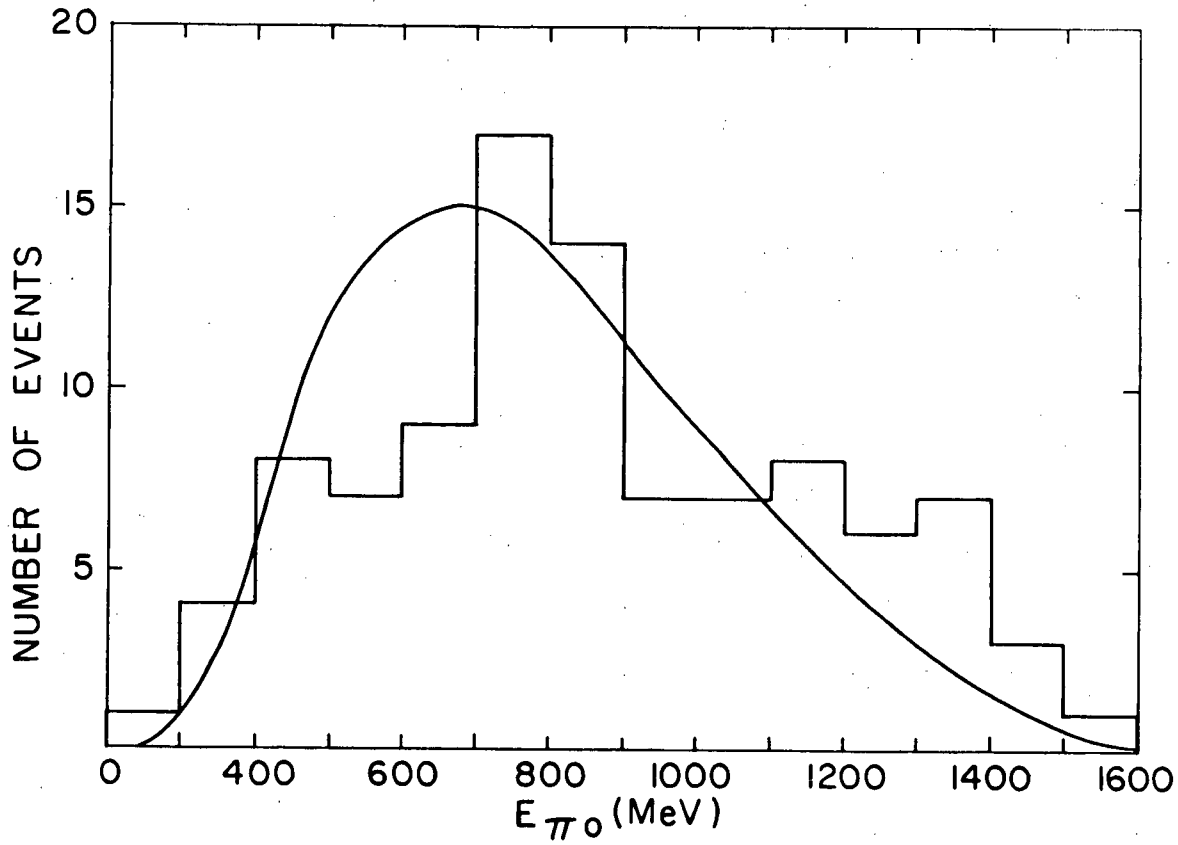
20
15
10
5
NUMBER OF EVENTS
0
400
600
800
1000
1200
1400
1600
E_{π^0} (MeV)

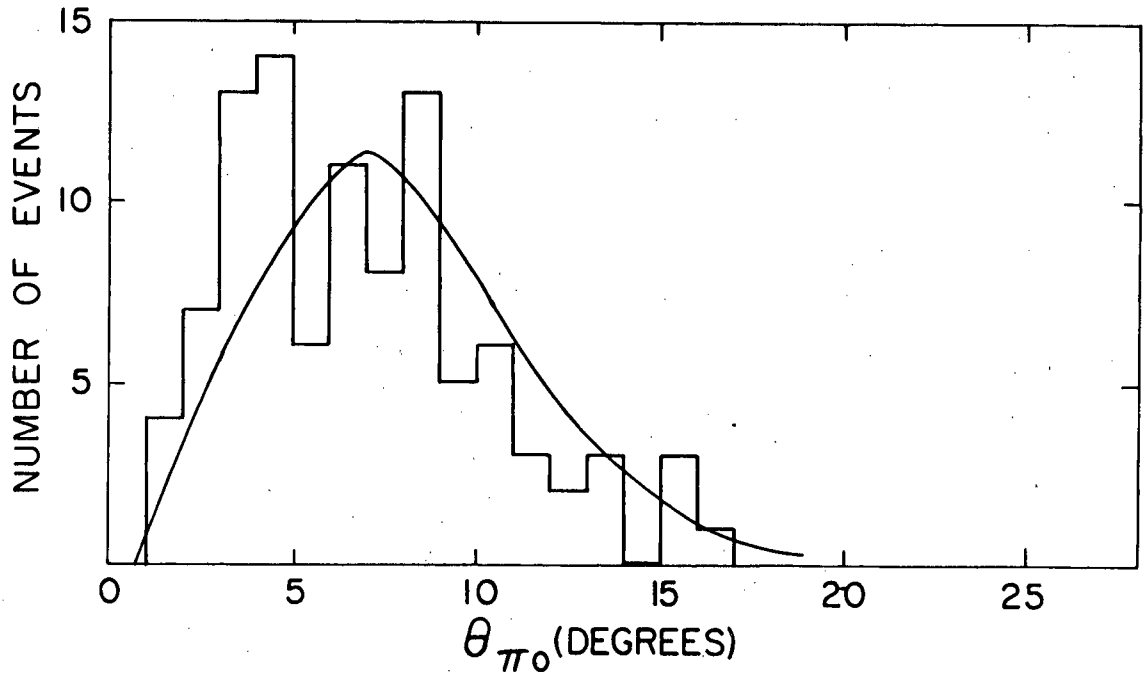
15
10
5
NUMBER OF EVENTS
0
5
10
15
20
25
θ_{π^0} (DEGREES)

The photon direction was taken to be the direction between the photon shower origin and the K^o decay vertex. A straightforward calculation then gave the photon energy as well as the direction and energy for the second photon from π^o decay.

No events were discarded on the basis of these calculations. However, the results are presented and compared to the Monte Carlo predictions in order to give an indication of the possible photon biases in the experiment.

Figure 21 shows a plot of the observed number of sparks vs. the calculated laboratory energy for the photons in the final $K^o_{\pi 3}$ sample. The average photon energy divided by the average number of sparks is 14.5 MeV per spark. This is consistent with the energy/spark ratio found for electron showers in the companion K^o_{e3} experiment.[13] The data points on the plot are roughly centered about the 14.5 MeV/spark line, which is drawn on the plot. The spread of points away from this line is partly due to the fact that 1.2 radiation lengths of lead is situated between the front and rear shower chambers to enhance the showering. Photons which lose a lot of energy in the lead tend to have fewer sparks than photons of the same energy which shower outside of the lead. In addition, some tracks reach the downstream end of the chambers before the showering is complete and thus have fewer sparks than might be expected from their energy.

Figure 22 shows histograms of the calculated photon laboratory energy and the photon angle θ_γ relative to the beam centerline. The Monte Carlo curves, normalized to the same number of photons, are shown for comparison. These plots suggest a low efficiency for detecting high energy, forward photons. One possible explanation is the following. In some frames, beam tracks appeared which were not part of the trigger but which passed through the spark chambers during their sensitive time. These tracks appeared very near the gap between

Figure 21. Observed number of sparks vs. calculated laboratory energy for photons in the final sample.

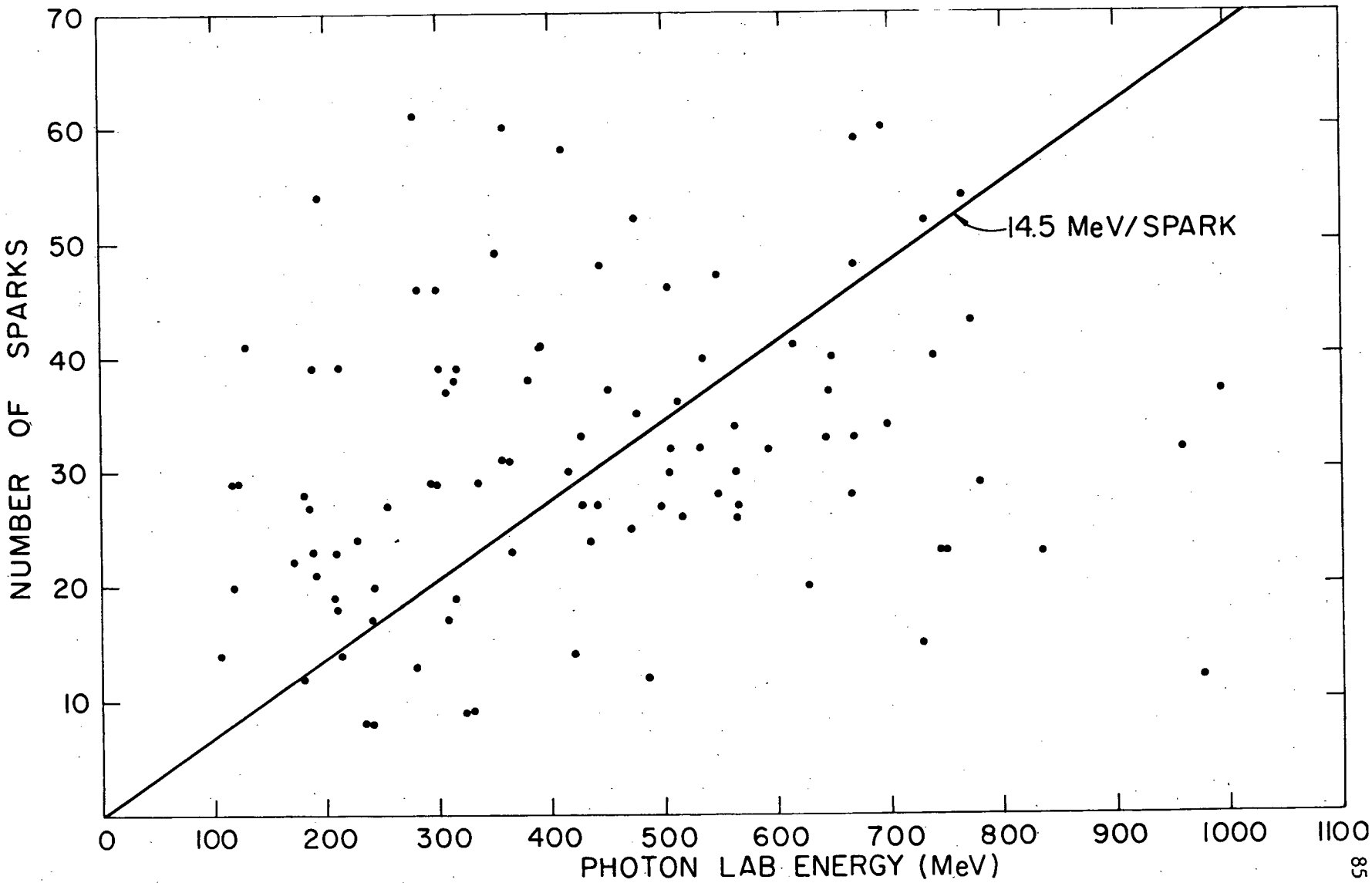
NUMBER OF SPARKS
70
60
50
40
30
20
10
0
100
200
300
400
500
600
700
800
900
1000
1100
PHOTON LAB ENERGY (MeV)
14.5 MeV/SPARK

Figure 22. Distributions of calculated laboratory energy and polar angle for photons in final sample. Smooth curves are Monte Carlo predictions.

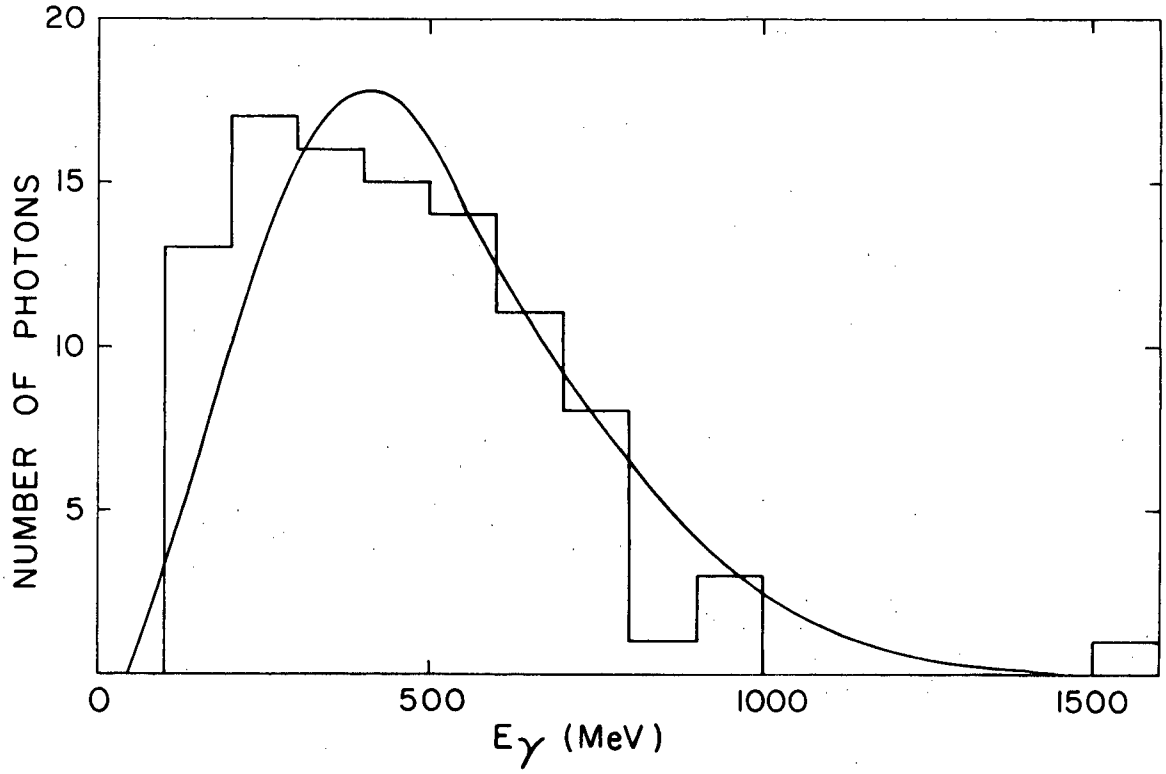
NUMBER OF PHOTONS
20
15
10
5
0
500
1000
1500
E_γ (MeV)

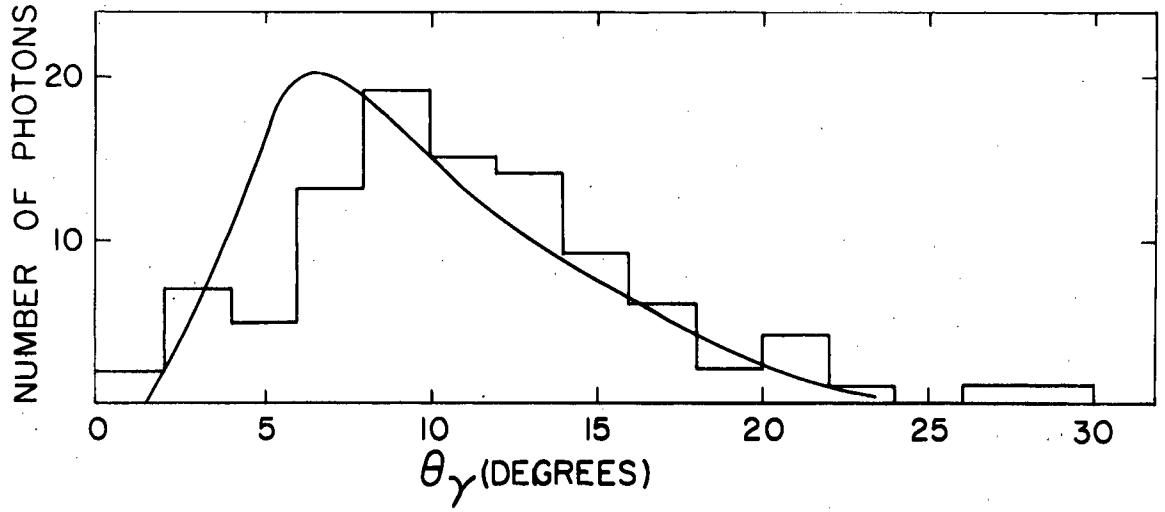
NUMBER OF PHOTONS
20
10
0
5
10
15
20
25
30
θ_γ (DEGREES)

the right and left pairs of shower chambers. Some entered the chambers from this gap. A substantial number of these accidental beam particles were electrons and hence showered in the shower chambers. If a photon appeared in the beam region of the shower chambers, it could have been mistaken for part of a "beam electron shower". If there was any doubt, tracks such as these were not accepted as photon tracks. Thus photons in the beam region could have been rejected to avoid confusing them with beam particles. The Monte Carlo program takes into account the existence of the gap between the shower chambers, but does not consider the effect of accidental beam tracks.

The Monte Carlo calculations indicate that in approximately 13% of the frames, two photons should appear in the shower chambers. For each frame, an approximate calculation was done to predict whether a second photon should appear in the shower chambers and, if so, where it should appear. The results were as follows:

14 photons seen in the predicted region of the chambers

2 seen, but not predicted

5 predicted, but not seen

49 not predicted, not seen

For the other 29 frames in the final sample, it was not clear whether the prediction and the photograph were in agreement. In some cases the predicted location was near the boundary of the chamber, so that a small error in the measured location of the first gamma could throw the predicted location of the second gamma out of the visible region of the spark chambers. In other cases, the assumed second photon track had very few sparks or did not have the characteristics of a usual photon track, so that is was not clear whether or not it should be called a photon.

Considering the approximate nature of the measurements of photon shower origins, these predictions for the locations of second photons give satisfactory agreement with the Monte Carlo results.

Photons from other sources besides $K^o \rightarrow \pi^+\pi^-\pi^o$ (with $\pi^o \rightarrow \gamma\gamma$) could occasionally appear in the shower chambers in connection with a valid $K^o_{\pi 3}$ decay. Extra photons could come from the following processes:

$\pi^- p \rightarrow \Sigma^o K^o$, with $\Sigma^o \rightarrow \Lambda\gamma$

$\pi^- p \rightarrow \pi^o K^o \Lambda^o$, with $\pi^o \rightarrow \gamma\gamma$

$\pi^- p \rightarrow \pi^o K^o \Sigma^o$, with $\pi^o \rightarrow \gamma\gamma$ and $\Sigma^o \rightarrow \Lambda\gamma$

The photons from Σ^o decays had laboratory energies < 20 MeV and thus were not energetic enough to produce showers in the shower chambers. On the other hand, the photons from the extra π^o's could produce visible showers in the chambers. The Monte Carlo program indicates that about 1% of the $K^o_{\pi 3}$ events which triggered the apparatus should have had a photon from the decay of an extra π^o as well as a photon from the decay of their own π^o appearing in the shower chambers. An additional 1% of the $K^o_{\pi 3}$ events which triggered the apparatus should have had a photon from the extra π^o, but no photon from their own π^o. However, no attempt was made to reject events which had the "wrong" photon. If a photon appeared in the shower chambers with a direction consistent with originating at the decay vertex and if the kinematical calculations were consistent with $K^o_{\pi 3}$ decay, the event was accepted.

In summary, the experiment appears to have a low efficiency for the events with the following characteristics:

1) Photons starting to shower in the first five gaps of the shower chambers
2) Photons in the beam region of the shower chambers
3) Low energy, wide angle π^o's.

The primary effect of the low photon detection efficiency and possible photon biases is to decrease the number of events in the final sample. The geometrical $K^o_{\pi 3}$ detection efficiency as a function of K^o decay time is only slightly affected by the type of photon requirement imposed. This conclusion was reached by calculating the geometrical detection efficiency with various cuts made to the photon energy spectrum in the Monte Carlo program. The final data were then fit using these different efficiencies. The results are presented in Table 5 . The relative likelihood maximum near the imaginary axis is given in cases where two likelihood maxima were found.

Table 5

Region of photon energy spectrum cut in Monte Carlo efficiency calculation	Results of maximum likelihood fit	
	x	y
No cut	$-.09 \pm .19$	$+.56 \pm .43$
$E_\gamma < 400$ MeV	$-.08 \pm .19$	$+.53 \pm .44$
400 MeV $< E_\gamma <$ 800 MeV	$-.04 \pm .19$	$+.38 \pm .50$
$E_\gamma > 800$ MeV	$-.06 \pm .19$	$+.48 \pm .46$
No photon required in Monte Carlo calculation	$-.25 \pm .18$	$+.73 \pm .33$

The results of these fits are consistent with each other, considering the limited statistics of the experimental data. We conclude that the

geometrical detection efficiency is relatively insensitive to any cuts made to the photon energy spectrum in the Monte Carlo program. For the final fit, which is discussed later, no photon energy cut was made in computing the Monte Carlo efficiency.

VIII. PREDICTION OF EXPECTED NUMBER OF $K^o_{\pi 3}$ EVENTS

Based on the number of $K^o_S \to \pi^+\pi^-$ events seen in the calibration roll, we have estimated the number of $K^o_L \to \pi^+\pi^-\pi^o$ that should have been seen.

An estimated 46,100 $K^o_S \to \pi^+\pi^-$ decays triggered the apparatus without hitting the walls of the magnet chambers or the magnet itself. The ratio of branching ratios[18] for the two decays is

$$\frac{\Gamma(K^o_L \to \pi^+\pi^-\pi^o)/\Gamma(K^o_L \to \text{all})}{\Gamma(K^o_S \to \pi^+\pi^-) \;/\; \Gamma(K^o_S \to \text{all})} = \frac{.126}{.687} = .184$$

The ratio of geometrical detection efficiencies integrated over the fiducial region is

$$\frac{\epsilon(K^o_L \to \pi^+\pi^-\pi^o)}{\epsilon(K^o_S \to \pi^+\pi^-)} = 2.22$$

Because of the difference in K^o_S and K^o_L lifetimes, virtually all of the K^o_S decay within the first 6.5 K^o_S lifetimes, but only $(1 - e^{-6.5/\tau_L}) = .010$ of the K^o_L decay within the first 6.5 K^o_S lifetime.) The expected number of $K^o_L \to \pi^+\pi^-\pi^o$ events expected is then $(46100)(.184)(2.22)(.010) = 188$ events. 99 $K^o \to \pi^+\pi^-\pi^o$ events were found in the experiment, indicating an overall detection efficiency of about 53%. This is consistent with the estimated photon detection efficiency of 55% given earlier, although neither estimate is claimed to be good to better than 10%. The agreement between these two independent estimates of efficiencies substantiates our belief that the low photon detection efficiency is the only significant reason for loss of good $K^o_{\pi 3}$ events.

IX. DISCUSSION OF FINAL $K^o_{\pi 3}$ SAMPLE

This section presents further comparisons between data and Monte Carlo-generated events and discusses the resolution of the experiment.

A. Dalitz Plot

Figure 23 shows the Dalitz plot for events in the final sample as well as a Monte Carlo-generated Dalitz plot containing the same number of simulated events. The smooth curve in each plot is the boundary of the kinematically-allowed region. The matrix element $\mathcal{M}$ assumed in the Monte Carlo calculation is

$$\mathcal{M} \sim 1 + 2\sigma_o(2T_{\pi^o} - T_{\pi^o max}) M_K/M_\pi{}^2 \quad 21/$$

with $\sigma_o = -0.204 \pm 0.018$, as given by Nefkens.

T_{π^o} = center of mass kinetic energy of π^o.

The experimental Dalitz plot has fewer events in the region of high energies than the Monte Carlo plot, but this difference is not regarded as significant, considering the limited statistics of the experiment. There are two points outside the allowed boundary in the experimental plot due to the measuring resolution of the experiment.

Figure 24 shows histograms of the laboratory energies for the π^- and π^+ with the normalized Monte Carlo curves superimposed. The π^- spectrum is shifted to slightly lower energies with respect to the π^+ spectrum as a result of the $M_{\pi^- p} < 1135$ cut which was applied to both the experimental data and the Monte Carlo events. The agreement between the experimental and theoretical spectra is satisfactory.

Figure 23. Predicted and experimental Dalitz plots.

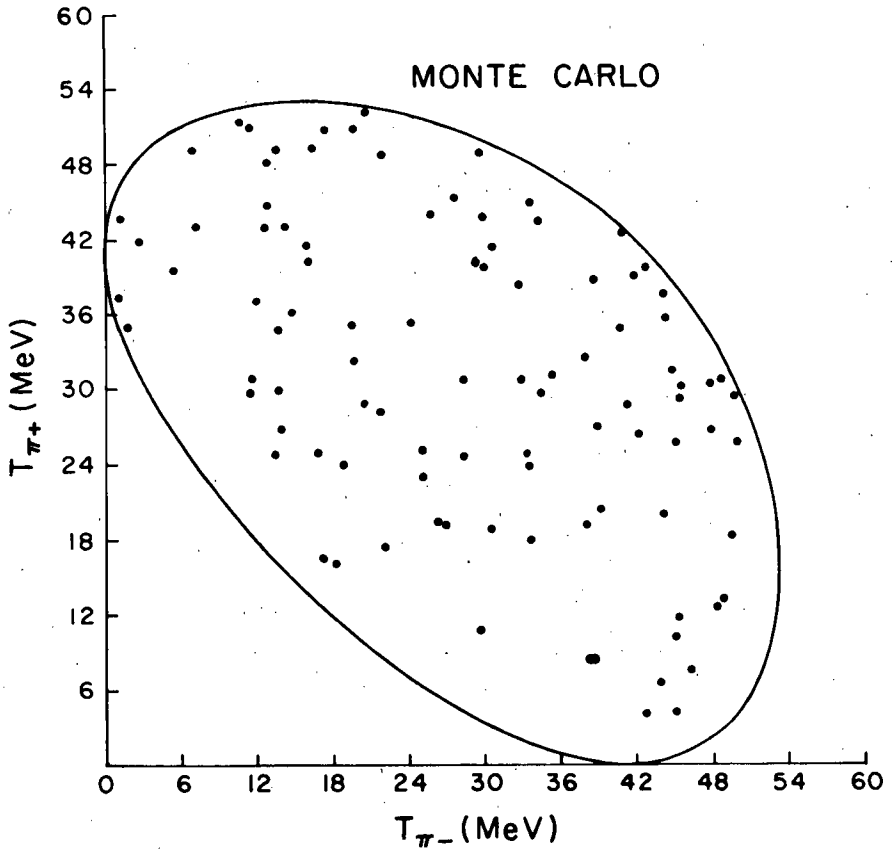
MONTE CARLO
60
54
48
42
36
30
24
18
12
6
0
6
12
18
24
30
36
42
48
54
60
$T_{\pi+}$ (MeV)
$T_{\pi-}$ (MeV)

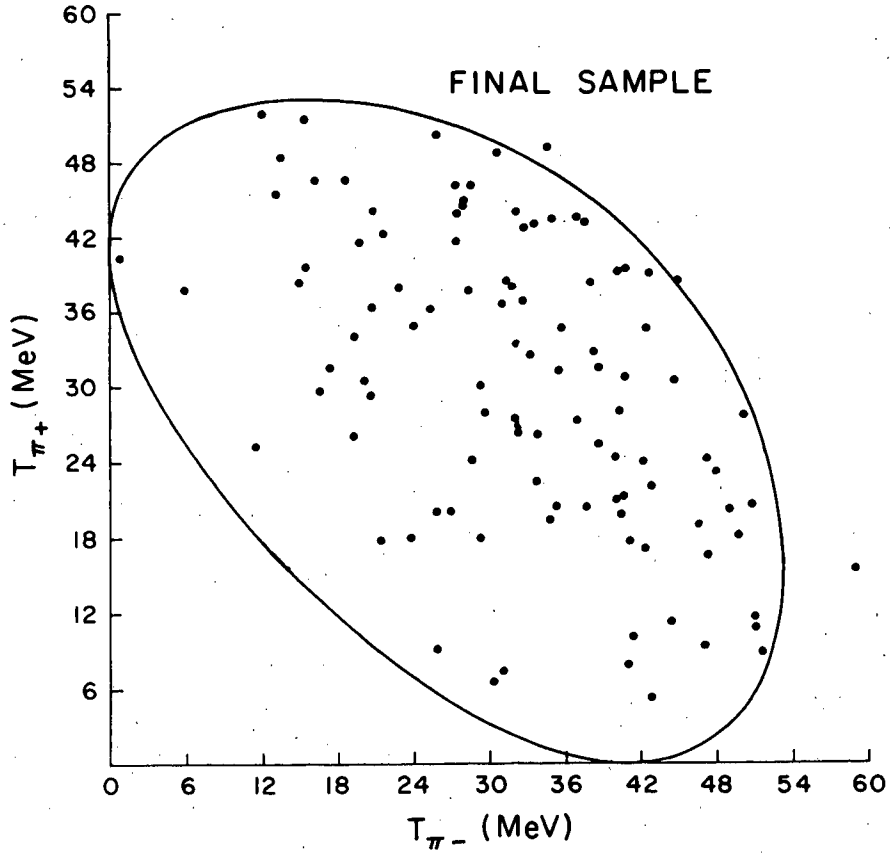
FINAL SAMPLE
60
54
48
42
36
30
24
18
12
6
0
6
12
18
24
30
36
42
48
54
60
$T_{\pi+}$ (MeV)
$T_{\pi-}$ (MeV)

Figure 24. Pion laboratory energies for events in the final sample. Smooth curves are Monte Carlo predictions.

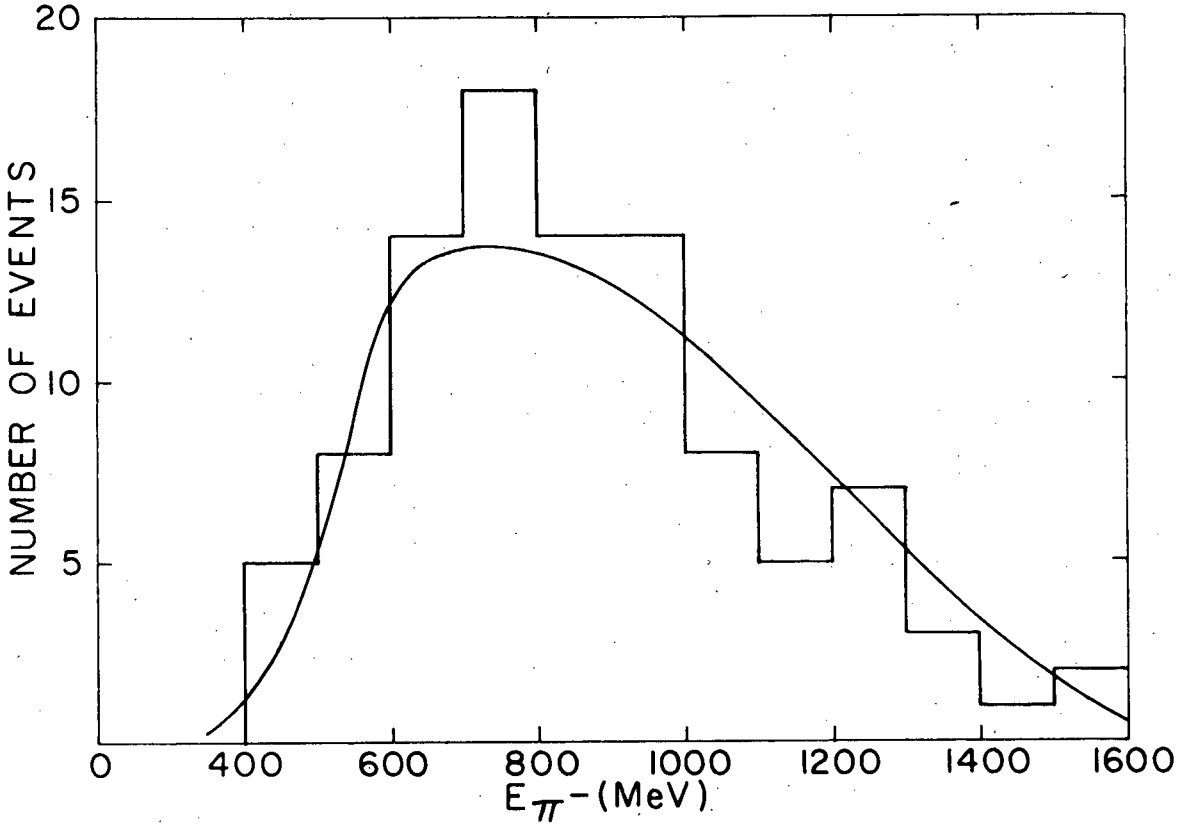
20
15
10
5
NUMBER OF EVENTS
0
400
600
800
1000
1200
1400
1600
E_{π^-} (MeV)

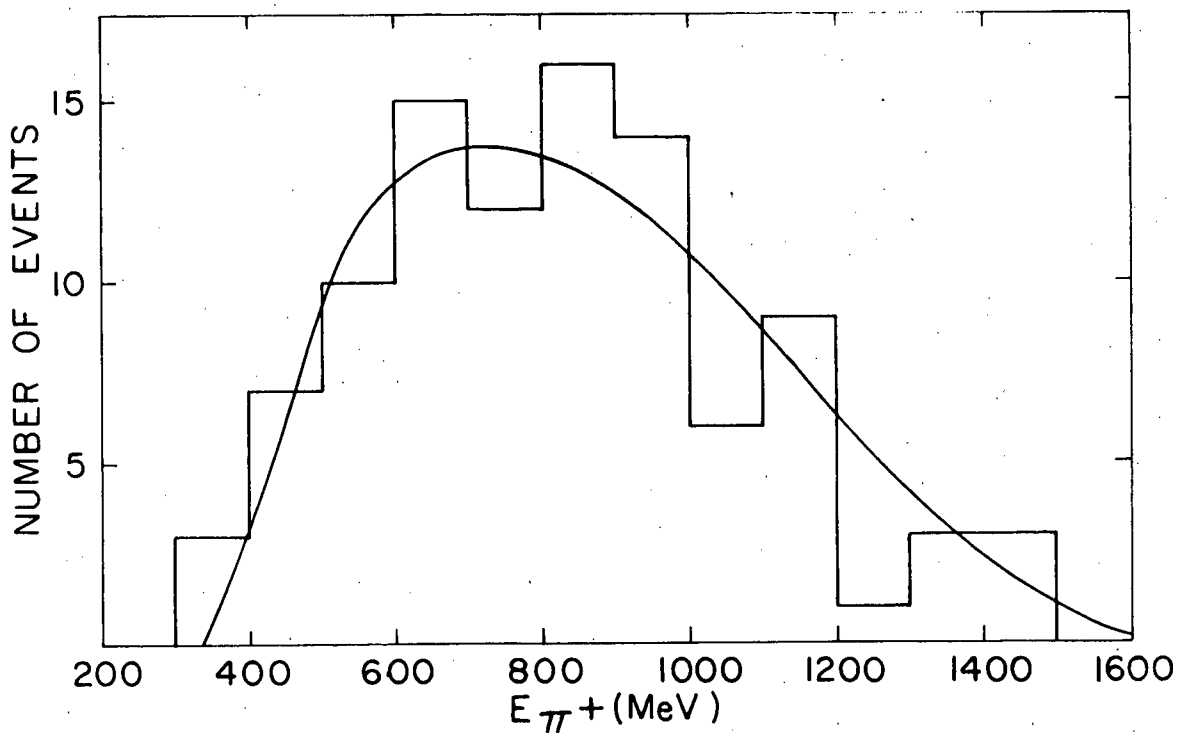
15
10
5
NUMBER OF EVENTS
200
400
600
800
1000
1200
1400
1600
E_{π^+} (MeV)

B. Experimental Resolution

This section discusses the errors in the determination of the quantities necessary for the calculation of t_K, the proper decay time of the K^o. t_k, expressed in units of the K_S^o lifetime, τ_S, is given by

$$t_K = \frac{d}{\gamma_K \beta_K c\tau_S}$$

where d is the K^o laboratory decay distance

γ_K is the K^o energy in units of the K^o mass

$\beta_K = \frac{\sqrt{\gamma_K^2 - 1}}{\gamma_K}$ is the K^o velocity in units of c.

γ_K can be calculated to within a two fold ambiguity, provided one knows the laboratory momenta of the π^+ and π^- and the laboratory direction of the K^o. This direction and the decay distance d are determined by the locations of the K^o production and decay points.

Momentum measurement. The error in measurement of the momenta of individual tracks is estimated to be ± 2.25% for 1 GeV/c particles.[22] This value was obtained by measuring events twice on the Hydel and comparing the momenta obtained from the two measurements.

Determination of the production point. For the majority of events, the production point was taken to be the intersection of the beam track trajectory with a perpendicular plane passing through the center of the target. In cases where a good vee from Λ decay was observed in the Λ chamber, the production point was taken to be the intersection of the plane formed by this vee and the beam trajectory. Since the length of the target

was 3 cm., the measured z coordinate (z axis being parallel to the beam centerline) of the production point could in extreme cases be wrong by as much as 1.5 cm. The measured transverse coordinates of the production point are correct to within 0.015 inch.

Determination of the decay point. Two methods were used. For events with early decays (decay point upstream of K chamber), straight line fits were made to the π^+ and π^- tracks in the Λ and K chambers, and the coordinates of the point of closest approach were calculated. In addition, the Miss, or smallest separation between the two tracks at the point of closest approach, was calculated. If the Miss was smaller than .100 inch, this point was taken to be the K^o decay point. For some events with early decays, this method could not be used because the tracks in the Λ and K chambers were not well enough defined to determine a good intersection point by this method, or the sparks from several tracks overlapped. For these events and for later decays, a second method was employed. Using the calculated momenta of the π^+ and π^- tracks and the calculated direction unit vectors for a point on each track near the center of the magnet chambers, a computer program stepped both tracks upstream through the field region into the fiducial region and determined the point of closest approach and the Miss. The table lookup of magnetic field values was used by the stepping program. The standard deviations for determination of decay point locations for all events were σ_x = .041 inch, σ_y = .081 inch, σ_z = .653 inch,[22/] where x is the vertical direction, y is the horizontal direction perpendicular to the beam centerline, and z is the direction parallel to the beam centerline.

Ths Miss distribution gives a further measure of the accuracy of determining the decay point locations. Figure 25 gives a histogram of the Miss for all events in the final sample.

Kinematic ambiguity. There is a two-fold ambiguity in the calculation of the K^o laboratory energy from the measured laboratory momenta of the charged pions and the measured laboratory direction of the K^o. For all events, we have taken the solution closest to $\gamma_K = 5.3$, where γ_K is the K^o laboratory energy in units of its mass. Monte Carlo calculations indicate that this method of choosing the K^o energy gives the correct solution for 88% of the events. Only 4% of the events should have a solution incorrect by more than 10%, according to the Monte Carlo program. For these events, the low energy solution was correct, but the high energy solution was chosen. Thus, the calculated value of the decay time would be too low.

Energy spectrum. Figure 26 shows a histogram of the calculated K^o laboratory energy E_K for the events in the final sample. Also shown is the Monte Carlo prediction (solid curve) normalized to the same number of events. Since no experimental error was included in the Monte Carlo calculation, the predicted curve is more peaked than the experimental one. We estimate that the experimental error in the determination of E_K is of the order of 5%. If a 5% Gaussian spread is included in the Monte Carlo result, the dashed curve is obtained, which more nearly approximates the experimental histogram.

The overall error in determination of t_K is estimated to be $\pm\ 0.25\ \tau_S$.

Figure 25. Miss at intersection for events in the final sample.

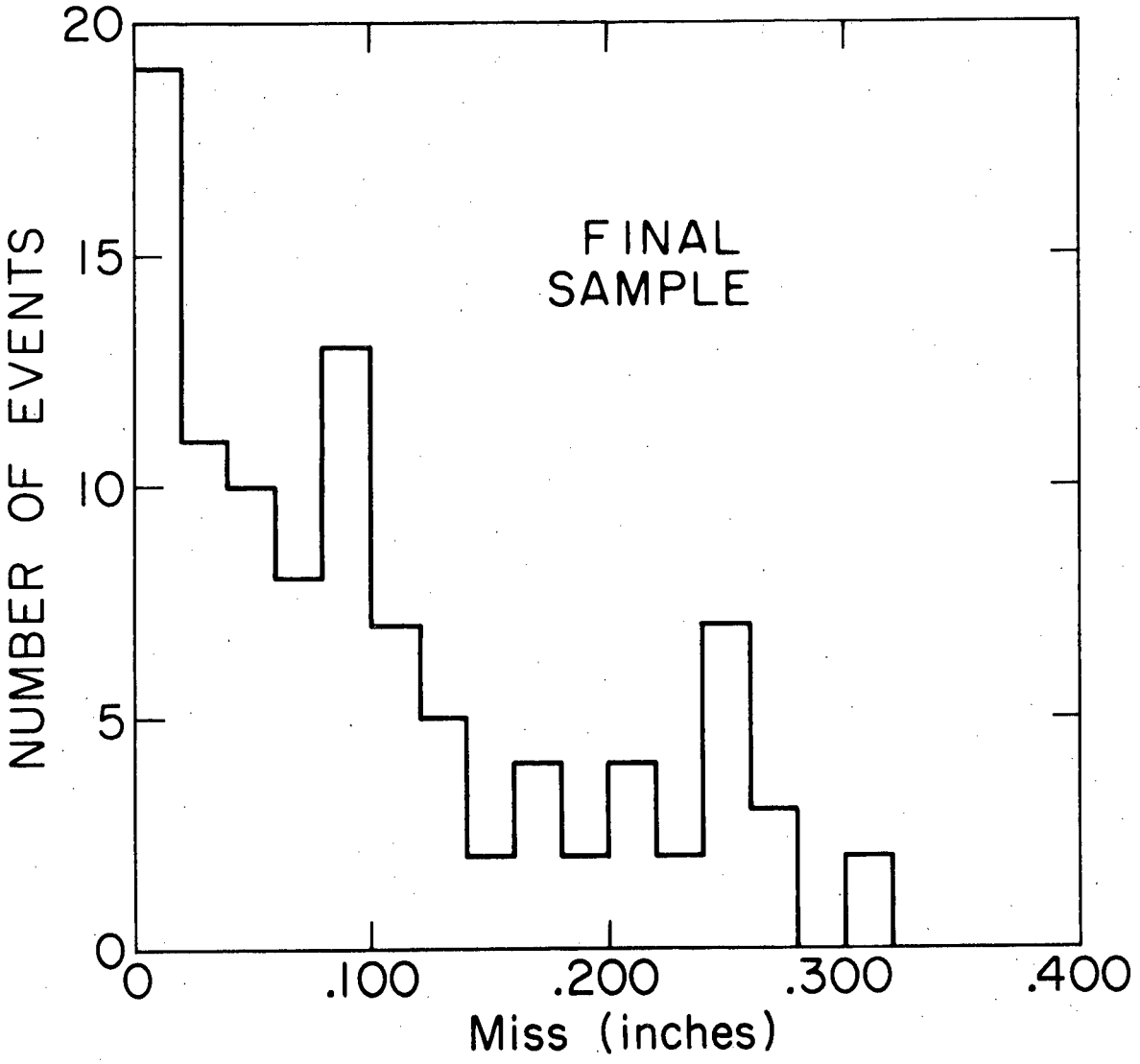
20
15
10
5
0
NUMBER OF EVENTS
FINAL
SAMPLE
0
.100
.200
.300
.400
Miss (inches)

Figure 26. K^{O} laboratory energy spectrum for events in the final sample. Smooth curve is Monte Carlo prediction with no error included. Dashed curve is Monte Carlo prediction with Gaussian error (σ = 5%) folded in.

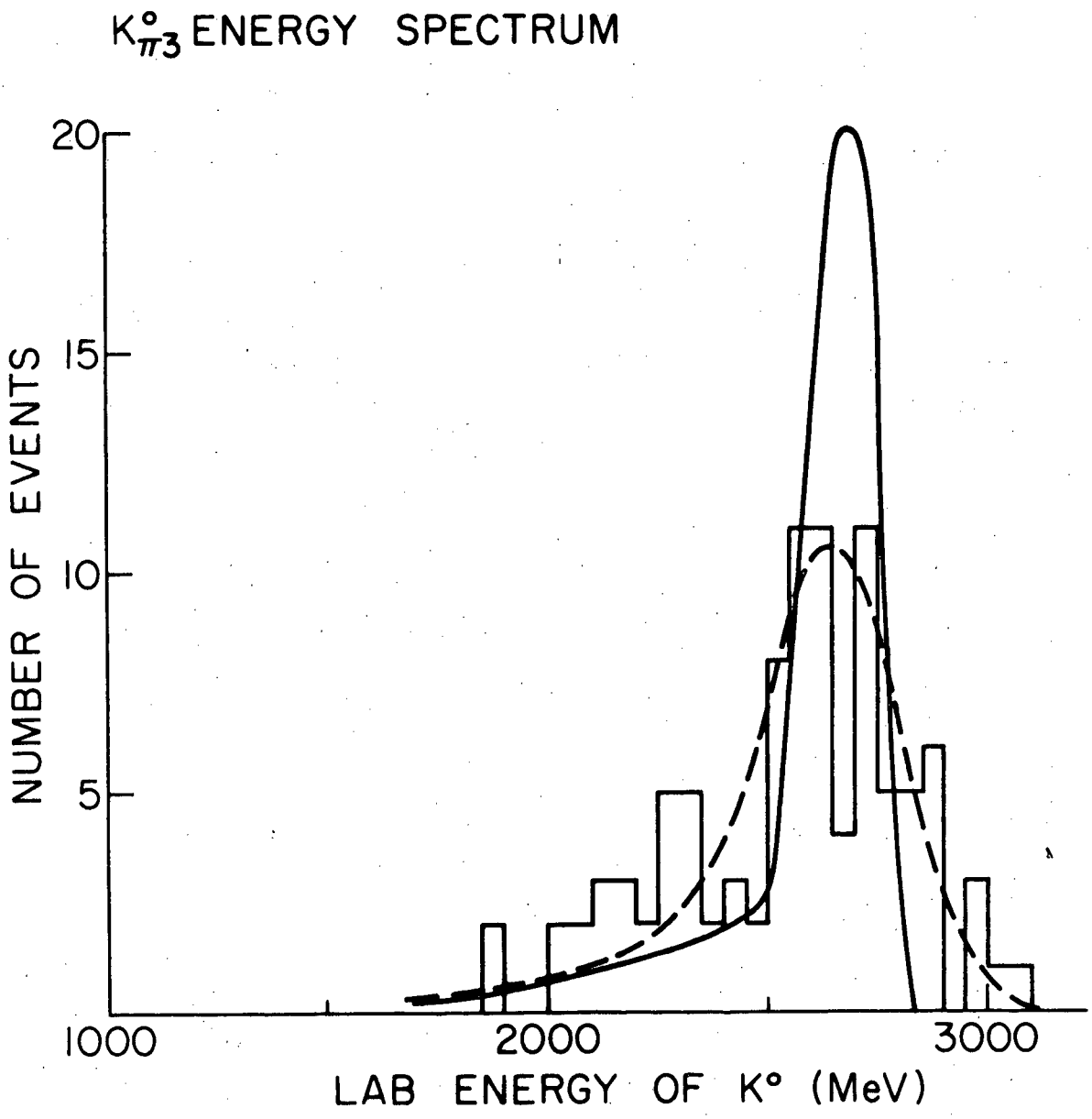
$K^{\circ}_{\pi 3}$ ENERGY SPECTRUM
NUMBER OF EVENTS
20
15
10
5
1000
2000
3000
LAB ENERGY OF K° (MeV)

X. RESULTS AND CONCLUSIONS

The final data were fit for the most probable values of x, y using both maximum likelihood and χ^2 minimum fitting programs. Both methods of fitting gave two values for (x,y).

The data used for these fits are tabulated in Appendix B. The expression for the time distribution of $K^o \to \pi^+\pi^-\pi^o$ decays, which was used in these fits, is

$$\Gamma(t;x,y) = \text{Const.}\ (x^2 + y^2)\ e^{-\gamma_S t} + e^{-\gamma_L t} + 2(x\cos\delta t - y\sin\delta t)\ e^{-1/2(\gamma_S+\gamma_L)t}$$

with

$$x + iy = \frac{a(K_S^o \to \pi^+\pi^-\pi^o)}{a(K_L^o \to \pi^+\pi^-\pi^o)}$$

$$\delta = 0.467$$

$$\gamma_S = 1.000$$

$$\gamma_L = \frac{\tau_S}{\tau_L} = \frac{0.862 \times 10^{-10}}{5.38 \times 10^{-8}} = 1.602 \times 10^{-3}$$ [18]

t is the K^o proper time in units of τ_S.

A. Maximum Likelihood Fit

The likelihood function used was

$$\mathcal{L}(x,y) = \prod_i \left[\frac{\Gamma(t_i;x,y)\epsilon(t_i)}{\int_{t=0.5}^{t=6.5} \Gamma(t,x,y)\epsilon(t)dt} \right]$$

$\epsilon(t)$ is the geometrical $K^o_{\pi 3}$ detection efficiency as a function of K^o proper decay time. This efficiency was calculated by the Monte Carlo program. Figure 27 shows a plot of $\epsilon(t)$. The integral in the denominator was evaluated numerically.

Figure 28 shows the likelihood map with contours of equal likelihood drawn. The contours shown indicate relative likelihood $e^{-n^2/2}$ with respect to the maximum. n is the number of standard deviations from the maximum. The likelihood maximum occurs at the point

$$x = -2.94 \pm 0.36, \quad y = -0.11 \pm 0.55$$

and a relative maximum occurs at the point

$$x = -0.09 \pm 0.19, \quad y = +0.56 \pm 0.43 \ .$$

The errors given are statistical only. The first maximum is favored by about two standard deviations over the second. Nevertheless, we place more confidence upon the second result, which is consistent with CPT and the $\Delta I = 1/2$ rule. In addition, other experimental data rule out the first result, as will be discussed later.

Figure 29 shows the time distribution for the 99 events used for this fit. The curves superimposed on the histogram are the theoretical distributions corrected for geometrical efficiency. The curves shown are for the two likelihood results as well as for $x = y = 0$.

Figure 27. Geometrical detection efficiency.

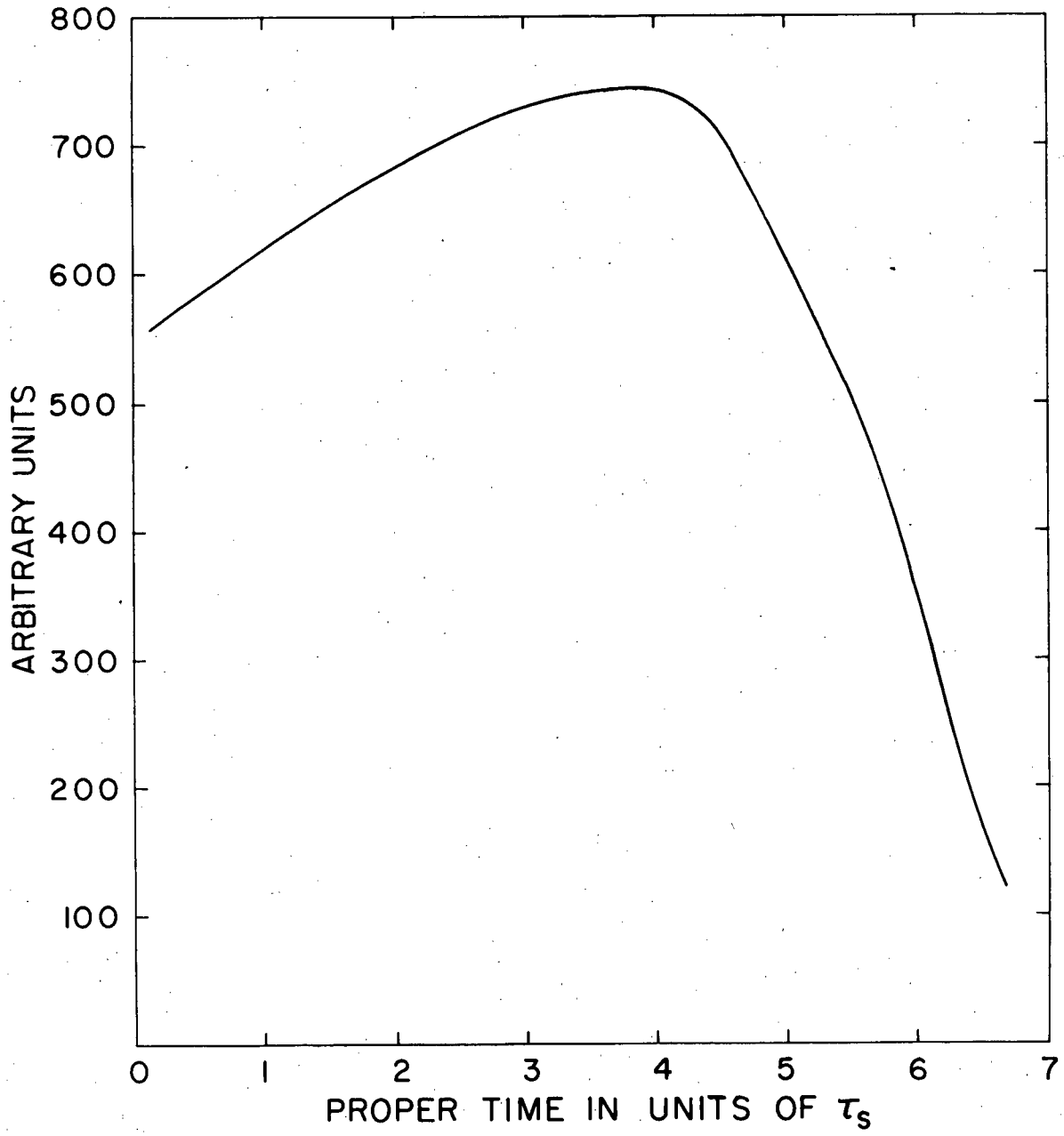
800
700
600
500
400
300
200
100
ARBITRARY UNITS
0
1
2
3
4
5
6
7
PROPER TIME IN UNITS OF τ_s

Figure 28. Contours of equal likelihood for the time distribution of 99 events. The contours shown indicate relative likelihood $e^{-n^2/2}$ with respect to the maximum.

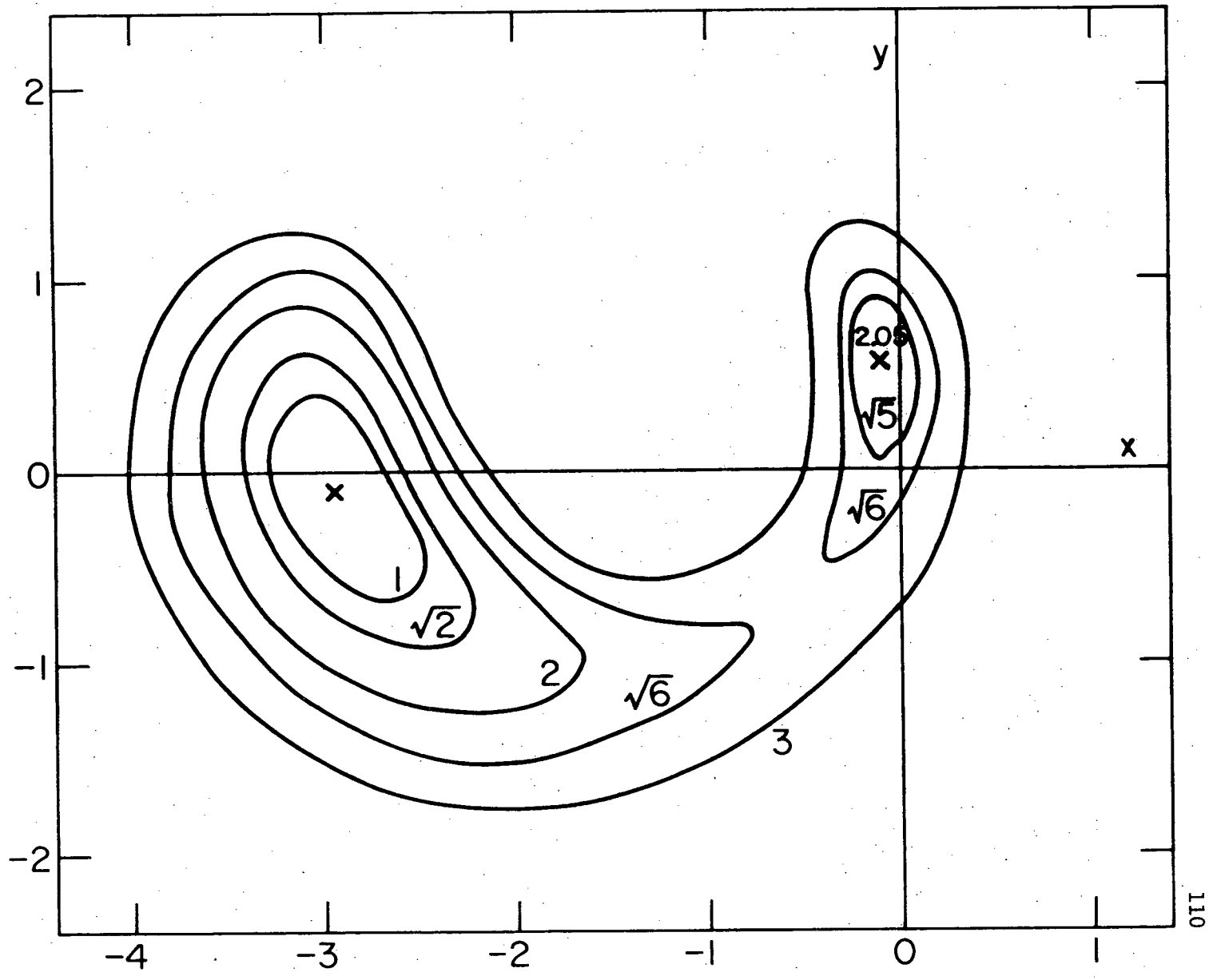
y
x
2
1
0
-1
-2
-4
-3
-2
-1
0
1
2.06
√5
√6
1
√2
2
√6
3

Figure 29. Time distribution for the 99 events in the final sample. The smooth curves are theoretical distributions corrected for efficiency.

TIME DISTRIBUTION FOR FINAL SAMPLE

CURVE A : X=-0.09 , Y= 0.56
CURVE B : X= 0.00 , Y= 0.00
CURVE C : X=-2.94 , Y=-0.10

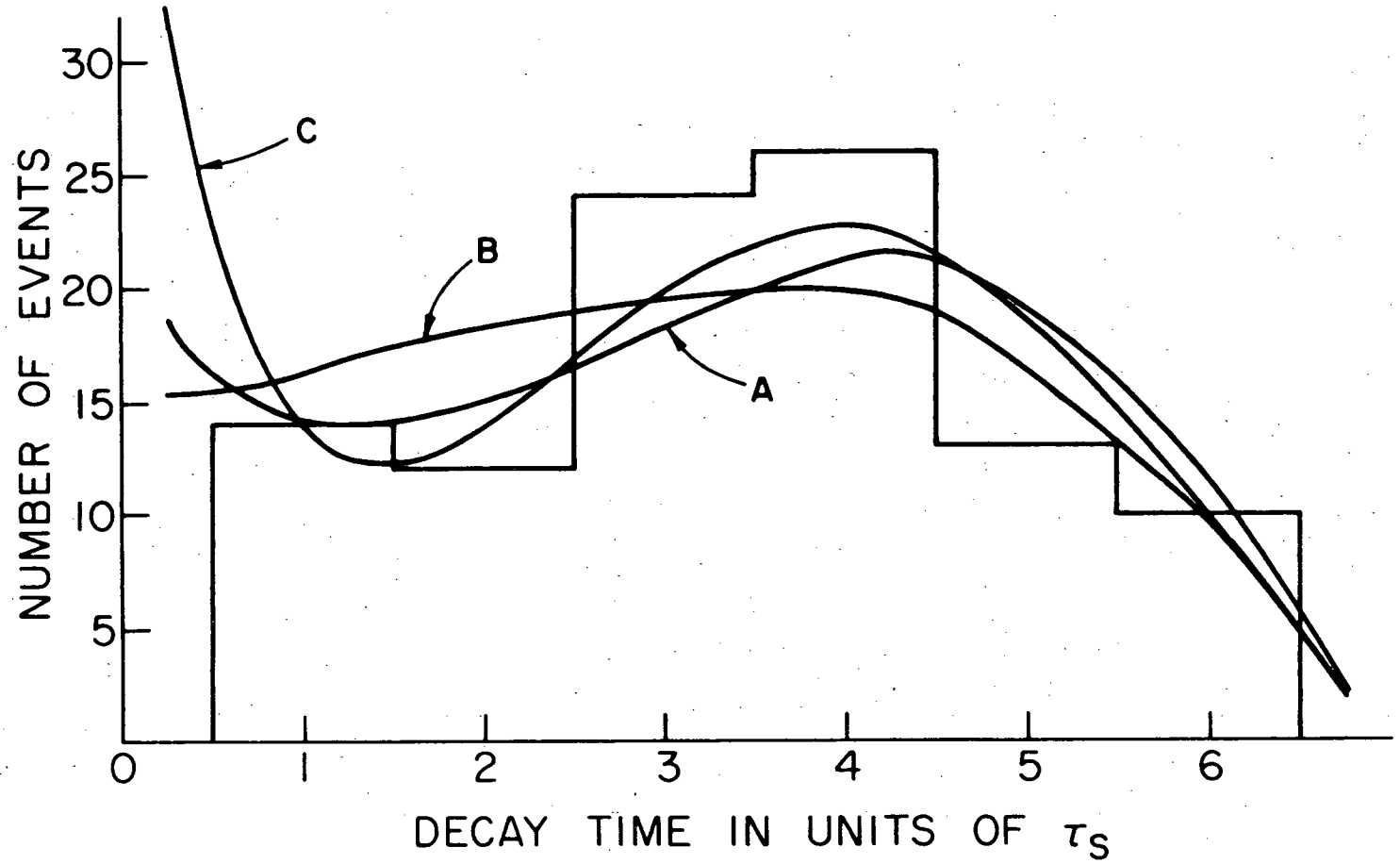

B. Chi Square Minimum Fit

The data were also fit by a χ^2 minimizing program. For this fit, the data were binned as shown in the histogram in Figure 29 , with bin width equal to one K_S^o lifetime. Two minima were found with the following values for x, y:

$x = -0.29 \pm 0.48, \quad y = -0.06 \pm 0.78$

$\chi^2 = 4.71$ for 4 degrees of freedom

Probability = 31.85%

$x = -2.82 \pm 0.61, \quad y = -0.30 \pm 0.68$

$\chi^2 = 3.23$ for 4 degrees of freedom

Probability = 51.05%

The errors are statistical only.

For x = y = 0 we obtained:

$\chi^2 = 6.10$ for 4 degrees of freedom

Probability = 19.2%.

Due to the limited statistics of the experiment, the χ^2 results are quite dependent on the binning used. Therefore, we place more credence upon the likelihood fits.

C. Estimate of ϵ

The contribution of $\pi^+\pi^-\pi^o$ states to the CP violating parameter ϵ may be estimated using the expression given by Haggerty.[5]

$$\epsilon_{3\pi} \approx 2y\ (10^{-4})(1-i)$$

If we use the value for y obtained in the maximum likelihood fit, $y = 0.56 \pm 0.43$, then we obtain

$$\epsilon_{3\pi} \approx (1\pm1) \times 10^{-4}\ (1-i)$$

which is about 1/20 the value of $\eta_{\pm}$.

D. Results of Other $K_S^o \rightarrow 3\pi$ Experiments

Table 6 presents the results of other experiments [5,23-26] which have sought to measure $x + iy$, along with the results of the present experiment. Figure 30 shows a plot of the other results, as well as the results of this experiment. Figure 31 shows the likelihood contour plots for 3 other experiments* which fit for $x + iy$ by the maximum likelihood method.

Two of the previous experiments [23,24] observed $\overline{K}^o$ decays; the others, including the present experiment, observed K^o decays. Since the same definition for $x + iy$ was used for both the K^o and the $\overline{K}^o$ experiments, the results may be directly compared. The only difference in the expression for the time distribution for K^o and $\overline{K}^o$ decays is the sign of the interference term.

The experiments by Behr *et al.* [25] and by Haggerty [5] assume x to be negligible and present their final results in terms of y only.

---

*The likelihood contour plot by Haggerty (Ref. 5) is one of six plots he presents for different subsets of his data.

Table 6. Results of $K_S \to \pi^+\pi^-\pi^o$ Experiments

Experiment	Ref.	Method	x	y	Events
Haggerty (Wisconsin)	5	Heavy liquid bubble chamber K^+ charge exchange	assumed 0	-0.03 ± 0.5	88 $\pi^+\pi^-\pi^o$
Meisner et al. (Mass.,BNL,Yale)	23	Hydrogen bubble chamber $K^-p \to \bar{K}^o n$	$2.75\ ^{+0.65}_{-0.60}$	$0.50\ ^{+0.70}_{-0.55}$	50 $\pi^+\pi^-\pi^o$
Webber et al. (LRL)	24	Hydrogen bubble chamber $K^-p \to \bar{K}^o n$	$0.5\ ^{+1.5}_{-0.6}$ *	$0.8\ ^{+0.4}_{-0.8}$ *	53 $\pi^+\pi^-\pi^o$
Behr et al. (Paris,Milano, Padova,Orsay)	25	Heavy liquid bubble chamber K^+ charge exchange	assumed 0	$-\left(0.34\ ^{+0.19}_{-0.59}\right)$	136 $\pi^+\pi^-\pi^o$ 54 $\pi^o\pi^o\pi^o$
Anderson et al. (LRL,Wisconsin)	26	Hydrogen bubble chamber $\pi^-p \to K^o\Lambda$	$0.1\ ^{+0.5}_{-0.4}$	0.6 ± 0.9	18 $\pi^+\pi^-\pi^o$
THIS EXPERIMENT		Optical spark chambers $\pi^-p \to K^o\Lambda$	-0.09 ± 0.19 -2.94 ± 0.36	0.56 ± 0.43 -0.11 ± 0.55	99 $\pi^+\pi^-\pi^o$

* Errors estimated from limits of 1 s.d. likelihood contour.

Figure 30. Results of $K_S^o \rightarrow \pi^+\pi^-\pi^o$ experiments.

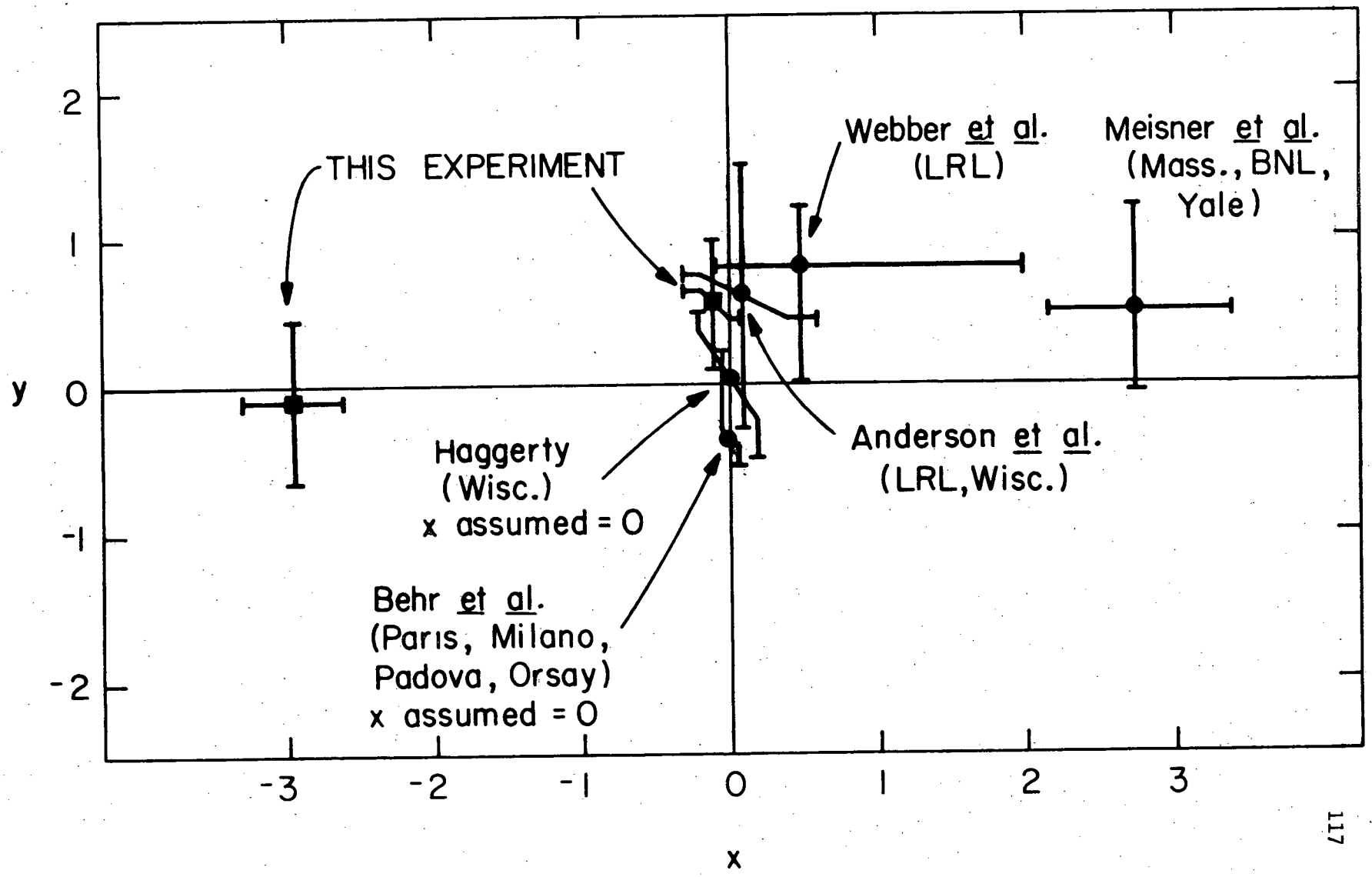
THIS EXPERIMENT
Webber et al.
(LRL)
Meisner et al.
(Mass., BNL,
Yale)
Haggerty
(Wisc.)
x assumed = 0
Anderson et al.
(LRL,Wisc.)
Behr et al.
(Paris, Milano,
Padova, Orsay)
x assumed = 0
y
x
2
1
0
-1
-2
-3
-2
-1
0
1
2
3

Figure 31. Likelihood contour plots for four $K_S^o \rightarrow \pi^+\pi^-\pi^o$ experiments.

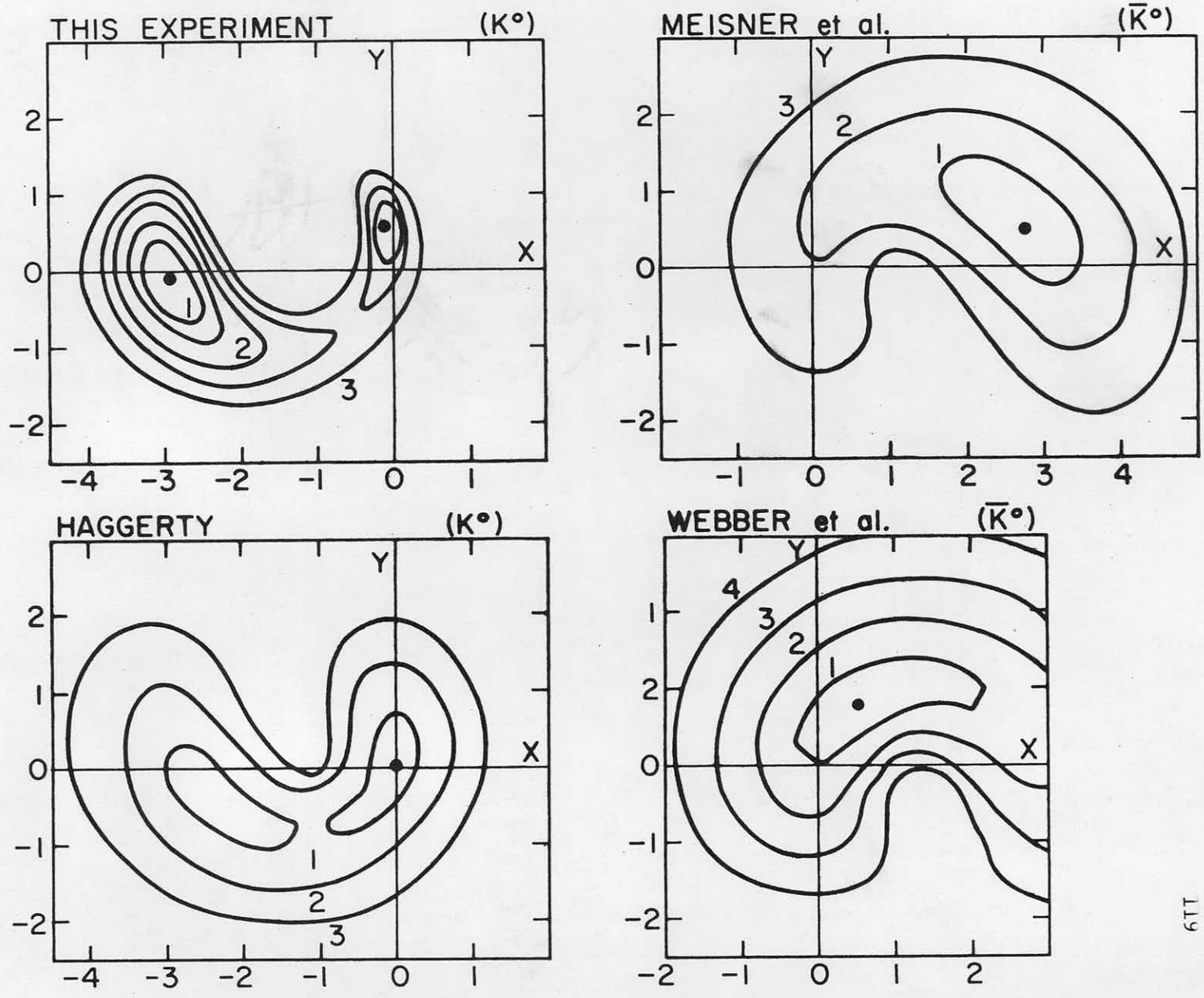
THIS EXPERIMENT
(K°)
MEISNER et al.
(K̄°)
HAGGERTY
(K°)
WEBBER et al.
(K̄°)
X
Y

E. Discussion of Experimental Results

Both the likelihood and χ^2 fitting programs have found results near $x = -3$ as well as results consistent with $x = y = 0$. We wish to argue that the results near $x = -3$ should probably be excluded on physical and experimental grounds.

As stated earlier, Glashow and Weinberg have shown[10] that if the magnitude of $x + iy$ is large, then CPT and the $\Delta I = 1/2$ rule require that the phase of $x + iy$ be nearly $\pm 90^\circ$. This result comes from a general proof that if a_1 and a_2 are amplitudes for decay of K_1^o and K_2^o into any CPT-conjugate channel which is an eigenstate of the strong interaction matrix then

$$\left| \frac{2\mathrm{Re}(a_1 a_2^*)}{|a_1|^2 + |a_2|^2} \right| < \frac{1}{50} .$$

We have shown earlier that this experiment is sensitive only to interference between K_S^o and K_L^o states both decaying to the symmetric I = 1 state of $\pi^+\pi^-\pi^o$, which is a CPT-conjugate channel and an eigenstate of the strong interaction matrix. Then $x + iy = a_1/a_2$.

If $a_1 \approx -3a_2$ then $\left| \frac{2\mathrm{Re}(a_1 a_2^*)}{|a_1|^2 + |a_2|^2} \right| = \left| \frac{2\mathrm{Re}[(-3a_2)a_2^*]}{10|a_2|^2} \right| = 0.6 > \frac{1}{50}$.

This suggests that $x + iy \approx -3$ is not a physically allowed solution.

Figure 31 shows the likelihood contours from three other experiments along with those of the present experiment. As indicated in the figure, two of these experiments had K^o initial states, and the other two experiments had

$\overline{K}^o$ initial states. All four experiments have kidney-shaped contours at a distance of two to three standard deviations out from the likelihood maximum. In each case, the two-standard-deviation contour includes the region of the imaginary axis near the origin. Two experiments find maxima in this region and the present experiment finds a secondary maximum in this region. But the two-standard-deviation controus also include the region near $x = +3$ for the K^o experiments and the region near $x = -3$ for the $\overline{K}^o$ experiments. The present K^o experiment finds its absolute maximum near $x = -3$, and one of the $\overline{K}^o$ experiments, finds its absolute maximum near $x = +3$. Since $x + iy$ is defined in the same manner for both K^o and $\overline{K}^o$ experiments, both types of experiments should obtain consistent results. Therefore, we maintain that the solutions near $x = \pm 3$ are experimentally inconsistent with each other and should be ruled out.

We then give as our final result

$$x = -0.09 \pm 0.19, \quad y = 0.56 \pm 0.43$$

This result is consistent with CPT conservation and the $\Delta I = 1/2$ rule. It indicates a possible violation of CP, but is also consistent with CP conservation at the one-standard deviation level.

APPENDIX A: THE MONTE CARLO CALCULATIONS

This appendix describes the Monte Carlo program which was written for the present $K^o_{\pi 3}$ experiment and for the concurrently run K^o_{e3} and $K^o_{\mu 3}$ experiments. The Monte Carlo program was used to compute the geometrical efficiency of the apparatus for triggering on K^o decays into various modes. This efficiency is calculated as a function of the proper time of the K^o, i.e., the time between the production and decay of the K^o in its own rest frame.

Simulated events are generated given the following constraints:

1) A π^- beam of specified momentum impinges on the carbon target.

2) A K^o and a Λ^o are produced in the target.

3) The Λ^o decays into a π^- and a proton.

4) The K^o decays into a specified mode at a specified proper time.

All other necessary kinematical quantities such as the angles and energies of the particles involved are chosen randomly as described below. Once the event has been generated, the program asks whether it would trigger the apparatus. The efficiency at the given value of the K^o proper time is then the ratio of the number of successful triggers to the number of simulated events.

For the initial discussion it will be assumed that the production mode is $\pi^- p \rightarrow K^o \Lambda^o$. Later, calculations of the effect of three body production modes will be discussed.

The following K^o decay modes have been considered:

$$K^o \rightarrow \pi^{\pm} e^{\mp} \overset{(-)}{\nu}$$

$$K^o \rightarrow \pi^{\pm} \mu^{\mp} \overset{(-)}{\nu}$$

$$K^o \rightarrow \pi^+ \pi^- \pi^o$$

$$K^o \rightarrow \pi^+ \pi^-$$

A description follows of the method for generating simulated events.

A. Choice of Production Point

The production point is chosen to lie along the beam trajectory, which is taken to be parallel to the z axis. The x and y coordinates of the beam pion (and hence of the production point) are chosen randomly to lie within .250 inches from the centerline of the cylindrical carbon target, assuming uniform density of beam particles in this cross sectional area. The z coordinate of the production point is chosen within the target volume using an exponentially weighted random number distribution. The weighting factor contains the interaction length for 3 GeV/c negative pions.

B. Choice of Production Angles and Energies for K^o and Λ^o

The beam pi interacts with a proton in the target. The proton is assumed to have a Fermi momentum p_F chosen randomly according to the distribution $p_F^2 e^{-p_F^2/p_o^2}$ with p_o = 250 MeV/c. The quantities $\cos\theta_F$ and ϕ_F, where θ_F and ϕ_F are the angles of the proton direction in spherical coordinates, are chosen randomly.

Next the production angles for the K^o (and hence of the Λ^o also) in the $\pi^- p$ rest frame must be chosen. The azimuthal angle ϕ is chosen randomly. $\cos\theta$, where θ is the polar angle, is chosen using a random number

distribution weighted according to an experimental angular distribution for K^oA^o production found in the literature.[27] The momenta and energies of the K^o and the Λ^o in the π^-p rest frame are calculated using the invariant mass of the π^-p system and two body kinematics. Using Lorentz transformations and Euler angle rotations, the energies and vector momenta of the K^o and the Λ^o are transformed to the standard laboratory system having the z axis parallel to the beam direction.

C. The Lambda Decay

The proper decay time of the lambda is now chosen randomly according to an exponential decay distribution. Using the decay time and vector momentum of the Λ^o, its decay point is calculated. The Λ^o is constrained to decay into the π^-p mode. The energies and momenta of the π^- and p in the Λ^o rest frame are known from two body kinematics. Their spherical angles in the Λ^o rest frame are chosen randomly assuming an isotropic angular distribution. This assumes that $\alpha\overline{P} = 1$, where α is the asymmetry parameter and $\overline{P}$ the polarization of the lambda. The energies and vector momenta of the π^- and p are then transformed to the standard lab system.

The program now asks whether the Λ^o decay will trigger the $\lambda dE/dx$ hodoscope. If the Λ^o decay is upstream of the anticounter or downstream of the $\lambda dE/dx$ hodoscope, the event is rejected. Using the vector momentum of the proton, the program determines whether it would hit a counter in the hodoscope and whether it would lose enough energy in the scintillator to cause a photomultiplier pulse above the threshold of the discriminator (The discriminators were set to accept 550 MeV/c protons.) If the proton would

not cause a trigger, the same questions are asked for the pi. If neither particle would trigger the hodoscope, the event is rejected.

D. The K^o Decay

The decay point of the K^o is now calculated using the proper time for the bin under consideration. If the K^o decay position is upstream of the anticounter or downstream of the ϕ hodoscope, the event is rejected.

Next the energies and angles of the K^o decay products in the K^o rest frame are chosen randomly according to theoretical Dalitz plot distributions. The procedure for the three-body decays is as follows: The kinetic energies of the two charged particles are chosen randomly between zero and their maximum allowed values. A calculation is performed to determine whether this choice of kinetic energies corresponds to a point within the Dalitz plot boundary. If not, a new pair of energies is chosen and the Dalitz boundary test repeated. When a pair of kinetic energies within the Dalitz boundary has been found, the Dalitz plot density for this choice of energies is calculated, using the expressions given below. A random number R is chosen between zero and the maximum allowed density. If R is smaller than the calculated density, the choice of energies is acceptable. Otherwise a new pair of energies must be picked and the whole process repeated. The Dalitz plot densities used are:

K^o_{e3}: Density $\propto \left[\frac{(2E^*_e E^*_\nu)}{M_K} + E^*_\pi - E^*_{\pi max} \right]$ 28/

neglecting the small form factor f_-.

$K^o_{\mu 3}$: Density $\propto [2M_K E^*_\nu - M_K^2 (E^*_{\pi max} - E^*_\pi] f_+$

$$- 2M_\mu^2 E^*_\nu f_+ f_2 + M_\mu^2 (E^*_{\pi max} - E^*_\pi) f_2^2 \quad 29/$$

where $f_2 = \frac{1}{2}(f_+ - f_-)$.

We use $f_- = -f_+$.

$K^o_{\pi 3}$: Density $\propto$ $1 - 1.042 \times 10^{-2}(2T^*_\pi - 53.80)$. 21/

E^*_i, T^*_i, M_K are the total energy, kinetic energy of particle i in the K^o rest frame and the mass of the K^o.

Knowing the momenta of the three particles in the K^o rest frame, the angles of two particles with respect to the direction of the third can be calculated in a straightforward manner. The azimuthal angle defining the orientation of the plane defined by the two particles is chosen randomly. The angles of the third particle in the laboratory are chosen randomly. Using the Lorentz transformation and several Euler angle rotations, the energies and vector momenta of the K^o decay products are then transformed to the standard lab system.

For the decay $K^o \rightarrow \pi^+\pi^-$, the foregoing calculations are much simpler. The energies of the two pis in the K^o rest frame are known from two-body kinematics. The decay is isotropic in this frame. One need only choose randomly two angles and then transform the energies and vector momenta of the two pis to the standard lab system.

E. Tracking the K^o Decay Products through the Magnetic Field

A subroutine steps the two charged particles from the K^o decay through the magnetic field. Measured values of the field components at three inch intervals are stored in a table look-up. The subroutine interpolates to obtain the average values of the field components for each step. Tests are made to determine whether the two charged particles would trigger the ϕ and ρ counters and whether they would hit the frame of the magnet spark chambers or any part of the magnet. If either particle fails to trigger the counters or hits an obstacle, the event is rejected. In addition, for K^o_{e3} decay, the event is rejected if the electron goes into the gap between the left and right shower chambers. This is necessary since visible identification of the electron shower in these chambers is required in the K^o_{e3} data analysis. For $K^o_{\mu 3}$ decay, a test is made to see whether the muon would trigger the muon hodoscope.

F. Photons

For $K^o_{\pi 3}$ decay, the center of mass angles of the two photons from π^o decay are chosen randomly, assuming the π^o decay is isotropic. The momenta and angles of the photons are then transformed to the laboratory system. Geometrical tests are made to determine whether one photon would pass through the shower chambers.

G. Summary Tape

A complete description of each successful event is stored on magnetic tape in order that histograms and plots of appropriate quantities

can be made for comparison with the experimental data. In addition, the effects of cuts on the data can be determined. For the unsuccessful events, a tabulation is made of the reasons for failure.

H. Three-body Production Modes

The experimental K^o energy spectra for K^o decays show a strong peaking in the region of 2640 MeV which is consistent with the Monte Carlo generated energy spectrum of K^o's from $K^o\Lambda^o$ production plus $K^o\Sigma^o$ production followed by $\Sigma^o \rightarrow \Lambda^o\gamma$. However, the observed spectrum also shows a low energy tail which is not predicted by the $K^o\Lambda^o$ plus $K^o\Sigma^o$ calculation. In order to reproduce this low energy tail, it is necessary to include three-body production modes in addition to the $K^o\Lambda^o$ mode. The main contribution is believed to come from the following processes:

$$\pi^- p \rightarrow K^{o*}\Lambda^* \rightarrow K^o\pi^o$$

$$\pi^- p \rightarrow K^oY^{o*} \rightarrow \Lambda^o\gamma$$

Several K^* and Y^* resonances are believed to contribute the low energy K^o's seen in the experiment. The presence of these low energy K^o's has the effect of raising the efficiency in the later lifetimes.

In order to determine whether resonance production can account for the lower energy K^o's and to modify the efficiency accordingly, an attempt was made to simulate resonance modes in the Monte Carlo program. Extension of the kinematics calculations described above to include three-body

production modes is straightforward. However, the angular distributions and resonance decay mechanisms are not well known. Therefore several approximations are employed in the resonance calculations. The same angular distribution is used for $K^*\Lambda$, KY^*, and $K\Sigma$ production as for $K\Lambda$ production with the meson peaked forward. The K^* and Y^* resonances are taken to decay isotropically in their own rest frames.

Ideally one would like to include all allowed production modes in the Monte Carlo calculations weighted according to their measured cross sections. Unfortunately, knowledge of the cross sections, angular distributions, and resonance decay mechanisms for modes other than $K^o\Lambda^o$ and $K^o\Sigma^o$ is limited. Therefore, it was deemed unfeasible to do a sufficiently accurate Monte Carlo calculation which would include all possible modes. It was found that $K^{o*}(890)\Lambda^o$ gives a reasonable fit to the low energy K^o tail. Therefore we have used this mode along with the $K^o\Lambda^o$ and $K^o\Sigma^o$ modes in the final calculation.

The percentages of the three production modes to use were determined by a study of the energy spectrum for $K^o_S \rightarrow \pi^+\pi^-$ events ($K^o_{\pi 2}$) from the calibration roll. Figure 32 gives a histogram of this $K^o_{\pi 2}$ energy spectrum. The $K^o_{\pi 2}$ spectrum was used rather than the $K^o_{\pi 3}$ spectrum because our determination of the K^o energy was more accurate for two-body than for three-body decays. For two-body decays, the K^o energy can be calculated by measuring the momenta of the two charged particles from the decay. For three-body decays, it is necessary to know the direction of the K^o as well as the momenta of the two charged particles from the decay. The K^o direction is determined from the measured locations of the production and decay points. In addition, there is a kinematic ambiguity in the K^o energy calculation for the three-body decays.

Figure 32. Laboratory energy spectrum for $K_S^o \rightarrow \pi^+\pi^-$ events from the calibration roll.

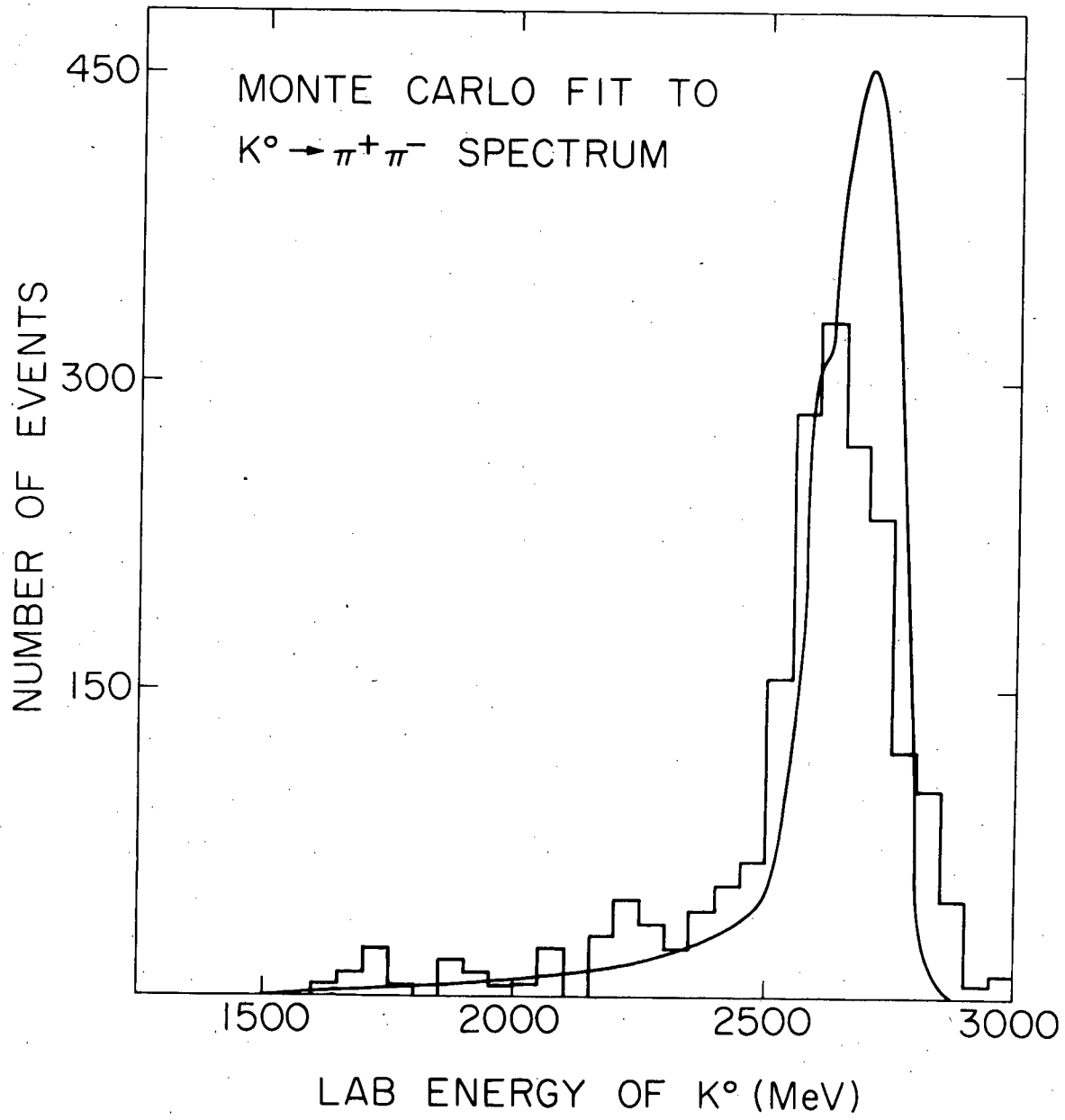
MONTE CARLO FIT TO
K° → π+ π− SPECTRUM
NUMBER OF EVENTS
450
300
150
1500
2000
2500
3000
LAB ENERGY OF K° (MeV)

The production cross sections for $K^oΛ^o$ and $K^oΣ^o$ are roughly the same,[27,30] and the geometrical detection efficiencies for detection of K^o's from these two production modes are nearly alike. Therefore, we have used equal mixtures of $K^oΛ^o$ and $K^oΣ^o$ in the Monte Carlo program. That is, equal numbers of $K^oΛ^o$ and $K^oΣ^o$ events were generated and subjected to the Monte Carlo tests. This gives about the same width to the main peak for the Monte Carlo energy spectrum and the experimental spectrum.

The percentage of $K^{o*}(890)Λ^o$ events to generate was determined as follows. The $K^o_{π2}$ energy spectrum (Figure 32) shows a main peak centered about 2640 MeV ($γ_K = 5.3$), which we assume is due to $K^oΛ^o$ and $K^oΣ^o$ production, and a low energy tail which we assume arises mostly from three-body production modes. The upper slope of the main peak was reflected about 2640 MeV to approximate the contribution to the K^o energy spectrum from $K^oΛ^o$ plus $K^oΣ^o$. 84.3% of the $K^o_{π2}$ events fell under this symmetrized peak. The events not within this peak (15.7%) were assumed to be from resonance production. We then calculated how long a $K^{o*}Λ^o$ run to make in order to obtain a ratio 15.7:84.3 of successful $K^o_{π2}$ resonance to non-resonance events. If was determined that if equal numbers of $K^oΛ^o$ and $K^oΣ^o$ events were generated, then the number of $K^{o*}Λ^o$ events generated should be .845 times the total number of $K^oΛ^o$ plus $K^oΣ^o$ events. Using this recipe for the $K^o_{π2}$ Monte Carlo events gives the smooth curve in Figure 32. The same formula was then used to generate Monte Carlo events for the $K^o_{π3}$ and $K^o_{μ3}$ decays. For K^o_{e3} decays, the mixing formula was determined from the experimental $K^o_{π3}$ energy spectrum rather than from the $K^o_{π2}$ spectrum.

I. Correction to Beam Momentum

A subtraction of 50 MeV/c was made from the beam momentum of 3000 MeV/c to account for the following effects. By giving the target proton a Fermi momentum, we artificially add ~30 MeV of energy to the $\pi^- p$ production system, so this extra energy should be subtracted out again. In addition, we estimate that ~20 MeV of energy goes into overcoming the binding energy of the proton in the target, recoil energy of the residual nucleus, and fragmentation energies if the target nucleus breaks up. How to treat all these effects rigorously is not understood. Therefore, we have employed the artificial method of subtracting 50 MeV/c from the beam momentum. The beam momentum used in the Monte Carlo program was 2950 MeV/c.

J. Comments on K^o Energy Spectrum

Comparison of the curves in Figure 32 for the experimental and Monte Carlo $K^o_{\pi 2}$ energy spectra shows that even after the 50 MeV/c subtraction from the beam momentum just described, the Monte Carlo spectrum peaks about 50 MeV higher than the experimental spectrum. We do not understand the reason for this discrepancy. However, its effect on the shape of the detection efficiency curves and on the calculation of other kinematical quantities for the K^o is very small.

For the K^o_{e3} experiment, an earlier version of the Monte Carlo program was used which had two differences from the final version described above. The $K^o\Sigma^o$ production mode was not included in the program. Only the $K^o\Lambda^o$ and $K^{o*}(890)\Lambda^o$ modes were used. This difference has the effect of making the main peak in the Monte Carlo K^o energy spectrum about half as wide as the peak in the experimental spectrum. Furthermore, the $K^o\Lambda^o$ plus $K^{o*}\Lambda^o$

spectrum peaks at higher energy than the $K^o\Lambda^o$ plus $K^o\Sigma^o$ plus $K^{o*}\Lambda^o$ spectrum. To correct for this effect, a beam momentum of 2850 MeV/c was used for the K^o_{e3} Monte Carlo runs.

K. Study of Backgrounds

Two possible backgrounds which would bias the K^o decay time distribution if undetected are 1) $\pi^- p \rightarrow K^o\bar{K}^o n$ and 2) $\Lambda \rightarrow pe^-\nu$ (lambda beta decay). Lambda beta decay is a background for K^o_{e3} decays only. These processes have been studied using a modified version of the Monte Carlo program.

The production process $\pi^- p \rightarrow K^o\bar{K}^o n$ could add $\bar{K}^o$ events to the sample of K^o events thus modifying the K^o_{e3} time distribution. This process is studied under two different sets of assumpsions:

a) K^o, $\bar{K}^o$, n produced isotropically in the $\pi^- p$ rest frame with no resonance

b) $\pi^- p \rightarrow A_2 n$ followed by $A_2 \rightarrow K^o\bar{K}^o$ using ΛK angular distribution for A_2 production with the A_2 peaked forward and assuming isotropic decay distribution for the A_2.

In both cases it is assumed that $\bar{K}^o \rightarrow \pi e\nu$ and $K^o \rightarrow \pi^+\pi^-$. For a successful event, the K^o decay products must trigger the $\lambda dE/dx$ hodoscope whereas the $\bar{K}^o$ decay products trigger the ϕ and ρ hodoscopes. It is found that these processes have a negligible efficiency. The principal reason is that the π^+ and π^- from K^o decay have momenta too high to trigger the $\lambda dE/dx$ hodoscope.

The lambda beta decay, $\Lambda \rightarrow pe\nu$, would add negative electron events to the sample if it were mistakenly identified as K^o_{e3}, thereby causing a serious bias to the data. A study of the raw data before selection of K^o_{e3}

candidates indicates that a sizeable number of triggers result from the decay $\Lambda \rightarrow \pi^- p$. Therefore it might be expected that $\Lambda \rightarrow pe^-\nu$ would also trigger the apparatus. The source of the Λ^0s seen in the raw data is unclear. They are too numerous and have too broad an energy spectrum to have resulted solely from ΛK production in which the Λ^0s are peaked strongly backward in the production frame. Many of the Λ^0s must therefore come from other processes for which the angular distributions are not well known. A comparison of the efficiencies of the two lambda decay modes was made. Due to the lack of information on the source of the Λ^0s, the following simplifications were made to the usual Monte Carlo program: 1) The $\lambda dE/dx$ hodoscope trigger was not required. 2) The lambda total energy was fixed at the values 1500, 2000, 2500, and 3000 MeV. 3) The lambda production angle in the lab system was fixed at the values 0^o and 5^o. It was found that in all cases the $\Lambda \rightarrow pe^-\nu$ efficiency is approximately 20% of the $\Lambda \rightarrow \pi^- p$ efficiency. Using this ratio along with the branching ratio for lambda beta decay and the $\Lambda \rightarrow \pi^- p$ triggering rate, the expected number of triggers from $\Lambda \rightarrow pe^-\nu$ may be calculated and used to correct the K^o_{e3} sample for this background.

APPENDIX B. TABULATION OF KINEMATICAL QUANTITIES

Table 6 presents a computer listing of kinematical quantities for the 99 $K^{o}_{\pi 3}$ events in the final sample. From the information given, other kinematical quantities such as invariant masses can easily be calculated. The following quantities are tabulated:

FRAME.....Frame number which identifies the event

TK.....Proper decay time of the K^{o} (units of τ_S)

EK.....Laboratory energy of the K^{o} (MeV)

EK2.....Second laboratory energy solution for K^{o} (MeV)

MISS.....Calculated distance of closest approach for the π^{+} and π^{-} tracks measured in the spark chambers (inches)

POPSQ.....Popsquare (defined in Backgrounds chapter) (MeV^2)

PL.....Total laboratory momentum of pion (MeV/c)

PLX,PLY,PLZ.....Components of pion laboratory momentum (z is beam direction, x is vertical direction, y is horizontal direction transverse to beam.) (MeV/c)

XPRO,YPRO,ZPRO...Coordinates of K^{o} production point (inches)

XDK,YDK,ZDK.....Coordinates of K^{o} decay point (inches)

Table 6

						POSITIVE PION				NEGATIVE PION									
FRAME	TK	EK	EK2	MISS	PCPSQ	PL	PLX	PLY	PLZ	PL	PLX	PLY	PLZ	XPRO	YPRO	ZPRO	XDK	YCK	ZDK
217521	3.1	2531	2189	.028	1357	738	31	-8	737	937	25	239	905	9.48	8.47	8.01	9.97	10.71	23.74
219808	1.7	2720	2317	.038	1652	982	-74	-88	975	679	-14	-181	654	9.23	8.46	7.00	9.13	7.25	16.10
223497	4.3	2641	2640	.062	-3690	1185	-68	124	1177	601	-66	-28	596	9.50	8.55	7.00	9.03	9.91	30.23
229880	3.7	2278	2278	.028	-362	843	33	14	842	787	74	-200	757	9.44	8.63	7.00	10.27	6.68	23.71
231424	5.9	2571	1616	.020	14525	836	-108	-13	828	465	43	10	463	9.30	8.56	7.00	8.29	7.58	37.99
234554	.7	2604	2769	.026	243	1128	84	153	1114	741	-68	197	711	9.29	8.65	7.00	9.43	9.31	10.66
236308	2.3	2898	2156	.061	5694	943	-22	36	942	711	57	-97	703	9.41	8.63	7.00	9.37	7.69	20.32
237314	6.1	2477	2372	.037	120	694	34	-61	691	1033	-97	131	1021	9.23	8.13	7.00	8.56	9.59	37.58
238650	4.2	2729	4445	.081	15371	734	66	-56	728	1545	79	71	1541	9.11	8.74	7.00	10.70	9.08	30.46
239412	2.1	2795	2063	.279	6014	916	50	132	905	709	-62	-30	705	9.47	8.08	7.00	9.63	8.61	18.80
247432	3.0	2822	2375	.047	1912	1175	-112	11	1170	640	11	131	626	9.30	8.43	7.44	8.35	10.11	24.53
253 44	3.6	2553	2056	.041	3058	902	-46	-176	883	633	-22	20	632	9.43	8.36	7.00	8.50	7.29	25.86
254652	.5	2544	4265	.002	17342	1293	80	10	1291	839	-70	26	835	9.50	8.30	7.00	9.52	8.37	9.78
260805	2.7	2851	1822	.238	13255	787	-88	-30	781	692	47	71	687	9.44	8.61	7.00	9.24	8.70	22.53
270185	1.0	2028	1934	.003	149	819	48	54	815	472	54	127	452	9.07	8.55	7.00	9.13	9.25	10.92
270249	2.5	2596	1917	.219	6032	910	-99	-120	897	599	59	7	596	9.11	8.80	7.00	9.10	7.68	20.25
274466	2.6	2157	1403	.241	12724	413	-9	62	409	701	1	-97	694	9.08	8.39	7.00	8.90	8.43	18.44
275 85	6.3	2044	1737	.165	1761	657	40	108	647	667	46	-114	655	9.33	8.38	7.00	10.74	8.29	32.82
276321	5.8	2555	2554	.063	-3536	1018	-21	91	1014	714	-110	155	688	9.38	8.27	7.00	8.76	12.84	36.67
278523	2.5	2724	3305	.092	2399	1410	-20	-134	1404	627	-30	35	625	9.13	8.41	7.00	8.54	8.12	20.94
283442	3.4	2847	3272	.148	1235	1312	-44	116	1306	662	-18	122	650	9.26	8.34	7.00	8.37	9.73	26.79
285 93	3.9	2792	2791	.085	-3638	550	-77	104	534	1426	-56	70	1423	9.42	8.17	7.00	8.61	9.73	29.20
287377	2.1	2700	1761	.135	12146	708	-42	-14	707	719	26	-178	696	9.25	8.42	7.00	9.15	7.11	18.56
287910	4.5	2284	3389	.273	10109	897	81	28	893	899	-45	113	891	9.25	8.66	7.00	10.23	10.89	27.75
288201	4.5	2313	1972	.055	1656	804	12	133	793	636	59	-48	631	9.11	8.53	7.00	9.25	10.27	27.93
294250	2.7	2303	1764	.180	4700	412	47	34	408	967	-93	-83	959	9.10	8.46	7.00	8.84	7.84	19.56
295922	6.1	2544	3324	.049	4612	1059	-78	79	1053	920	87	153	903	9.17	8.59	7.00	9.08	13.14	38.27
296432	3.9	2593	2852	.054	586	637	8	46	635	1193	-49	-109	1187	9.37	8.38	7.00	9.15	8.75	27.68
300719	3.8	2726	4159	.059	11502	741	8	60	738	1515	-147	-33	1507	9.40	8.43	7.00	8.02	8.60	28.10
302538	2.8	2417	2192	.278	620	1124	-110	-4	1118	490	22	95	480	9.55	8.47	7.00	9.14	9.35	20.46
310312	4.1	2595	3023	.117	1502	898	-22	133	888	1048	-9	-63	1046	9.22	8.65	7.00	8.74	9.99	28.37
313612	3.4	2444	1914	.245	3916	349	-34	61	341	1126	82	123	1117	9.42	8.60	7.00	10.00	11.12	23.45
316552	3.6	2958	1735	.133	19008	606	13	-35	605	756	56	47	752	9.44	8.44	7.00	10.50	7.29	28.86

Table 6 (continued)

						POSITIVE PION				NEGATIVE PION									
FRAME	TK	EK	EK2	MISS	PCPSQ	PL	PLX	PLY	PLZ	PL	PLX	PLY	PLZ	XPRO	YPRO	ZPRO	XDK	YDK	ZDK
320113	3.2	2547	1348	.000	6780	644	1	112	634	830	6	-80	826	9.33	8.28	7.00	9.27	8.87	23.40
321991	1.8	2742	1555	.260	21858	688	-6	1	688	583	-61	-111	569	9.47	8.54	7.00	8.97	7.32	16.96
331440	3.6	2624	2623	.037	-1394	591	42	-37	588	1239	-104	83	1231	9.33	8.11	7.00	9.35	8.75	25.99
336562	2.5	2855	1922	.116	10287	888	57	34	886	621	-23	130	607	9.36	8.48	7.00	10.28	10.25	21.19
341303	4.1	2278	2095	.025	457	643	-49	-11	641	829	63	-171	808	9.15	8.66	7.00	9.01	7.22	26.05
348797	4.5	2119	2118	.088	-2250	797	54	-208	767	731	-60	-3	728	9.29	8.64	7.00	9.43	6.43	25.90
358646	4.8	2467	3765	.004	11573	910	-32	-60	907	1125	-52	129	1117	9.48	8.27	7.00	8.44	8.87	31.21
365843	.5	2900	2170	.004	5465	1180	65	262	1149	539	29	5	538	9.59	8.11	7.00	9.73	8.54	9.97
367423	2.9	2708	1850	.099	9591	551	47	11	549	923	15	-183	905	9.34	8.32	7.00	9.56	6.66	22.79
374473	5.5	2679	2190	.085	2623	834	14	-66	831	858	64	142	844	9.51	8.14	7.00	10.41	9.24	37.23
377599	4.7	2649	1713	.089	12637	602	-61	60	596	716	-60	-55	711	9.22	8.50	7.00	8.16	7.52	32.22
378523	4.5	2149	1691	.212	3835	351	27	102	335	962	-94	72	954	9.49	8.62	7.00	8.29	11.20	26.49
382512	.6	2976	3906	.001	4719	902	-38	104	896	1288	-6	15	1288	9.24	8.65	7.05	9.29	8.75	10.56
387149	4.0	2815	2849	.027	10	1064	-34	192	1046	787	-81	40	782	9.52	8.51	7.00	9.13	10.69	29.75
388498	1.3	2182	1630	.003	5694	389	-32	-43	385	881	10	135	871	9.42	8.54	7.00	9.17	8.88	12.88
389983	2.1	2151	3501	.010	15565	637	52	116	624	1105	53	42	1103	9.40	8.52	7.00	10.23	9.41	15.93
390530	.6	2427	2426	.029	-367	1132	48	129	1123	501	11	-31	500	9.62	8.24	7.00	9.79	8.53	9.76
394902	4.7	2243	3744	.221	17177	1003	19	-28	1003	831	83	87	822	9.21	8.27	6.63	10.96	8.69	27.91
403762	5.6	2513	1720	.075	9574	524	-35	-37	522	840	29	132	829	9.45	8.74	7.91	8.60	11.39	36.18
406607	1.9	2353	3026	.052	4095	1046	34	155	1034	797	-7	-53	795	9.48	8.14	7.00	9.74	8.78	15.95
409125	1.6	2603	1382	.000	27791	505	-10	103	494	597	2	36	596	9.46	8.30	7.00	8.92	9.13	15.38
417902	4.4	1870	1428	.026	4983	404	-11	15	403	622	-58	-125	607	9.65	8.66	7.00	9.52	8.01	23.52
423880	2.7	2794	2085	.000	5565	782	34	-69	778	708	36	17	706	9.28	8.36	6.78	9.11	7.12	21.84
423976	.7	2517	1803	.128	7371	423	1	12	423	913	80	-38	909	9.27	8.33	7.37	9.50	8.52	11.07
424683	6.0	2793	2792	.005	-3625	821	-90	-26	815	1069	-60	137	1058	9.42	8.65	7.00	8.02	9.43	40.96
430851	3.3	2071	1764	.047	1701	623	-47	-104	613	717	57	89	709	9.30	8.27	7.00	9.65	8.10	20.77
433698	1.0	2674	1703	.251	13602	850	54	-116	840	542	-59	22	539	9.31	8.54	7.00	9.35	8.20	12.46
438392	1.6	3035	3034	.111	-432	790	-46	95	783	1219	75	51	1216	9.30	8.56	7.00	9.57	8.82	17.07
449932	3.1	2266	1653	.176	6644	574	27	-44	571	623	-32	45	620	9.39	8.34	7.00	8.98	9.54	21.37
458715	4.0	2389	2962	.099	2984	729	30	92	722	1061	-94	-21	1056	9.23	8.22	7.00	8.94	9.64	26.45
459286	4.7	2534	3254	.185	4024	574	-27	-4	573	1388	46	195	1374	9.30	8.34	7.00	9.79	10.13	31.15
459903	3.0	3065	2097	.000	9392	410	22	52	407	1274	69	8	1272	9.44	8.72	7.17	10.55	9.80	26.01
464958	4.6	2631	1576	.043	17738	851	36	69	847	440	-48	-35	436	9.27	8.45	6.43	9.19	9.53	30.94

Table 6 (continued)

						POSITIVE PION				NEGATIVE PION									
FRAME	TK	EK	EK2	MISS	PCPSQ	PL	PLX	PLY	PLZ	PL	PLX	PLY	PLZ	XPRO	YPRO	ZPRO	XDK	YDK	ZDK
475240	4.3	1878	1404	.255	5820	605	7	-113	594	466	43	68	459	9.29	8.28	7.00	10.83	7.28	23.14
477361	1.2	2109	4153	.010	30584	939	17	-67	936	857	-49	-160	841	9.30	8.57	7.00	9.22	7.90	11.97
484247	5.9	2636	1378	.120	29139	539	-27	-1	528	576	-2	95	568	9.46	8.81	7.00	7.02	11.50	38.41
494316	2.9	2873	2083	.133	6726	627	-6	26	626	903	34	-72	899	9.13	8.35	7.00	10.36	8.48	23.93
504624	2.7	2541	2167	.183	1647	364	33	89	351	1288	6	108	1284	9.33	8.18	7.00	9.52	9.87	21.05
515513	.8	2314	4213	.001	23603	891	53	75	887	968	5	133	959	9.36	8.16	7.00	9.51	8.41	10.71
517651	1.0	2209	2208	.005	-4165	904	47	-8	903	528	-22	-59	524	9.52	8.54	7.00	9.96	8.35	11.41
524572	3.3	2954	2002	.010	9909	810	-57	-108	800	790	-23	63	787	9.32	8.18	7.00	7.71	7.59	26.53
524871	4.6	2698	2977	.112	624	860	-91	-8	855	1150	108	84	1142	9.39	8.23	7.00	9.14	9.16	32.08
530336	3.8	2736	3397	.067	3002	1462	-146	92	1452	636	-53	144	618	9.53	8.13	7.00	8.01	10.40	28.14
531 70	3.0	2587	1823	.163	8090	980	-98	112	968	462	58	43	457	9.47	8.39	7.00	9.12	9.61	22.62
531636	4.1	2308	3023	.099	4713	754	-52	-102	745	1055	112	-10	1049	9.50	8.15	6.62	9.81	6.65	25.56
544104	1.6	2382	1972	.318	2330	801	29	112	793	717	71	-100	706	9.27	8.53	7.00	9.89	8.66	14.67
544936	5.8	2603	3287	.085	3495	1302	-52	211	1284	754	63	1	751	9.06	8.24	7.00	9.04	11.33	37.52
549 12	4.3	2595	2594	.016	-2485	830	-37	-135	818	978	19	42	977	9.31	8.56	7.00	10.03	7.27	29.66
556199	3.4	2801	2800	.094	-3653	510	20	-91	501	1373	85	-131	1364	9.47	8.42	7.00	10.00	7.00	26.35
568659	4.6	2684	3528	.074	4802	1446	-137	-87	1437	693	-6	69	690	9.31	8.29	7.00	7.85	8.00	32.06
571385	.5	2887	3786	.031	4693	1141	87	53	1136	1138	-68	-73	1134	9.24	8.36	7.00	9.22	8.36	10.02
572355	4.9	2726	2334	.083	1556	766	62	-1	763	1030	-35	-227	1004	9.27	8.26	7.00	9.68	4.75	33.72
580410	4.5	2733	2066	.055	5104	603	-61	115	589	1001	11	-5	1001	9.33	8.59	7.50	7.74	10.20	32.62
581788	4.5	2742	2741	.153	-731	637	-83	35	631	1240	-56	-130	1232	9.49	8.54	7.00	8.24	6.43	32.11
584656	2.7	2604	4399	.126	17872	1269	-87	77	1264	906	54	1	904	9.45	8.24	6.53	9.33	8.57	20.91
600254	4.2	2650	1809	.016	9624	612	69	-19	608	835	-10	152	821	9.39	8.55	7.66	9.74	10.92	30.16
602520	1.4	2798	2798	.211	-20	1163	21	-124	1156	815	36	87	810	9.32	8.58	7.00	9.37	8.45	15.09
605512	4.1	2320	2319	.096	-134	959	-18	241	928	708	-24	-16	707	9.43	8.25	7.00	9.01	10.97	25.92
608 66	3.7	2426	2425	.248	-4467	818	-3	94	813	898	-105	-84	888	9.45	8.64	7.42	8.78	9.40	25.63
634312	3.2	2616	2828	.119	395	1050	37	-46	1048	827	-56	-184	805	9.64	8.67	7.00	9.14	7.07	23.99
635662	4.2	2066	2066	.118	-3096	509	-46	0	506	876	-59	192	852	9.41	8.76	7.00	9.30	11.34	24.33
649238	5.4	2565	2276	.259	922	1092	-72	-80	1087	517	33	-101	506	9.16	8.50	7.00	9.23	4.03	35.03
655504	2.3	2268	3698	.202	15621	534	18	17	524	1328	86	185	1312	9.50	8.63	7.00	9.89	9.89	17.29
677434	3.9	2581	2580	.080	-1420	708	-31	38	706	970	-95	-84	962	9.57	8.41	7.00	9.18	8.52	27.22
678230	2.8	2806	2111	.317	5264	671	-29	-32	670	948	14	148	937	9.28	8.70	7.00	8.56	10.20	23.14
678282	4.4	2568	1981	.061	4392	434	-13	103	421	1081	49	59	1078	9.30	8.14	7.00	9.22	10.00	30.04

REFERENCES

1. J. H. Christensen, J. W. Cronin, V. L. Fitch, and R. Turlay, Phys. Rev. Letters 13, 138 (1964).

2. A. Abashian, R. J. Abrams, D. W. Carpenter, G. P. Fisher, B. M. K. Nefkens, and J. H. Smith, Phys. Rev. Letters 13, 243 (1964).

3. T. T. Wu and C. N. Yang, Phys. Rev. Letters 13, 380 (1964).

4. N. Cabibbo, Symmetries in Elementary Particle Physics, 1964 International School of Physics "Ettore Majorana", edited by A. Zichichi (Academic Press, New York, London, 1965), p. 258.

5. H. F. Haggerty, Ph.D. thesis, University of Wisconsin, 1970.

6. L. Wolfenstein, Theory and Phenomenology in Particle Physics, 1968 International School of Physics "Ettore Majorana", edited by A. Zichichi (Academic Press, New York, London, 1969), p. 218.

7. T. D. Lee and C. S. Wu, Ann. Rev. Nucl. Sci. 16, 471 (1966).

8. S. Eliezer and P. Singer, Phys. Rev. 165, 1843 (1968).

9. S. L. Glashow, Phys. Rev. Letters 14, 35 (1965).

10. S. L. Glashow and S. Weinberg, Phys. Rev. Letters 14, 835 (1965).

11. K. Terwilliger et al., Summary of Beam Design Studies for 17° Secondary Beam Experiment E-3 (ANL Report, 1964), unpublished.

12. D. Hodges (ANL Applied Mathematics Division, Technical Memorandum No. 127), unpublished, July, 1966.

13. P. M. Mantsch, Ph.D. thesis, University of Illinois, 1970.

14. M. F. Graham, Ph.D. thesis, University of Illinois, 1971.

15. D. Luers, I. S. Mittra, W. J Willis, and S. S. Yamamoto, Phys. Rev. 133, B1276 (1964).

16. B. R. Webber, Ph.D. thesis, University of California (Berkeley), 1969, UCRL-19226.

17. P. Franzini, L. Kirsch, P. Schmidt, J. Steinberger, and J. Plano, Phys. Rev. 140, B127 (1965).

18. A. H. Rosenfeld, N. Barash-Schmidt, A. Barbaro-Galtieri, L. R. Price, P. Söding, C. G. Wohl, M. Roos, and William J. Willis, Rev. Mod. Phys. 42, 87 (1970).

19. M. Derrick, J G. Fetkovitch, T. H. Fields, and J. Deahl, Phys. Rev. 120, 1022 (1960).

20. N. P. Samios, Phys. Rev. 121, 275 (1961).

21. B. M. K. Nefkens, A. Abashian, R. J. Abrams, D. W. Carpenter, G. P. Fisher, and J. H. Smith, Phys. Rev. 157, 1233 (1967).

22. M F. Graham, private communication, 1971.

23. G. W. Neisner, W. A. Mann, S. S. Hertzbach, R. R. Kofler, S. S. Yamamoto, D. Berley, S. P. Yamin, J. Thompson, W. J. Willis, Phys. Rev. (to be published).

24. B. R. Webber, F. T. Solmitz, F. S. Crawford, M. Alston-Garnjost, Phys. Rev. D 1, 1967 (1970).

25. L. Behr, V. Brisson, P. Petiau, E. Bellotti, A. Pullia, M. Baldo-Ceolin, E. Calimani, S. Ciampolillo, H. Huzita, A. Sconza, B. Aubert, L. M. Chounet, J. P. Lowys, and C. Pascaud, Phys. Letters 22, 540 (1966).

26. J. A. Anderson, F. S. Crawford, Jr., R. L. Golden, D. Stern, T. O. Binford, and V. G. Lind, Phys. Rev. Letters 14, 475 (1965); 15, 645 (1965); 16, 968 (1966).

27. O. I. Dahl, L. M Hardy, R. I. Hess, J. Kirz, D. H. Miller, J. A. Schwartz, Phys. Rev. 163, 1430 (1967).

28. L. J. Verhey, Ph.D. thesis, University of Illinois, 1968.

29. D. W. Carpenter, A. Abashian, R. J. Abrams, G. P. Fisher, B. M. K. Nefkens, J. H. Smith, Phys. Rev. 142, 871 (1966).

30. R. W. Hanft, Ph.D. thesis, University of Illinois, 1967.

VITA

Lewis H. Jones was born in [redacted]

He attended elementary and secondary schools in East Cleveland, Ohio, and was graduated from Shaw High School in February, 1959.

From September, 1959, to June, 1963, he was a student at Ohio Wesleyan University, Delaware, Ohio. He was graduated with Honors with a B.A. degree in Physics in June, 1963.

In September, 1963, he enrolled in the Graduate College of the University of Illinois. In February, 1965, he received his M.S. degree in Physics. While at Illinois he has held Teaching and Research Assistantships in the Department of Physics.

He has been a summer employee of the Joint Committee on Atomic Energy, U.S. Congress, Washington, D.C.; the N.A.S.A. Lewis Research Center, Cleveland, Ohio; and the U.S. Naval Research Laboratory, Washington, D.C.

He has co-authored the following publications:

"Investigation of Isobaric Analog States by (p,n) Reaction followed by Proton Emission", Phys. Rev. Letters 16, 1049 (1966)
(with A. I. Yavin, R. A. Hoffswell and T. M. Noweir) and

"Search for the Decay $K_S^0 \rightarrow \mu^+ + \mu^-$", Phys. Rev. 177, 2009 (1969)
(with R. D. Stutzke, A. Abashian, P. M. Mantsch, J. R. Orr, and J. H. Smith).

He is a member of the American Physical Society, Phi Beta Kappa, Pi Mu Epsilon, and the Simian Outing Society.